

Micro-strip module production for the ATLAS Semi-conductor Tracker

John Melone



UNIVERSITY
of
GLASGOW

Submitted in fulfilment of the requirements for the
Degree of MSc by research

University of Glasgow
Department of Physics and Astronomy

July, 2006

©J. Melone July 31 2006

Abstract

This report will discuss the development and implementation of a process to wire-bond and electrically test ATLAS semiconductor tracker silicon micro-strip detectors. It will detail the specific requirements for successful wire-bonding, the steps taken to improve and streamline the process and the criteria to be met during testing before the modules are deemed suitable for use. These detectors form part of the inner detector of the ATLAS experiment which is scheduled to begin in 2007 at the large hadron collider at CERN in Switzerland. The ATLAS experiment will observe and record the products of head on collisions of protons at very high energy. It is expected to shed light on many as yet unanswered questions about the fundamental particles of matter and forces of nature.

Table of Contents

<u>Chapter 1.....</u>	<u>14</u>
<u>1 Introduction.....</u>	<u>14</u>
<u>2 The ATLAS Detector.....</u>	<u>20</u>
<u>2.1 Introduction.....</u>	<u>20</u>
<u>2.2 The ATLAS Experiment.....</u>	<u>20</u>
<u>2.3 The ID layout.....</u>	<u>22</u>
<u>2.4 ATLAS Semiconductor Tracker (SCT) overview.....</u>	<u>24</u>
<u>2.5 ATLAS physics and simulated results.....</u>	<u>25</u>
<u>2.6 End-cap module description.....</u>	<u>29</u>
<u>2.7 Inner, middle and outer modules of the SCT End-cap.....</u>	<u>31</u>
<u>2.8 Summary.....</u>	<u>34</u>
<u>Chapter 3.....</u>	<u>36</u>
<u>3.1 Introduction.....</u>	<u>36</u>
<u>3.2 ATLAS SCT Collaboration.....</u>	<u>36</u>
<u>3.3 The UK-V collaboration.....</u>	<u>37</u>
<u>3.4 Electrical/Mechanical characteristics of SCT end-cap modules.....</u>	<u>38</u>
<u>3.5 Production Overview.....</u>	<u>40</u>
<u>3.6 Production statistics.....</u>	<u>41</u>
<u>3.6.1 SCT Production Database.....</u>	<u>42</u>
<u>3.6.1.1 DB Structure.....</u>	<u>43</u>
<u>3.6.1.2 Items.....</u>	<u>44</u>
<u>3.7 Module Tracker and E-Log.....</u>	<u>46</u>
<u>3.8 Other Internal Production Software.....</u>	<u>46</u>
<u>3.9 Summary.....</u>	<u>47</u>

Chapter 4.....	48
4 Wire-bonding Methods.....	48
4.2 Basics of wire-bonding.....	48
4.3 The physical stages of bonding.....	50
4.4 Parameters.....	51
4.4.1 Mechanical Parameters.....	52
4.4.2 Programmable parameters.....	54
4.4.3 Loop Parameters.....	56
4.4.4 Other Bonder Parameters.....	60
4.5 Criteria for good bonder performance.....	61
4.5.1 Ultrasonic settings.....	61
4.5.2 Clamping.....	61
4.5.3 Material condition.....	63
4.6 External factors affecting bonding.....	63
4.7 Bonding program optimisation.....	63
4.7.1 Bonding zones.....	65
4.8 Bonder parameter optimization.....	66
4.8.1 Over-bonding.....	67
4.8.2 High impact damage.....	69
4.8.3 Bond footprint profile analysis.....	70
4.8.4 Bonding zone foot-print profile comparison.....	73
4.9 Summary.....	77
Chapter 5.....	78
5 Electrical testing.....	78
5.1 Introduction.....	78
5.3 Electrical Test Equipment and Procedure.....	79
5.3.1 Data Acquisition System (DAQ).....	79
5.4 Thermal cycling.....	83
5.5 Electrical Tests.....	84
5.6 Summary of Full Module Testing Sequence.....	89
5.7 Anomalous channel tolerances.....	90

5.8 Criteria and Selection for Assembly to Disks.....	92
5.9 Summary.....	93
Chapter 6.....	94
6 Production Results.....	94
6.1 Introduction.....	94
6.2 Collaboration overview.....	94
6.4 Production and early bonding problems.....	97
6.5 Wire-bond reworks.....	100
Module Number.....	102
6.6 Bonding parameter evolution.....	103
6.7 Rework Analysis.....	105
6.8 Mechanical tolerances.....	106
6.9 Module Failure Modes.....	108
6.10 Final yield.....	109
6.11 Post production.....	110
6.12 Conclusions and Summary.....	112
Appendix A.....	115
List of information provided by SCT system DAQ.....	115
Appendix B.....	121
List of Failed Modules.....	121
Visual Inspection Failures.....	123
List of information provided by SCT system DAQ.....	Error: Reference source not found
Appendix B.....	Error: Reference source not found
List of Failed Modules.....	Error: Reference source not found
Appendix C.....	Error: Reference source not found
Visual Inspection Failures.....	Error: Reference source not found

List of Figures

<i>Figure 1-1 Quarks and leptons in the Standard Model.....</i>	<i>15</i>
<i>Figure 2-2 General layout of the ATLAS detector at the LHC.....</i>	<i>21</i>
<i>Figure 2-3 Three-dimensional cutaway overview of the layout of the ATLAS ID.....</i>	<i>23</i>
<i>Figure 2-4 Simulated Higgs event with the neutral higgs boson subsequently decaying predominantly into another bb pair. Note how the tracks are accurately reconstructed by the detectors of the SCT.....</i>	<i>27</i>
<i>Figure 2-5 Simulated side-on view of event in the ATLAS detector.....</i>	<i>28</i>
<i>Figure 3-6 The ATLAS end-cap SCT section contributors [].....</i>	<i>37</i>
<i>Figure 3-7 Thirteen parameters specify the geometry of an outer or middle module in the XY plane. Blue spots represent the sensor centres and blue lines the detector orientations. These points are checked after bonding and testing, to ensure each module remains within specification. Several modules were rejected for failing these tests (see section 6.9).....</i>	<i>39</i>
<i>Figure 3-8 Z survey points on an outer module</i>	<i>40</i>
<i>Figure 3-9 User access scheme for recording the data into the SCT production database.....</i>	<i>42</i>
<i>Figure 4-10 Wedge bond geometry [].....</i>	<i>49</i>
<i>Figure 4-11 Physical stages of a single wire bond.....</i>	<i>50</i>
<i>Figure 4-12 The three stages of bonding: source, loop and destination.....</i>	<i>51</i>
<i>Figure 4-13 H&K 710 Bond-head.....</i>	<i>52</i>
<i>Figure 4-14 Left and right views of bond-head showing detailed layout of the bond-head components</i>	<i>53</i>
<i>Figure 4-15 The parameter window, showing the range of adjustable parameters for one of the process windows</i>	<i>54</i>
<i>Figure 4-16 Deformation chart.....</i>	<i>55</i>
<i>Figure 4-17 Detailed breakdown of loop height parameters.....</i>	<i>57</i>

<i>Figure 4-18 ATLAS module mounting jig.....</i>	<i>62</i>
<i>Figure 4-19 ATLAS outer module bonding map.....</i>	<i>64</i>
<i>Figure 4-20 Close-in view of high and low bonds on module detector area.....</i>	<i>65</i>
<i>Figure 4-21a/b IV curve of module 253/falls of leakage current in time.....</i>	<i>68</i>
<i>Figure 4-22a Examples of over-bonding.....</i>	<i>68</i>
<i>Figure 4-23 Module 236 showing evidence of high impact damage on the high voltage bias line.....</i>	<i>70</i>
<i>Figure 4-24 Module 236, high current 1 nA@110 V and 6 uA@400 V.....</i>	<i>70</i>
<i>Figure 4-25 3D profile of wire-bond.....</i>	<i>71</i>
<i>Figure 4-26 X and Y profiles of bond from previous figure.....</i>	<i>72</i>
<i>Figure 4-27 Kinematic arrangement of H&K bond-head.....</i>	<i>73</i>
<i>Figure 4-28 2D and 3D images of a single wire-bond footprint on the chip bonding zone 74</i>	
<i>Figure 4-29 3D image from horizontal view point.....</i>	<i>74</i>
<i>Figure 4-30 2D and 3D profiles of missed wire-bond on the detector.....</i>	<i>75</i>
<i>Figure 4-31 Footprint profile from bond on the detector.....</i>	<i>76</i>
<i>Figure 4-32 3D profiles of two bonds on the fan-in bonding zone.....</i>	<i>77</i>
<i>Figure 5-33 Photograph of a patch card linked to an end-cap module.....</i>	<i>81</i>
<i>Figure 5-34 Module readout modes.....</i>	<i>82</i>
<i>Figure 5-35 Schematic diagram of the SCTDAQ system.....</i>	<i>83</i>
<i>Figure 5-36 Thermal cycling humidity profiles.....</i>	<i>83</i>
<i>Figure 5-37 Outer module supported by its transport frame inside an aluminium test box. The dry-air and coolant inlets are visible as is the support card on the lower right of the image.....</i>	<i>84</i>
<i>Figure 5-38 Strobe delay results from module 82. Each chip (top side of the module in this case M0 to E5) is readout simultaneously. This scan is performed to find the delay between the calibration pulse injection and comparator changing its state. The second row of results show the signal from the comparator must fall within a 25 ns window. (Note chip S1 is damaged and so is not reading out).....</i>	<i>85</i>
<i>Figure 5-39 Typical set of plots obtained with the Response Curve procedure before trimming for one data stream, corresponding to six chips (768 channels). From top to bottom the vt50 value, the gain, the offset and the noise are shown for each channel</i>	<i>87</i>
<i>Figure 5-40 The vt50 value after trimming for the same module as in Figure 5-6.....</i>	<i>87</i>

<i>Figure 5-41 Noise occupancy plot for one data stream: 2D plot of occupancy vs. channel number and vs. threshold (left); average occupancy for the stream vs. threshold (right). The threshold is expressed with respect to the 1 fC point (0 mV) as determined during the trimming procedure.....</i>	<i>88</i>
<i>Figure 5-42 Long-term test results for six modules showing from top to bottom: hybrid temperature; analogue (Icc) and digital (Idd) current; detector leakage current (Idet); and noise occupancy as a function of time. Each modules results are represented using different colours as indicated on the right of the figure.....</i>	<i>88</i>
<i>Figure 5-43 IV curve of module 652.....</i>	<i>89</i>
<i>Figure 6-44 Module production performances, the filled histograms show the cumulative number of modules built as a function of time (Starts) and the number of finished, assembled and tested modules of each flavour. Also shown is the production yield (right scale) both considering just GOOD modules and also GOOD+PASS modules.....</i>	<i>95</i>
<i>Figure 6-45 Results of qualification, this chart lists the number of defects per qualification module and the defect types. Bonding errors are defects that are deemed a result of poor bonding. Visible defects are defects that are seen at visual inspection (such as scratches). Non-visible defects are defects that are neither seen at visual inspection nor caused by poor bonding (such as dead/stuck channels.....</i>	<i>97</i>
<i>Figure 6-46 Number of reworked channels during early stages of production.....</i>	<i>98</i>
<i>Figure 6-47 Failed wire-bonds caused by bonding system fault, wire is seen to form a loop between consecutive source points.....</i>	<i>98</i>
<i>Figure 6-48 Graphical image of bonding system bond head.....</i>	<i>100</i>
<i>Figure 6-49 Example of good wire-bonding on the fan-in to detector zone of module 258 101</i>	
<i>Figure 6-50 Final totals for reworked channels per module.....</i>	<i>102</i>
<i>Figure 6-51 Frequency of reworked channels per module.....</i>	<i>103</i>
<i>Figure 6-52 Deformation charts provided by the H&K bonding system software. Wire deformation is measured in the Z axis.....</i>	<i>104</i>
<i>Figure 6-53 Breakdown of reworked channels per bonding zone on selected modules. This figure shows the total number of defects per module and breaks down that number into which bonding zone each rework was performed in.....</i>	<i>106</i>

<i><u>Figure 6-54 Analysis of the effects of Z-deviation in the detector on module rework numbers.....</u></i>	<i><u>107</u></i>
<i><u>Figure 6-55 Module 81 cracked spine (left, identified by arrow) undamaged spine (right).....</u></i>	<i><u>108</u></i>
<i><u>Figure 6-56 Disk 4 of SCT end-cap C.....</u></i>	<i><u>111</u></i>
<i><u>Figure 6-57 ATLAS SCT end-cap C.....</u></i>	<i><u>112</u></i>
<i><u>Figure C-0-58 Module 144 Scratches on fan-in.....</u></i>	<i><u>123</u></i>
<i><u>Figure C-0-59 Module 245 failed IV. Scratch on detector.....</u></i>	<i><u>124</u></i>
<i><u>Figure C-0-60 Scratches on fan-in of Module 488.....</u></i>	<i><u>124</u></i>
<i><u>Figure C-0-61 Module 38 Dead channels on fan-in, caused by scratches.....</u></i>	<i><u>125</u></i>
<i><u>Figure 6-13 Disk 4 of SCT end-cap C.....</u></i>	<i><u>Error: Reference source not found</u></i>
<i><u>Figure 6-14 ATLAS SCT end-cap C.....</u></i>	<i><u>Error: Reference source not found</u></i>
<i><u>Figure C-0-1 Module 144 Scratches on fan-in.....</u></i>	<i><u>Error: Reference source not found</u></i>
<i><u>Figure C-0-2 Module 245 failed IV. Scratch on detector. .</u></i>	<i><u>Error: Reference source not found</u></i>
<i><u>Figure C-0-3 Scratches on fan-in of Module 488.....</u></i>	<i><u>Error: Reference source not found</u></i>
<i><u>Figure C-0-4 Module 38 Dead channels on fan-in, caused by scratches.....</u></i>	<i><u>Error: Reference source not found</u></i>

List of Tables

<u>Table 1 Detailed breakdown of loop parameters.....</u>	<u>59</u>
<u>Table 2 Other useful bonding parameters.....</u>	<u>61</u>
<u>Table 3 Final program list including H&K program codes used to generate program information.....</u>	<u>66</u>
<u>Table 4 Results of pull tests on modules 52 and 53 (pre-qualification).....</u>	<u>67</u>
<u>Table 5 Anomalous channel defect tolerances.....</u>	<u>91</u>
<u>Table 6 Module category statistics (as defined in Chapter 5).....</u>	<u>95</u>
<u>Table 7 Failure modes of rejected modules.....</u>	<u>108</u>
<u>Table 8 Final yield figures of all SCT module production sites.....</u>	<u>110</u>

Acknowledgements

Many colleagues and friends have been a positive influence and source of support during this period of study and I would like to thank some of them for their contributions. My brother Jody helped at key stages during early production, and was jointly responsible for achieving such a reliable process and high production yield. My colleagues in the other production sites have also been a great resource and I am indebted to Mike Wormald at Liverpool for his help identifying a suitable system and subsequent training. Vicki Davis at RAL and the other members of the “league of bonders” have also been available to discuss bonding issues.

Many people in the group are responsible for the success of the ATLAS module production run and I would like to thank Sasha for his work and feedback on production testing. Sasha continued the work of Will and Richy who both made massive contributions. My colleagues in the lab, Fred, Lina and Fifi have all been helpful and good pals along the way. Long days of bonding were often broken up nicely with trips to Byers road for lunch where I enjoyed heated debates with Liam, Andy and Jambihno on some of my favourite topics.

I reserve special thanks to Val for offering me the opportunity to embark on this project. His guidance has helped me during the dark days of early production and he was always available for advice and to remind me that I was “just a bonder” when in danger of getting carried away! Other members of the group have assisted with their expertise and I would like to thank Keith for his advice at the writing up stage and for encouraging me to ignore Val and leave in that super-symmetry reference. Thanks also to Andy for helping with Origin and Liam for his proof reading.

As always, my parents have been more supportive than I could have wished, I am grateful for their patience and encouragement. Last but not least, my love and thanks to Loz for putting up with months of boring chat about deformation charts and bonding parameters.

Authors Declaration

This thesis represents work performed from 2002 to 2005 in the Experimental Particle Physics group in the Department of Physics and Astronomy at the University of Glasgow. Except where explicit reference is made to the work of others, this dissertation is the result of my own work. None of this material has been submitted for any other degree at the University of Glasgow or any other institution.

John Melone

Chapter 1

1 Introduction

In the last 50 years, the study of the basic constituents of matter and their interactions has led to an extraordinarily detailed understanding of subatomic phenomena (phenomena on the scale of atomic nuclei or smaller). This work culminated in the unification of electromagnetism and radioactivity, by which we mean that they are now understood to be different aspects of the same phenomenon. These discoveries were the results of experiments involving:

- Particle accelerators that produce proton and electron beams of ever increasing energy.
- Detectors capable of measuring the complex interactions produced by the collisions of these high-energy beams.

Accelerator experiments have revealed that the world of particles is very rich; many new particles similar to protons and neutrons (called *baryons*) and a whole new family of particles called *mesons* have been discovered. By the early 1960s over one hundred new types of particles had been identified. Discoveries have also shown that there are six types of quarks (given the names of *up*, *down*, *strange*, *charm*, *bottom* and *top* in order of increasing mass). In addition, there are six types of particles (including the electron) called *leptons*. The standard model ^[1] (Figure 1-1) accounts for the strong,

weak and electromagnetic interactions of the quarks and leptons, and thus explains the patterns of nuclear bindings and decays.

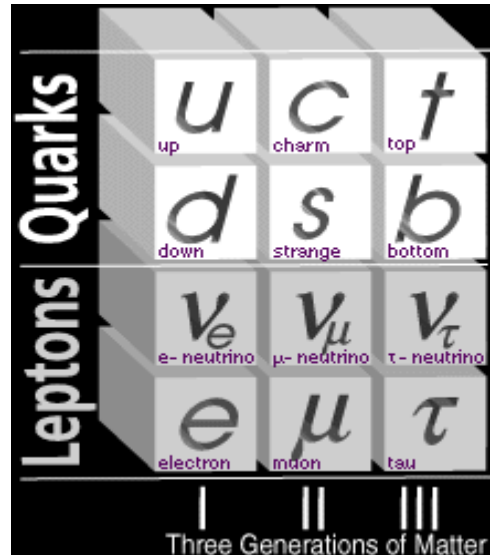


Figure 1-1 Quarks and leptons in the Standard Model

In contrast to the leptons, none of the six quarks may be found by itself. The *electron* is the best known lepton. Two other charged leptons, the *muon*, (discovered in 1936) and the *tau* ^[2] (discovered in 1975) differ from the electron only in that they are more massive than it is. The other three leptons are very elusive particles called *neutrinos*, which have no electric charge and very little, if any, mass. There is one type of neutrino corresponding to each of the three types of electrically charged leptons. For each of the six leptons there is an anti-lepton with equal mass and opposite charge.

Atoms are made of protons, neutrons, and electrons. Protons and neutrons are made of quarks, which are possibly made of more fundamental objects. The *strong* force holds quarks together to form hadrons; its carrier particles are called *gluons* because they so successfully "glue" the quarks together. The binding of protons and neutrons to form nuclei is the result of the residual strong interaction due to their strongly interacting quark and gluon constituents. Leptons undergo no strong interactions. *Weak* interactions are the only processes in which a quark can change to another type of quark, or a lepton to another lepton. They are responsible for the fact that all the more massive quarks and leptons decay to produce lighter quarks and leptons. That is why

stable matter around us contains only electrons and the lightest two quark types (*up* and *down*). The carrier particles of weak interactions are the *W* and *Z bosons* ^[3]. Beta-decay of nuclei was the first observed weak process: in a nucleus where there is sufficient energy a neutron becomes a proton and gives off an electron and an anti-electron neutrino. This decay changes the atomic number of the nucleus. Beta-ray is the name given to the emerging electron. So now we have explained beta-rays; what about the alpha? The *alpha-particle* is a helium nucleus - one of the products of a nuclear fission. Fission is the break-up of a massive nucleus into smaller nuclei; this occurs when the sum of the masses of the smaller nuclei is less than the mass of the parent nucleus. This is a residual strong interaction effect. The Standard Model answers many of the questions of the structure and stability of matter with its six types of quarks, six leptons, and the four forces.

But the Standard Model leaves many other questions unanswered:

- Why are there three types of quarks and leptons of each charge?
- Are there more types of particles and forces to be discovered at yet higher-energy accelerators?
- Are the quarks and leptons really fundamental, or do they, too, have substructure?
- What particles form the dark matter in the universe?
- How can the gravitational interactions be included in the Standard Model?

Questions such as these drive particle physicists to build and operate new accelerators, such as the Large Hadron Collider (LHC) with the ATLAS detector, in the hope that higher-energy collisions can provide clues to their answers. In recent years physicists have pushed to higher and higher energies, because much of the complexity observed at low energies may disappear when the energy becomes sufficiently large. Thus while radioactivity and electromagnetism have been separately known for 100 years, it

is only in the last 25 years that particle accelerators have provided beam energies sufficiently high to “unmask” the fundamental relationship between the two phenomena. In collisions involving high energy particles, some of the incoming energy can be used to create new particles ($E=mc^2$ means energy can be transformed into mass). The more massive the new particles, the larger the incoming energy must be to create them. The particles that underlie radioactivity turn out to be very massive (about 100 times as massive as a hydrogen atom), and therefore can only be created in the collisions of very high energy beams. To study the nucleus and the interactions of neutrons and protons that form it, physicists needed a tool that could probe within the tiny nucleus, as earlier scattering experiments had probed within the atom. The *accelerator* is a tool that allows physicists to resolve very small structures by producing particles with very high momentum and short wavelength. The wavelength (λ) of the associated wave is inversely proportional to the momentum (p) of the particle ($\lambda = h/p$), where h is Planck's constant. The greater the momentum, the shorter the wavelength and the smaller the structures that can be studied.

As the energy levels of experiments increase, the technology used to detect particles becomes more advanced, larger in scale and, crucially, greater in precision. The study of particles has progressed at a rate governed by the technology available at the time. In 1900 the first particle detector “The Cloud Chamber” was built. In the cloud chamber, the high energies of alpha and beta particles mean that a trail of vapour is left, due to the many ions produced along the path of the charged particle. These tracks have distinctive shapes (for example an alpha particle's track is broad and straight, while an electron's is thinner and shows more evidence of deflection). When a vertical magnetic field is applied, positively and negatively charged particles will curve in opposite directions. In the 1950's the “Bubble Chamber” was invented. In a bubble chamber, the whole chamber is subject to a constant magnetic field. As the particles enter the chamber, a piston suddenly decreases the pressure in the chamber. This brings the liquid to a superheated state, in which a tiny effect, such as the ionization produced by the passing of a charged particle near an atom, is sufficient to nucleate a bubble of vaporized liquid. At this moment, the camera records the picture. The magnetic field causes charged particles to travel in helical paths whose radius is determined by the particle momentum and by the ration of charge to the mass of the

particle. In this way charge particles can be observed and their mass measured. For these types of experiments it is also valuable to observe the particles path. For a long time, the bubble chamber was used for this purpose, but with the improvement of electronics, it became desirable to have a detector with fast electronic readout (in bubble chamber, photographs were made and films were looked through). The next technology was the wire chamber, which is a chamber with many parallel wires, arranged as a grid and held at high voltage, with the metal casing being on ground potential. As in the Geiger counter, a particle leaves a trace of ions and electrons, which drift toward the case or the nearest wire, respectively. By marking off the wires which had a pulse of current, one can see the particles path. The wire detector was the first detector with the ability to trace particle paths (or vertices) and has been used as a vertex detector ^[4]. As we move into the new century the vertex detector has become well established. A vertex detector gives the most accurate location of any outgoing charged particles as they pass through.

The origins of semiconductor detector arrays for particle physics event reconstruction lie in a project undertaken in 1965 by the IKO-Phillips group in Amsterdam ^[5], who built a ball shaped scattering chamber surrounded by 64 modules with several layers of silicon detectors ^[6]. Even with the limited number of channels (<8000) an enormous effort was required to provide the bulky readout electronics, the ADC and the computing power for event reconstruction. 40 years and several silicon chip revolutions later the progress made has been immense. There are now a large variety of silicon detectors in use in collider experiments. The associated local electronics has shrunk spectacularly and at the same time become faster and more powerful. In modern experiments, large multi-layered detectors surround the collision point. Each layer of the detector serves a separate function in tracking and identifying each of the many particles that may be produced in a single collision. The front-end readout electronics used in the ATLAS experiment detectors have been developed over many years to deal with the demands made by the ultra-high resolution pixel and micro-strip detector that will be used.

This thesis concentrates on the production and testing of silicon micro-strip detectors for use in the ATLAS experiment. The work will look at the process of module

manufacture, the technology and processes required to electrically connect the channels to the readout electronics, and the system used to test the modules. Chapter 2 looks in depth at the detector that will be used for the ATLAS experiment. This Chapter will look at the different sections of the detector with an emphasis on the sections for which Glasgow provided deliverables. This Chapter will also address the physics goals of the ATLAS detector (section 2.5) and provide some examples of simulated results. Chapter 3 details the specific responsibilities of the Glasgow group to ATLAS and explains the groups position within the wider collaboration. This Chapter will introduce the different stages of the production process and the methods of recording information for statistical analysis. The next Chapter, Chapter 4, will focus more in depth on the processes of wire-bonding with specific reference to parameters required for stable bonding and parameter optimisation. Next, in Chapter 5 the focus switches to the electrical testing of the silicon micro-strip detectors, where the modules are tested for IV, stream delay and digital/analogous tests. This Chapter will explain all processes performed before the modules are passed fit for assembly in the experiment. Chapter 6 is concerned with the problems encountered during production and the steps taken to resolve them. Specific attention will be paid to the overall success of the module wire-bonding and testing.

The work concludes with a discussion of the main results which will show that the Glasgow production site completed 273 modules for the ATLAS detector. To achieve this, 420,000 readout channels were connected using 1.3 million wire bonds and over 10 km of bonding wire. It will also show that the Glasgow site achieved an overall production yield of 94.5%.

Chapter 2

2 The ATLAS Detector

2.1 Introduction

This chapter will introduce the ATLAS detector ^[7], and looks in depth at the four sections of the Inner Detector (ID) ^[8]. The section of the ID of primary importance to this thesis is the Semi Conductor Tracker (SCT) which uses silicon micro-strip detector modules, some of which were wire bonded and tested in Glasgow. The construction of the modules and the different sizes of module will be discussed as will how the finished modules are assembled onto the eighteen rings of the SCT before shipment to the ATLAS cavern in CERN, Geneva in summer 2006. Some simulated results are included to indicate the kind of data expected during the experiment.

2.2 The ATLAS Experiment

The ATLAS collaboration proposes to build a general-purpose experiment, which is designed to exploit the full discovery potential of the LHC at CERN. The ATLAS experiment is concerned with the construction of a very large array of sensors for charged particle detection and accurate track measurement at the 27km superconducting accelerator which is presently under construction at CERN. The LHC will

accelerate protons at very high energies of 7 TeV as they collide in the detector. The detector (see Figure 2-1) consists of four major components:

- The inner detector, which measure the momentum of each charged particle
- The calorimeter, which measures the energy carried by the particles
- The muon spectrometer, which identifies and measure muons
- The magnet system, which is used for bending charged particles for momentum measurement

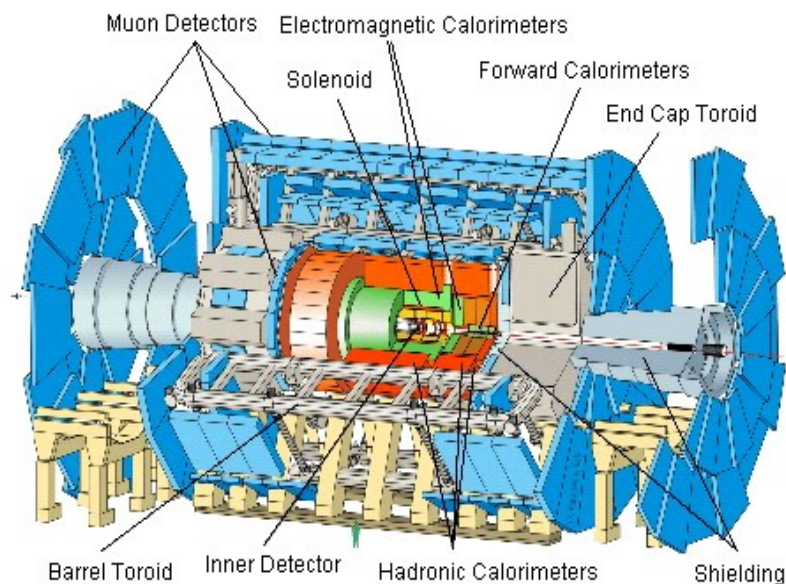


*Figure 2-2
General layout of the ATLAS detector at the LHC*

Many of the interesting physics questions at the LHC require extremely high luminosity ^[9]. Luminosity defines the intensity of a collider and is a product of the number of particles in both beams per unit area per second. The primary goal is to operate at a luminosity of $10^{34}\text{cm}^{-2}\text{s}^{-1}$ using a detector that provides as many reaction signatures as possible. Electron, photon, muon, jet and missing transverse energy will be measured, as well as b-quark tagging ^[10] (the identification of jets of particles originating from the bottom quark). The variety of signatures is considered to be important in the high-rate environment of the LHC in order to achieve robust and redundant physics

measurements with the capability for internal cross-checks. The interactions in the ATLAS detectors will create an enormous dataflow. To digest this data there is:

- A trigger system – selecting 100 “interesting” events out of 1000 million others. An interesting event is one from which new physics can be explored.
- A data acquisition system – channelling the selected data from the detectors to mass storage.
- A computing system analysing 1000 million events recorded per year.

ATLAS is designed as a general-purpose detector. When the proton beams produced by the LHC interact in the center of the detector, a variety of different particles with a broad range of energies may be produced. Rather than focusing on a particular physical process, ATLAS is designed to measure the broadest possible range of signals. This is intended to ensure that, whatever forms any new physical processes or particles might take, ATLAS will be able to detect them and measure their properties. Experiments at earlier colliders, such as the Tevatron and Large Electron-Positron Collider, were designed based on a similar philosophy. However, the unique challenges of the LHC - its high energy and extremely high rate of collisions require ATLAS to be larger and more complex than any detector ever built.

2.3 The ID layout

The challenges for the tracking detector systems at the LHC are unprecedented in terms of the numbers of channels, the required read-out speed and the expected radiation level. It combines high-resolution detectors at inner radii with continuous tracking elements at outer radii, all contained in a solenoidal magnet with a central field of 2 T. Mechanically, the ID consists of three units: a barrel section extending over 80 cm on each side of the interaction point, and two identical end-caps covering the rest of the cylindrical cavity. In all 2000 modules will be built, tested and prepared for the ATLAS end-caps.

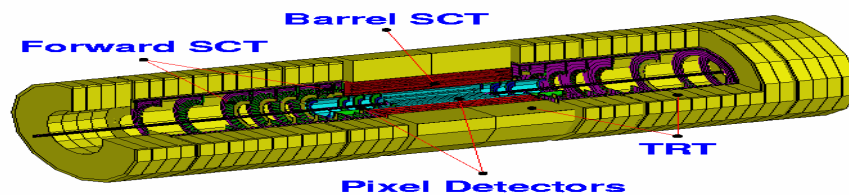


Figure 2-3 Three-dimensional cutaway overview of the layout of the ATLAS ID

The forward SCT of ATLAS ^[1] has 3 million electronics channels each reading out every 25 ns into its own on-chip 3.3 μ s buffer. A three-dimensional cutaway view of the layout of the ID is shown in Figure 2-2. A large number of tracking points (typically 36 per track) is given by a straw tube transition radiation tracker (TRT) which provides the possibility of continuous track-following with much less material per point and at lower cost. The combination of the high resolution detectors at inner radii of the SCT and the TRT give very robust pattern recognition and high precision in both transverse and longitudinal directions. The straw hits at the outer radius contribute to the momentum measurement due to the magnetic field, with the lower precision per point compared to the silicon being compensated by the large number of measurements and the higher average radius. The relative precisions of the different measurements are well matched, so that no single measurement dominates the momentum resolution. This means that the overall performance is robust, even in the event that a single system does not perform to its full specification. In addition, the electron identification capabilities of the whole experiment are enhanced by the detection of transition-radiation photons in the straw tubes.

2.4 ATLAS Semiconductor Tracker (SCT) overview

Within ATLAS, the UK's largest contribution is to the silicon micro-strip based SCT, composed of the 4-layer barrel section and two 9-layer end-cap sections within the ID. The ID has over 60 m² of active silicon detectors. The tracker has 4000 modules, each of 1536 channels with spatial resolution ~ 10 μm . The task of the SCT is to reconstruct tracks and vertices and to supply the important extra signature for short-lived particle decay vertices. The momentum and vertex resolution targets require high precision measurements to be made with fine granularity detectors given the large track density expected at the LHC. Semiconductor tracking detectors, using silicon micro-strip technology offer these features. The SCT system is designed to provide four precision measurements per track in the intermediate radial range, contributing to the measurement of momentum, impact parameter and vertex position as well as providing good pattern recognition due to the use of high granularity ^[11]. This is done using four layers of silicon micro-strip detectors to provide precision points, with a small stereo angle on each layer to obtain the Z measurement. The readout chain consists of a front-end amplifier and discriminator, followed by a binary pipeline, which stores the hits above threshold until the first level trigger decision. The forward SCT end-cap detector contains 60 m² of silicon detectors, with 6.2 million readout channels. The spatial resolution is 16 μm in R_0 and 580 μm in Z . Tracks can be distinguished if separated by more than 200 μm . The forward modules are mounted in up to three rings on 9 wheels, and their pattern recognition performance in the tracker is fundamentally limited by occupancy. In the case of the SCT, which has binary readout, the only way to resolve two tracks is to see them as two hit strips with at least one empty strip in between.

The noise occupancy of the SCT is very low (< 0.1 %) by design, and its occupancy due to underlying events at full luminosity is also low at around 0.5 %. These levels do not pose a significant problem for track reconstruction. However, the occupancy of a module hit by a b jet is typically 1.5 % and this can make track finding difficult. The efficiency drops further to 78 % near the core of the jet, indicating pattern recognition difficulties. An indication of the importance of the SCT in track finding jets is that the average efficiency of the whole tracker is 89.5% with a fake rate of 0.24 %. If one

layer of the SCT is removed, the efficiency only drops to 89.0 %, but the fake rate doubles to 0.46 %. These numbers show that high occupancy is already a cause of some tracking inefficiency with 80 μm pitch and would be worse with larger pitch of SCT module.

2.5 ATLAS physics and simulated results

The high energy and luminosity of the LHC offers a large range of physics opportunities that can potentially provide answers to the imperfections of the standard model outlined in Chapter 1. Additionally, the ability to probe the electroweak scale leads to a major focus on the Higgs boson ^[12]. Other physics goals of the detector include:

- The search for phenomena possibly related to the symmetry breaking, such as particles predicted by supersymmetry ^[13] or technicolour theories.
- The search for new gauge bosons and evidence for composite quarks and leptons.
- The investigation of CP violation ^[14] in B decays and the precision measurements of W and top-quark masses and triple gauge boson couplings.

As outlined, one of the main goals of the ATLAS experiment is to discover and study the Higgs particle (or Higgs boson). The Higgs particle is of critical importance in particle theories and is directly related to the concept of particle mass and therefore to all masses. What is the Higgs particle? Why do the fundamental particles have mass, and why are their masses different? Most of us are familiar with electric, magnetic, and gravitational fields. A person in the Earth's gravitational field feels a force. Electromagnetic waves (such as radio waves) travel through space in the same way that ripples in a pond travel through water. If the pond was described in quantum language, the water surface that carries the waves would be called a "field". The Standard Model proposes that there is another field not yet observed, a field that is almost indistinguishable from empty space. This has come to be known as the Higgs

field. All of space is potentially filled with this field, and that by interacting with this field, particles acquire their masses. Particles that interact strongly with the Higgs field are heavy, while those that interact weakly are light. The Higgs field has at least one new particle associated with it, the Higgs particle. The ATLAS detector at the LHC may be able to detect this particle if it exists.

When protons collide at the LHC, some events are "interesting" and may tell us about exciting new particles or forces, whereas many others are "ordinary" collisions (often called "background"). The ratio of their relative rates is about 1 interesting event for 10 million background events. One of the key needs is to separate the interesting events from the ordinary ones. The differentiation between these is based on the observed products of each collision - their identities, energies, directions of motion etc. For example, it may be possible to demonstrate that some observed configurations of outgoing collision products arise from the decay of a new particle. Such observations would then represent the discovery of this new particle. This information must be obtained and analyzed very rapidly. Only 10 to 100 of the billion collisions that occur each second must be flagged as potentially interesting and recorded for further study, while all the others are rejected.

The search for the source of symmetry breaking is a primary goal of the LHC programme. In the Standard Model, the as yet unobserved Higgs boson is responsible for particle masses. In addition, internal consistency arguments suggest that other new physics is super-symmetry. In many super-symmetry models, there is a large probability for production of neutral Higgs bosons in association with a $b\bar{b}$ -quark pair, with the neutral Higgs Boson subsequently decaying predominantly into another $b\bar{b}$ -pair. Figure 2-3 is a display of a simulated Higgs decay in the ATLAS SCT ID. Precision hits are shown and fitted tracks in red are shown just in the precision tracker. It is possible to identify the different layers of the ID from this simulation. The two innermost rings closest to the event depict the layers of the ultra high precision pixel detector. The next four larger rings represent the four layers of the SCT barrel and finally the outer section give an indication of the output of the TRT. These simulations represent the anticipated output of the SCT barrel section.

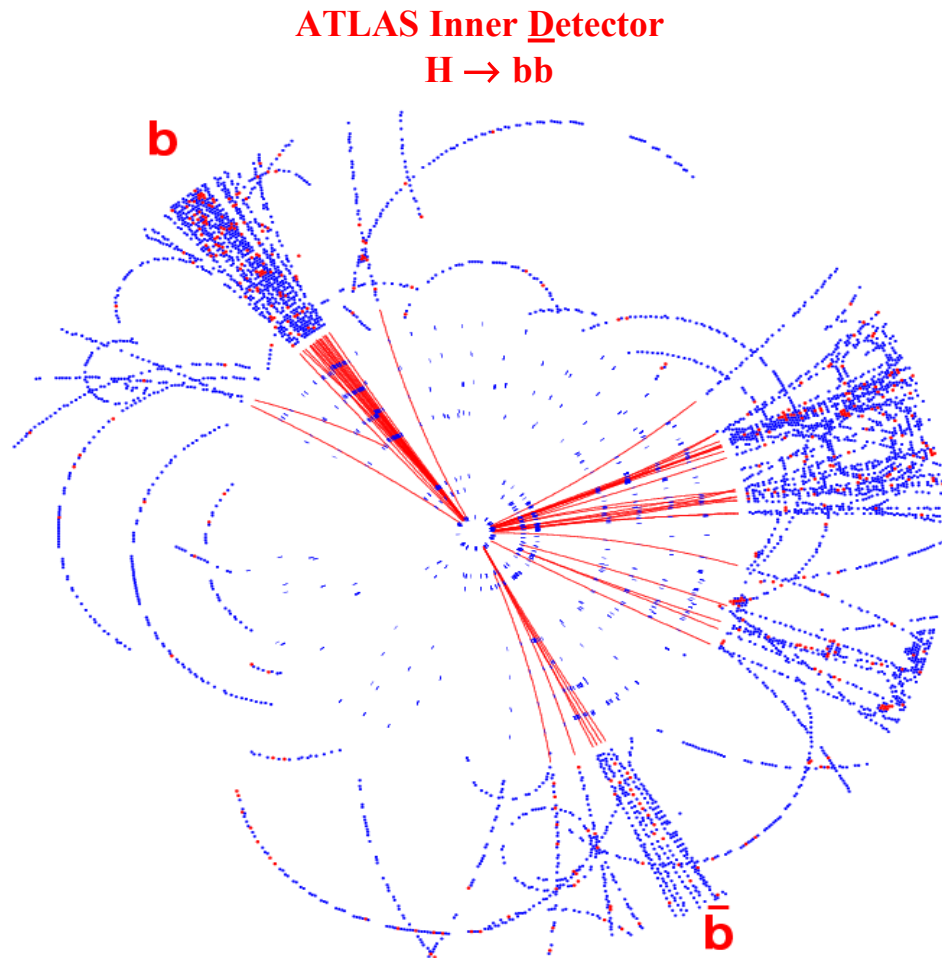


Figure 2-4 Simulated Higgs event with the neutral higgs boson subsequently decaying predominantly into another bb pair. Note how the tracks are accurately reconstructed by the detectors of the SCT

Another simulated collision event viewed from the side (beam is horizontal in centre) in Figure 2-4. The event is one in which a mini-*black hole* was produced and decayed immediately.

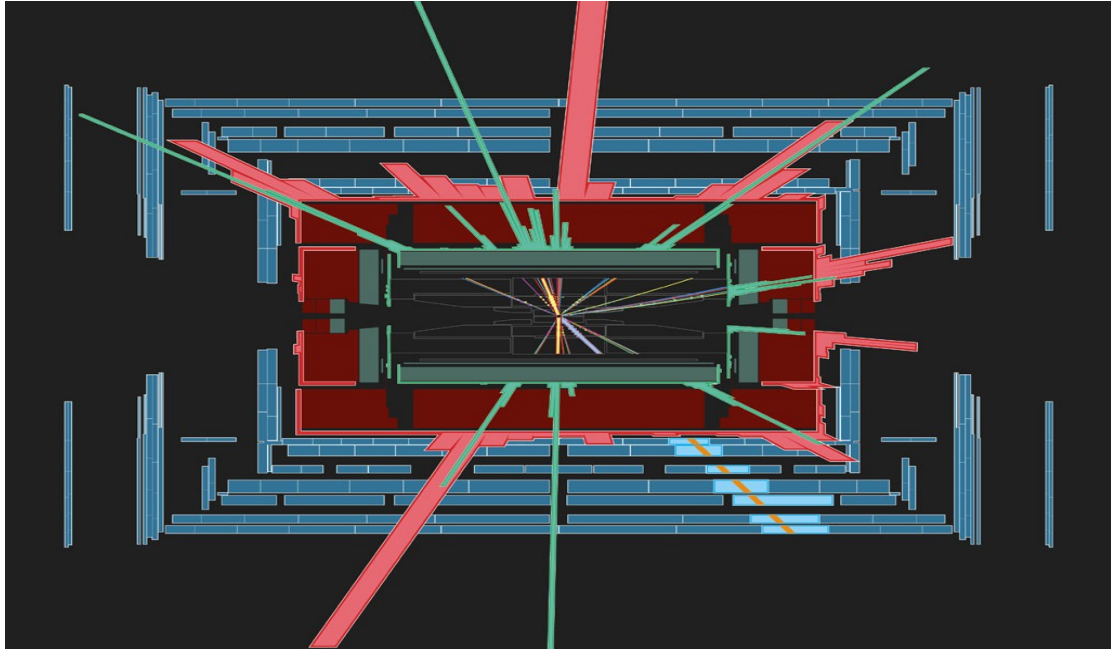


Figure 2-5 Simulated side-on view of event in the ATLAS detector

The black area in the centre with many particle tracks represents the ID (pixel detector, semiconductor tracker, and transition radiation tracker), which has been enormously magnified relative to the rest of the detector (in this view). The colours of the thin tracks have no significance. The thick yellow lines show the tracks of two electrons in this event. The green area is the electromagnetic calorimeter, while the red area is the hadronic calorimeter. The green and red histograms show the energy deposits by particles in the electromagnetic and hadronic calorimeters. A muon was added by hand to the event to show how it would look in the detector; it is a thick blue line in the ID and orange in the (blue) muon chambers surrounding calorimeters.

Comprehensive study of the SCT performance has also been undertaken ^[15]. As an example of the simulation results (in Figure 2-5) the reconstruction efficiency for isolated tracks detected in the SCT is presented as a function of the fraction of noisy strips in an SCT module. It is seen that even with 2% of noisy channels presented in the module the total efficiency is still higher 99% with a low fake rate of about 10^{-3} .

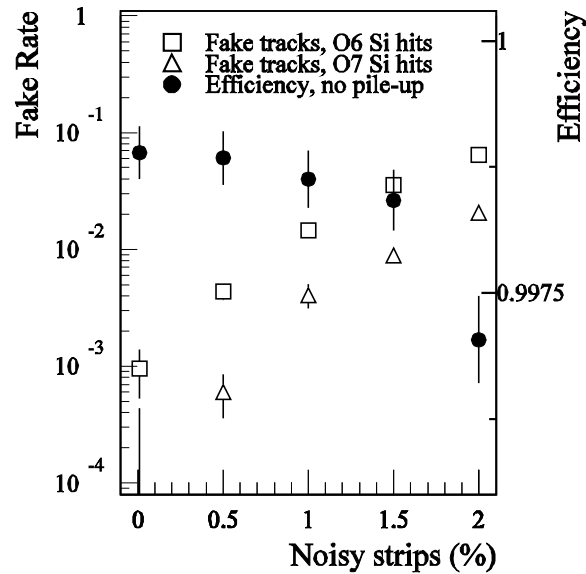


Figure 2-5 Reconstruction efficiency as a function of the fraction of noisy strips in an SCT module

2.6 End-cap module description

Each end-cap of the SCT is made up of end-cap modules arranged in rings. To form one layer of an end-cap SCT module, a trapezoid of active silicon semiconductor, representing two smaller trapezoids are bonded together. Each silicon detector is $6.36 \times 6.40 \text{ cm}^2$ with 768 readout strips each of $80 \mu\text{m}$ pitch. Each module consists of four detectors. Two such detector pairs are glued together back to back at a 40 mrad angle, separated by a heat transport plate and the electronics are mounted above the detectors on the electronics hybrid. The electronics board is 3 cm long, $320 \mu\text{m}$ thick, and the same width as the base of the sensor trapezoid closest to it. The exact size and shape of the sensor trapezoid depends upon what radial position it will occupy within the ID: for example a module destined for the outermost possible radial position is 12.4 cm high. A dead area is left all around each of the two smaller trapezoids, and each is divided into 768 strips. These strips are keystone-shaped, that is, their width is uniform in θ when they are placed in their final position. Because the width of the modules depends upon which wheel they will be mounted, the strip pitch does too. It varies between 80 and $120 \mu\text{m}$ at the centre of a module. To form an end-cap SCT module, two of these trapezoid-rectangle combinations are attached to a $300 \mu\text{m}$ thick beryllium substrate, with one being attached on one side so that its strips will be radial

and the other on the other side with a 40 mrad rotation (stereo angle). This stereo rotation has opposite signs for adjacent wheels. The module is mounted on a supporting aluminium block, which is also used to cool the modules.

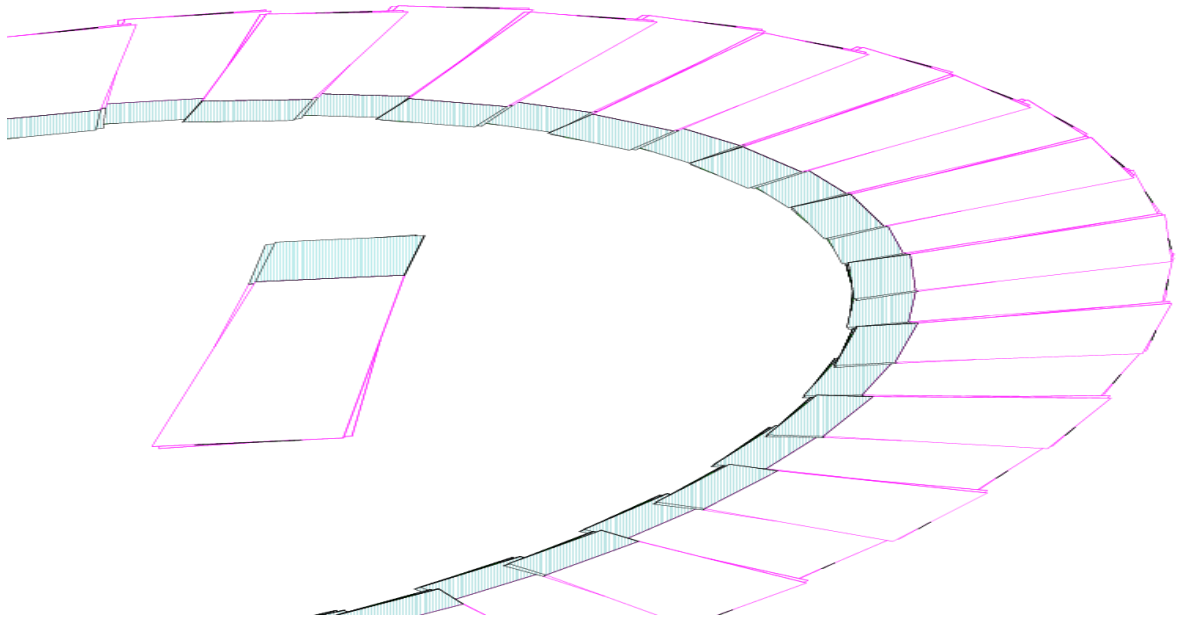


Figure 2-6 End-cap SCT outer module with part of a ring, the hybrid/electronic readout is shade

Figure 2-6 shows an end-cap SCT module and illustrates how these modules are arranged in rings. On the ring, modules that are adjacent in θ , are separated by 0.25 cm in Z to allow active over-lapping in the θ -direction: this overlap is on average about 1mm wide. There are four types of rings, each of which is intended to cover a different radial range. The rings are in turn arranged on nine wheels, which are numbered from 1 to 9 with increasing distance from the interaction point. As can be seen in Figure 2-7, rings that are adjacent in R are positioned on alternate sides of the wheel support disks to provide projective overlap of the active regions. The high spatial resolution of the silicon detectors will be required to identify and accurately measure the hundreds of charged particle tracks produced every 25 ns by the ultra-high energy head-on collisions of protons at the LHC. From this information, evidence for the Higgs and/or super-symmetric particles, etc, will be extracted from the Peta-Bytes of data to be recorded by the experiment.

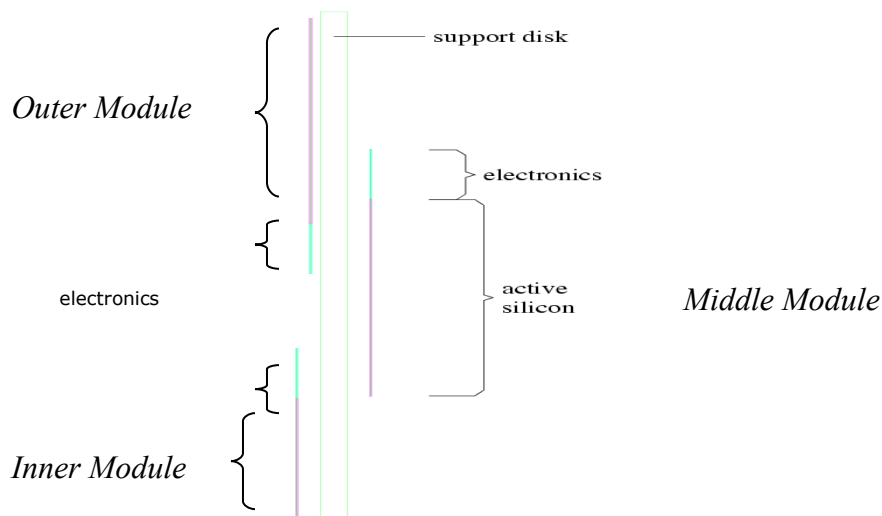


Figure 2-7 Cross-section of SCT wheel. For clarity, only the modules and support disks are shown. It shows how the middle module on the rear of the disk provides active silicon detector at every point on the disk.

2.7 Inner, middle and outer modules of the SCT End-cap

On the face of the ring facing the event (proton interaction point) there are the inner and outer modules, and on the rear of the disk is the middle module providing projective overlap in the active regions. During production Glasgow was required to produce outer and inner modules. Figure 2-8 shows the different types of modules, the modules are held in colour coded plastic holders to assist handling and clamping during bonding.



Figure 2-8 The three types of end-cap module: outer, middle and inner

The main difference between these types of module is in size. As the innermost module on the ring the inner module is required to cover the smallest area and hence the inner module has only one trapezoidal silicon detector.

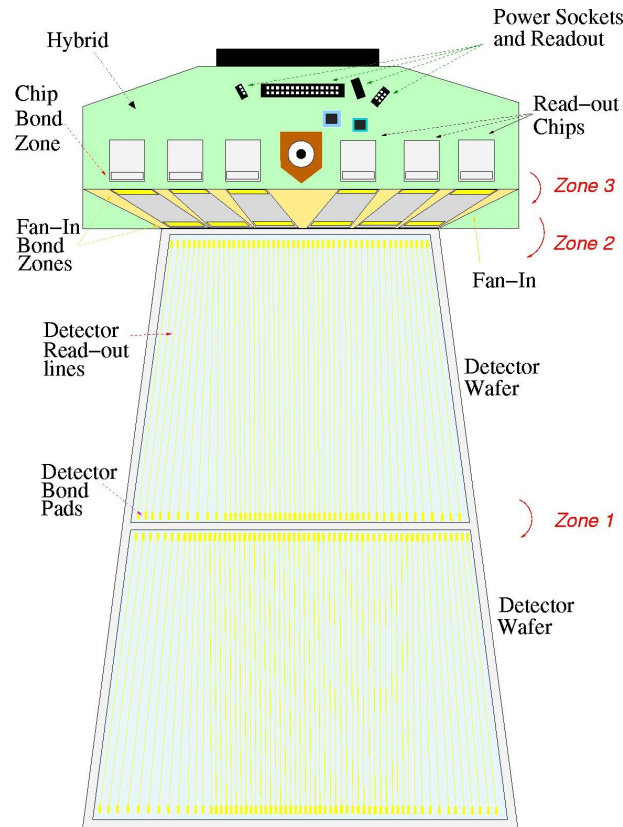


Figure 2-9 Graphical image of outer module. Bonding zones appear in red (see chapter 4 for bonding zone description)

In Figure 2-9 the hybrid (hybrid is a type of printed circuit board) is clearly shown at the top of the image, the term hybrid defines the interaction of different functions which the electronics board performs. Each module type has the same hybrid electronic readout. The aluminium micro-strips are also included on this image (depicted in yellow, along with the bond pads) and with a pitch of around 80 micron at some places on the detector are only visible under magnification. Both sides of the modules are virtually identical. The main differences being in the additional readout electronics required on the top side of the hybrid and the slight difference in stereo angle displacement. Channel numbers, detector area and chip configuration are the same.

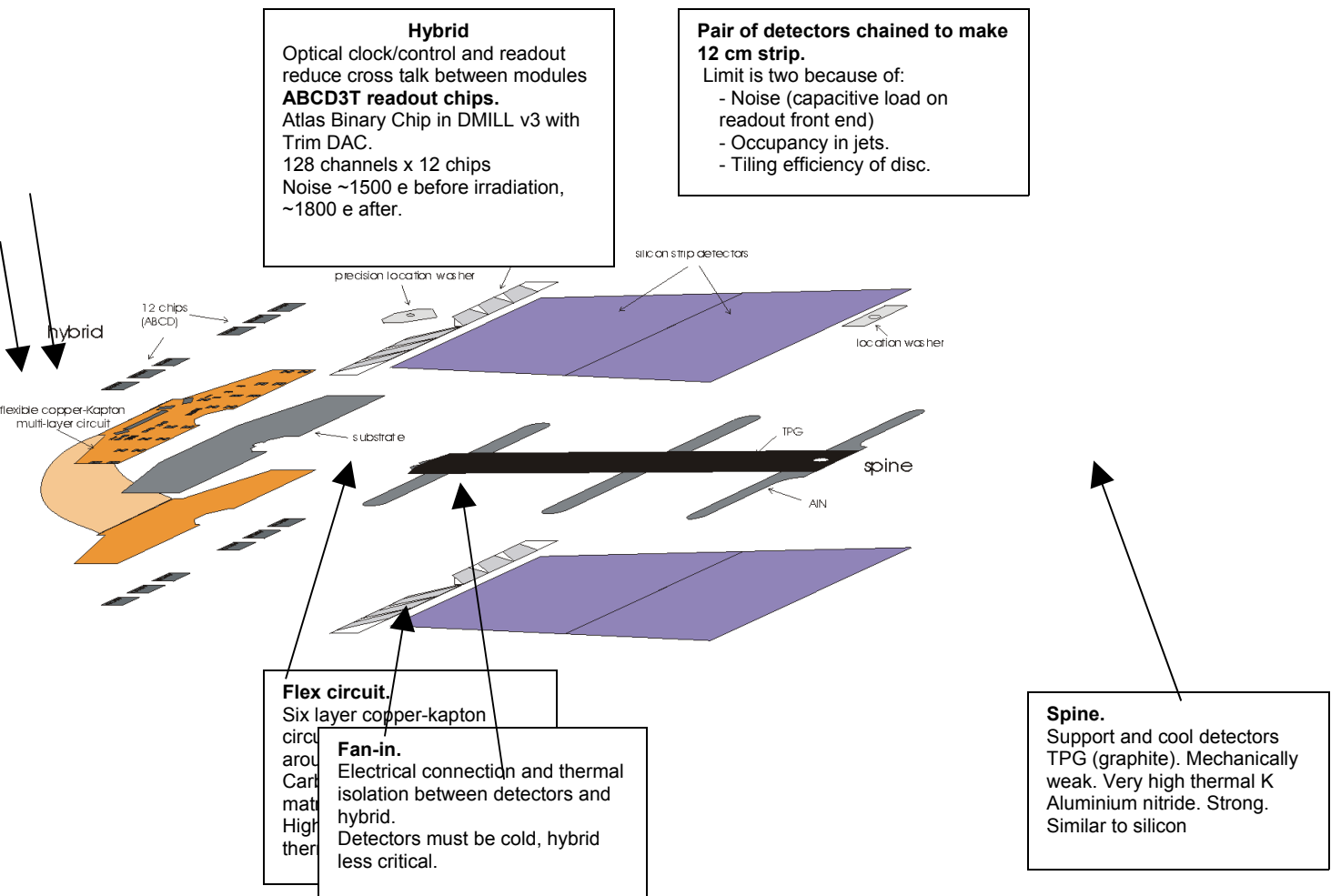


Figure 2-10 Breakdown of SCT outer module components

Figure 2-10 shows a breakdown of all parts of an ATLAS SCT outer module. Each part is briefly described in the caption from the 4 separate silicon detectors to the electronics and the locating washer. Positioning of the individual components of the module is critical. Each module is read out by 12 ABCD3T ASIC's ^[16] mounted on a hybrid circuit (Figure 2-11). Each chip provides binary readout of 128 detector channels. The amplified and shaped input signal is compared to a programmable threshold having two components: a single 8-bit DAC applied across the whole chip, and a channel-specific 4-bit DAC designed to compensate for channel-to-channel variations. In ATLAS, an optical stage ^[17] will be used to transmit data from the detector modules to the off detector electronics and to distribute Timing, Trigger and Control (TTC) data from the counting room to the front-end electronics.

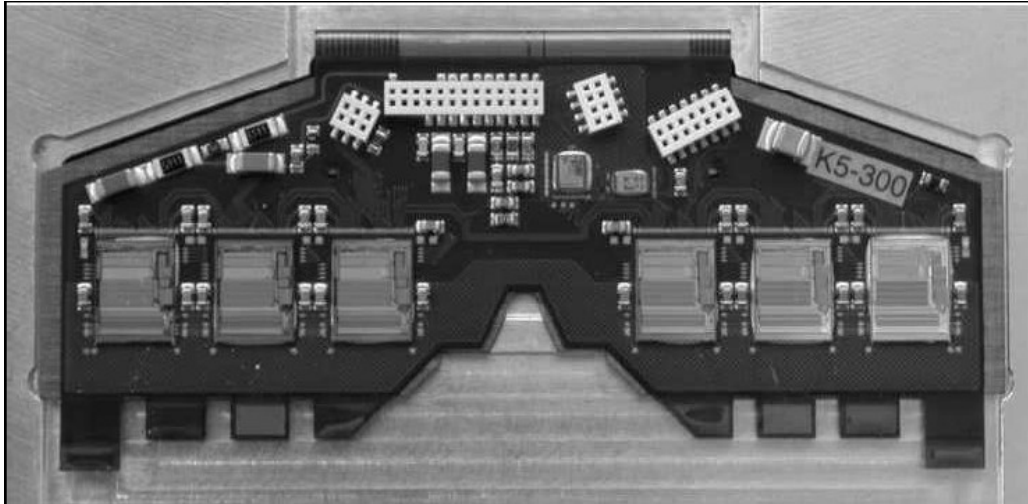


Figure 2-11 SCT module hybrid showing the six readout chips on the top side of the module

An extensive suite of hardware and software has been developed to facilitate hybrid and module testing during the production. The readout system for this testing setup is based on custom-designed VME boards and high-voltage boards developed specifically for SCT production testing. The electrical measurements performed as part of detector module quality assurance are drawn from a pool comprising around 13 component tests (for details, see Chapter 5). Each test has been designed to determine a certain set of parameters and to identify a number of specific defects or failure modes. Passing all the tests demonstrates the complete functionality of a hybrid or a module and provides measurements of all electrical parameters considered important to monitor module quality.

2.8 Summary

The ATLAS detector is concerned with the construction of a general experiment, which is designed to exploit the full discovery potential of the LHC at CERN. The ID systems of the detector can be broken down into four different sections; TRT, pixel, SCT barrel and the SCT end-caps. The SCT end-caps are two 9-layer disk sections used for the reconstruction of tracks and vertices. Forward module production in the UK is geared toward the production of modules for the end-cap disks and which consist of three flavours of silicon micro-strip module providing active silicon detector at every point on the disk. When the experiment is in use, the micro-strips on

the active detectors areas will flag when hit by charged particles. The eighteen disks on the two end-caps will allow charged particle vertices to be traced as they pass the length of the end-caps.

SCT end-caps provide information tracking particles helping decide the origin of the vertices. SCT software can then provide B jets vertices flavour tagging, particle momentum and other vital information. Results of simulations and test beam experiments have proved that the SCT will provide accurate data which is crucial for future ATLAS discoveries.

Chapter 3

3 SCT End-cap Module Production

3.1 Introduction

The Glasgow production site is one of many around the world. This chapter will describe the responsibilities of the Glasgow group and how they fit into the greater picture. Each production site has different expertise and equipment, and contributions are subsequently diverse. This chapter will give an overview of the production contribution of the Glasgow site and will take an initial look at the electrical and mechanical requirements for the SCT end-cap modules. It will also introduce the methods, internal and external, used to log important module data during production

3.2 ATLAS SCT Collaboration

In total there were fourteen institutes involved in the development and production of the SCT end-caps. Of these fourteen institutes, eleven were universities and three were large laboratories. The collaboration spent 10 years developing the module specification before concentrating on production for 2 years. The collaborating institutes were divided into three subgroups. These subgroup or clusters were grouped together by region or site specialisation.

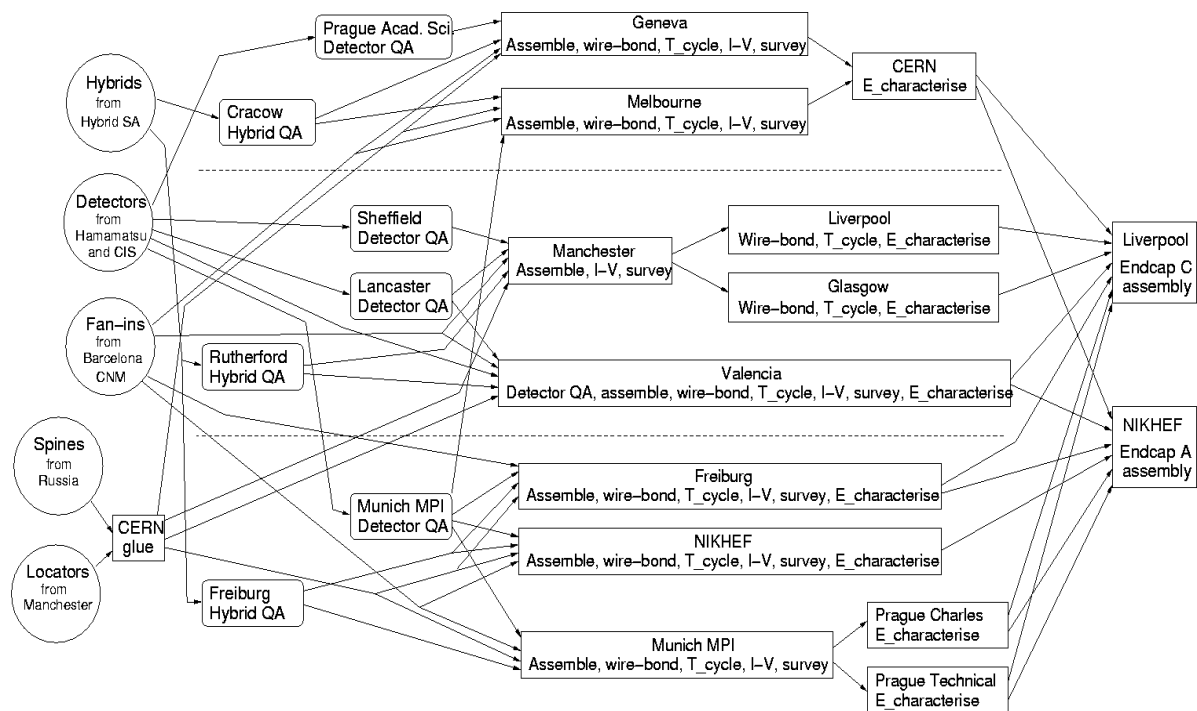


Figure 3-6 The ATLAS end-cap SCT section contributors ^[18]

3.3 The UK-V collaboration

The UK-V collaboration consists of 6 UK institutes – Liverpool, Glasgow, Manchester, Sheffield, Lancaster, Rutherford and Valencia. Other collaborations were Central Europe, consisting of the Freiburg, NIKHEF, Munich, CERN and Prague production sites, and the CS collaboration consisting of Geneva, Melbourne, Krakow and CERN groups. Within the UK-V collaboration SCT module production was split into three areas. Detector quality assurance (QA) was the responsibility of Sheffield, Lancaster and Rutherford. Manchester was responsible for the module assembly. Module bonding, testing and characterisation were carried out at Liverpool and Glasgow. Finally all modules are sent to Liverpool to be mounted on end-cap C. The modules of end-cap A are assembled, bonded and tested within the other collaborations. The ATLAS SCT end-cap module production at the University of Glasgow was the largest user of the Detector Development Laboratory in the Particle

Physics Experimental (PPE) group during the period between July 2002 and June 2005. The end-cap, which is being assembled at Liverpool, represents roughly half the UK's deliverables to the tracker.

Glasgow is part of the UK north cluster. In conjunction with Manchester and Liverpool we are responsible for the manufacture, wire bonding and testing of around 634 modules. This number breaks down into 192 Inner, 192 Middle and 250 Outer modules for the SCT end-cap. Manchester has exclusive responsibility for the module manufacture, leaving Glasgow and Liverpool to bond and test the modules. It was planned that Glasgow and Liverpool will share the 634 modules equally. This would result in the total number of readout channels bonded at Glasgow exceeding five hundred thousand. As each readout channel is bonded in at least 3 areas, the total number of bonds made on ATLAS modules in Glasgow would exceed 1 million. Once the modules have been assembled in Manchester they arrive in the production sites where they undergo rigorous visual inspection in preparation for wire bonding. At all times the modules are kept in a clean, static free environment. After wire bonding the module undergoes IV characterisation and thermal cycling tests. After the IV test, the modules are tested again for confirmation of defects before undergoing further characterisation and Long Term Testing (LTT). The modules are then visually inspected one last time before shipment.

3.4 Electrical/Mechanical characteristics of SCT end-cap modules

Throughout production the modules are tested at each to ensure they conform to the strict mechanical and electrical characteristics required. Each module has 12 ABCD3T readout chips each reading out 128 channels, this results in a total of 1536 channels. The main electrical guidelines during production were:

- **Dead channels.** Each module has 1536 channels. It was decided that for a modules to pass the maximum number of dead channels permitted was 15, less than 1% (15/1536) ^[19]

- **Noise occupancy.** Each module must achieve noise occupancy of less than 5×10^{-4} at 1 fC threshold.
- **Leakage Current.** The leakage current in the detector has to be less than $20 \mu\text{A}$ per detector at 350 V.
- **Thermal characteristics.** Must operate for 24 hours cold. (thermistor on hottest part of hybrid at $\sim 10^\circ \text{C}$)^[20]
- **Critical tolerances,** Thirteen parameters define the positions of detectors and location holes in the XY plane (for details see Figure 3-2). These had to remain within the following limits:

detector angles	-	a1-a4, stereo: ± 0.13 mrad
detector front-back alignment	-	midyf ± 5 microns
location holes	-	mhx,mhy,msy ± 20 microns

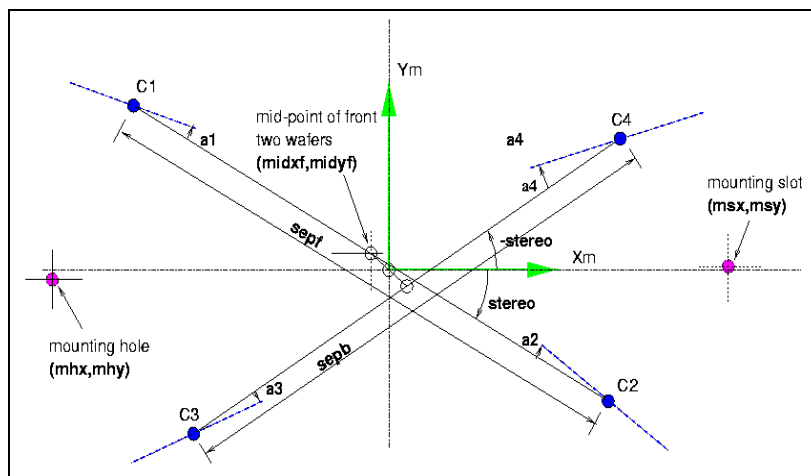


Figure 3-7 Thirteen parameters specify the geometry of an outer or middle module in the XY plane. Blue spots represent the sensor centres and blue lines the detector orientations. These points are checked after bonding and testing, to ensure each module remains within specification. Several modules were rejected for failing these tests (see section 6.9)

In addition, the Z level of detector surface relative to mounting block surface is measured on a grid of 5×5 points per detector (see Figure 3-3). All points must be within (875 ± 115) microns (front) or (-375 ± 115) microns (back).

These XY & Z tolerances define modules that are within design specification. In practice we were able to increase some tolerances by 50% to define a "pass" category, while keeping within the physics specifications.

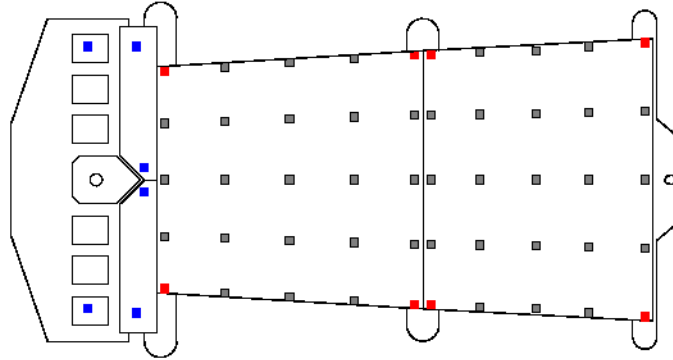


Figure 3-8 Z survey points on an outer module

- **Other specifications**

Another requirement to take into account during all stages of production is the requirement for the module to survive 10 thermal cycles from -30 to $+35$ C and remain in tolerance.

3.5 Production Overview

All the institutes involved in the module construction have clean room areas for the assembly activities which comply with BS class 10000 for clean-room. This standard indicates the dust particle count within a certain cubic area. Clean rooms incorporate temperature and humidity control as well as anti-static floor and mats. Dust, metal debris or oil vapour deposition can be a problem for electrical behaviour and also for wire bond-ability. Static discharge can damage the detectors and chips. Operators are required to take rigorous precautions to ensure to protect the modules, all work is carried out wearing ESD clean-room shoes with grounding straps and working with mask, cap and gloves. During the various assembly steps the modules move from one working place to a test bench or storage place for queuing into the pipe line. The internal organization of this was left to the individual institutes which put the basic

information for every module onto a traveller document that was signed off at each stage. The process in Glasgow was divided into 7 different stages: Visual Inspection, wire-bonding, testing, assessment, long term testing, thermal cycling and dispatch. Important information like identity of components and details of wire bonding and tests were uploaded into the SCT production database.

- **Visual inspection.** Each module is thoroughly inspected on reception from Manchester. The inspection results are compared with the results from visual inspection at Manchester. Information logged.
- **Wire-bonding.** The modules are mounted and clamped onto the wire bonding system. When wire bonding is completed a further visual inspection is carried out. Faulty bonds are reworked. Number of reworked channels and other relevant information is logged.
- **Electrical tests.** Modules are removed from the bonding system and placed in a cooling box for testing. Test information provided by the DAQ is logged.
- **Assessment.** Results from electrical tests will determine the next move. If the module fails, it will be relocated at visual inspection or wire bonding for rework.
- **Long term testing.** If electrical tests are passed the module will undergo a prolonged period of tests to ensure long term reliability.
- **Thermal cycling.** Thermal cycling is needed to check and ensure stability of the module metrology. It requires 10 cycles of temperature from +35 to -30°C. Each cycle takes a minimum of two hours: half an hour to stay at a certain temperature level and half an hour to change it. Humidity and temperature profiles are logged.
- **Dispatch.** A module that passes all the tests is then packed and posted to Liverpool.

3.6 Production statistics

Each module and its components were tracked through their history by means of the SCT production database. This meant that details of tests, component trees, movements between sites and overall status of modules were available to the whole collaboration, and fostered a culture of transparency. The database also allowed easy

monitoring of site production statistics and component supplies, and was a crucial tool in the project management. Additionally, the full raw test data is archived at each test site, together with traveller documents, check sheets and high resolution optical scans of assembled modules.

3.6.1 SCT Production Database

The complexity of the SCT project prompted development of a relational database (DB) ^[21] to manage it. The DB and most of the features needed were already working when module production started. It has proved a powerful tool to monitor the location, the assembly and QA progress of the module production. For storing the data, the utilities that are available to the user are the web interface and a java client application for mass data upload. The upper access scheme is presented in Figure 3-4.

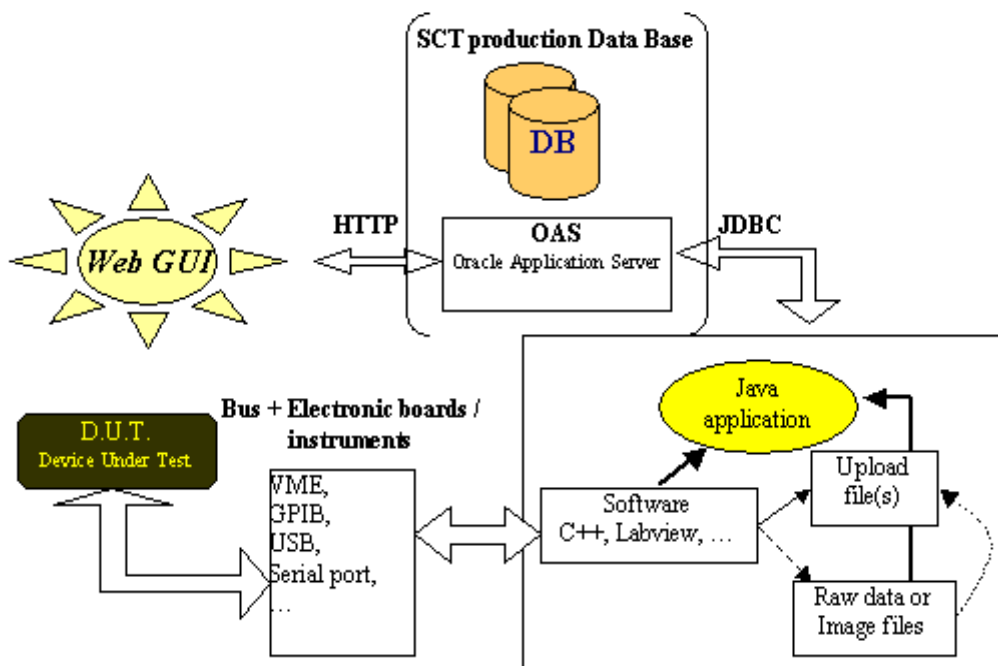


Figure 3-9 User access scheme for recording the data into the SCT production database

Two separate Oracle databases (kernel 9i) with the latest application server were set up on a server at University of Geneva ^[22]. One database is used only for developer validation purposes. New features are fully proved here before they are exported to the production database. This allows a safe evolutionary system for extension of the data structure or implementation of new features.

The Oracle Designer 6i rapid application development tool was used for the data structure and web applications ^[23]. The tool facilitated development of the entity relationship model and helped ensure the integrity of the overall structure. The tables with primary, foreign keys and attributes are then automatically generated as well as the code for the web browser Graphical User Interface (GUI).

Additional client applications were developed:

Java applications for uploading mass data. Text files generated by, e.g., module test applications can be used to upload large amounts of test, item, assembly or shipment data.

GUI query and report: All SCT users are allowed to view any tables of the SCT DB. Several tools have then been implemented using java or other object oriented languages.

Special users' java applications: several users have written java applications for extracting statistics or creating summary web pages from SCT DB data.

3.6.1.1 DB Structure

The database is largely self describing in that metadata and data are both present in the entity relationship diagram. The main entities are items, assemblies, tests, and shipments which cover most of the DB use. The data structure has been defined with 3 classes of tables:

- class 1: Definitions or metadata tables for the description of items, tests, and assemblies. These are only modified by the administrator.
- class 2: User data tables that hold the actual data. Each record has a column for its ownership, and only the owner of the record can update or delete it.
- class 3: A history structure for assemblies. When a deletion is made as for a disassembly the data are stored automatically in a log table by a trigger. The data in the disassembly history log table are readable by any authorized users.

The DB is protected by integrity rules - the laws that decide which operations on the data and the structures are allowed. Some additional rules have been created to protect and share the status, location and ownership of items and assembly. Special events are triggered in the following action cases:

- Shipment validation: Set the shipped items with ITEMS.OWNER = 'sent', ITEMS.LOCATION = 'unknown' and SHIP_ITEMS.OWNER = (Destination Location)
- Shipment reception: Set the shipped items with ITEMS.OWNER = (Destination OWNER), ITEMS.LOCATION = (Destination Location).
- Assembly: Set ITEMS.ASSEMBLED = 'YES'
- Disassembly: Set ITEMS.ASSEMBLED = 'NO', ITEMS.LOCATION = (Location of the Assembly), ITEMS.OWNER = (OWNER of the assembly), fill ASSEMBLY_HISTORY

3.6.1.2 Items

The item entity is at the heart of the SCT production DB and only after an item is registered will the user be allowed to enter assembly, shipment, event and test data.

All SCT items recorded into the DB have a 14 digit serial number (SerNo) which follow the ATLAS part number rule [46] , with the following structure:

2	0	2	2	0	I	I	x	x	x	x	x	x	x
---	---	---	---	---	---	---	---	---	---	---	---	---	---

where:

- 2022: means that it is SCT project of the ID of ATLAS.
- 0II: 2 digits are reserved for the SCT institute number. 099 and above are reserved for web interface sequential number.
- xxxxxxx: 7 digits that are set by the institute when items are uploaded using the java application.

Labels with bar-coded serial numbers can be printed together with the item type and the manufacturer serial number. The items are always recorded with a minimum number of mandatory fields plus some optional fields if desired, as listed below:

- SER_NO - NUMBER(14,0) – MANDATORY : Serial number set by the web application or by the user if java is used as the upload tool.
- TRASHED - DEFAULT 'NO' – MANDATORY : Trash status, set to 'NO' by default, and updatable
- SUBSYST - DEFAULT 'S' – MANDATORY : Inner detector subsystem set to SCT by default.
- ENTRY_DATE - DATE – MANDATORY : Entry date set by the user.
- ASSEMBLED – MANDATORY : 'YES' If the item is already assembled. This is set automatically, triggered by insertion of an assembly record.
- PASSED - MANDATORY : Overall test status of the item.
- LAST_MOD - DATE DEFAULT sysdate – MANDATORY : Last modification timestamp of the record, set automatically by the system.
- OWNER - DEFAULT user – MANDATORY : Owner set by the API to the name of the current user's institute.
- INITLS – MANDATORY : Initials of the user who is making the registration.
- LOCN_NAME – MANDATORY : Current location name
- MFR – MANDATORY : Manufacturer of the item, selected by the user from the manufacturer table.
- MFR_SER_NO - Manufacturer serial number, set optionally by the user.
- RECEIPT_DATE – DATE : Reception date of that item, set optionally by the user.

In addition to the attributes above the user can record a comment, text or picture or/and an event that is linked to the item. The event list is non exhaustive and records information such as irradiation, annealing, thermal cycling, chip dicing.

3.7 Module Tracker and E-Log

During production the progress of each module was charted using a simple, manually incremented java program called the Module Tracker developed by W. Bell. A new module from Manchester would be entered into the program using an infra red scanner to scan the 22-bit barcode on each module. The module would pass through each stage of production, entry, visual inspection, wire-bonding, electrical tests, thermal cycling, LTT and dispatch. A module that encountered a problem at any of these stages could then be relocated to the appropriate stage. For example, if a module was found to flag more than 15 defects at electrical test, it would be relocated to wire-bonding to await rework. The Tracker also enabled the group to keep a track of production numbers and rates. At the height of production the group achieved a throughput of 12 modules per week. The other internal production information recorder used was the E-Log. The E-Log was used to record any information useful to production and often replicated the information entered into the official database. The E-log enabled the group to fine tune the process while keeping a track of all wire-bonding information and test results.

3.8 Other Internal Production Software

Other internal software was developed by W.Bell to assist with the proper logging of production information.

BondingUploadGUI: a program to speed entry of bonding defect data.

BondingDataUploader: a program to upload bonding data. Data are entered in a simple manner and are directly uploaded to the database via ATLAS JAVA applications.

VisualUploadGUI: a program to speed entry of visual inspection data and edit digital photos.

3.9 Summary

Glasgow is part of the UK-V north collaboration, which has responsibility for the manufacture, bonding and testing of 634 modules which will form end-cap C. Each production site has responsibility for the development and implementation of their individual production process. Production at Glasgow was broken down to visual inspection, wire-bonding, electrical testing, assessment, LTT, thermal cycling and dispatch. Information relating to the process was logged both on the official ATLAS database and the groups own internal records and web pages.

Chapter 4

4 Wire-bonding Methods

4.1 Introduction

The different stages of the process have now been identified. The next two chapters look in depth at the two most important stages, wire-bonding and testing. The primary technology utilised in our production process is wire-bonding. This chapter will look at the history and development of wire-bonding techniques while introducing the Hesse and Knipps (H&K) 710 wire-bonding system used by the group. The process of wire-bonding is controlled and refined using the system parameters, which are used to describe any aspect of the system process which can be adjusted. Good parameters are essential for wire-bonding and extensive effort was made to ensure that the parameters were well adjusted prior to production. Some of this effort is discussed in the section 4.7. Additionally, reference is made to improvements made in bonding quality at the production stage. This effort and its results are discussed further in chapter 6.

4.2 Basics of wire-bonding

Wire-bonding is an electrical inter-connect technology developed by the micro-electronics industry and used today extensively in (solid state) detector construction. It allows inter-connection of electronic chips, printed circuit boards, pitch adapters and solid-state sensors (usually silicon). Ultrasonic (US) wedge bonding has been used in

micro-electronics industry since about 1960, mainly for device production. In High Energy Physics (HEP) applications, US wedge bonding is the predominant method, as it does not require any substrate heating and therefore is very versatile. US wedge bonding is mainly used to bond Al wires (diameter in the range 17 - 75 μm and even over 0.5 mm in special cases) to Al or Au bond pads. The basic mechanism, common to most bonding methods is the transfer of ultrasonic energy via the resonating bond tool to the interface between the bond wire and the bond pad in order to form a metallurgical bond, a kind of micro weld. The ultrasonic power creates a localised heat increase sufficient to “weld” the bond foot to the substrate surface. As the wire, in wedge/wedge bonding (a wire bond in which both source and destination bonds are made by the wedge, is known as wedge/wedge bonding) is fed beneath the flat bonding face of the wedge tool, the second bond must be placed in-line with the first to ensure correct location beneath the tool. This effectively slows down the rate of bonding, as the operator (in the case of a manual machine) must orientate the substrate to maintain the bonding direction. Figure 4-1 shows a schematic representation of the geometry of a wedge/wedge bond.

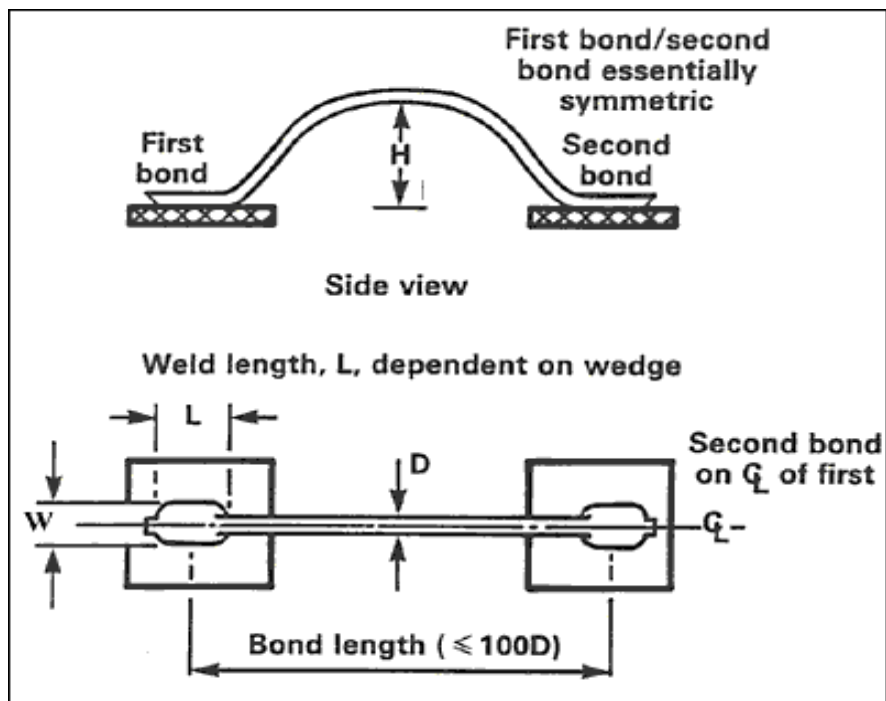


Figure 4-10 Wedge bond geometry ^[24]

A good wedge bond can be determined (in most cases) by the degree of deformation of the wire. The width of the flattened area should be approximately 1.7 times the diameter of the wire, e.g. for 25 μm diameter wire, the width should be 42 μm . Figure 4-1 represents a perfectly symmetrical wire bond. The wire bonding system used during production was the Hesse and Knipps 710 bondjet. This system is a high speed thin wire automatic ultrasonic wire bonder. It includes wire deformation control and multiphase bonding capability (see section 4.4.2). With the H& K 710 all aspects of this wire bond are variable.

4.3 The physical stages of bonding

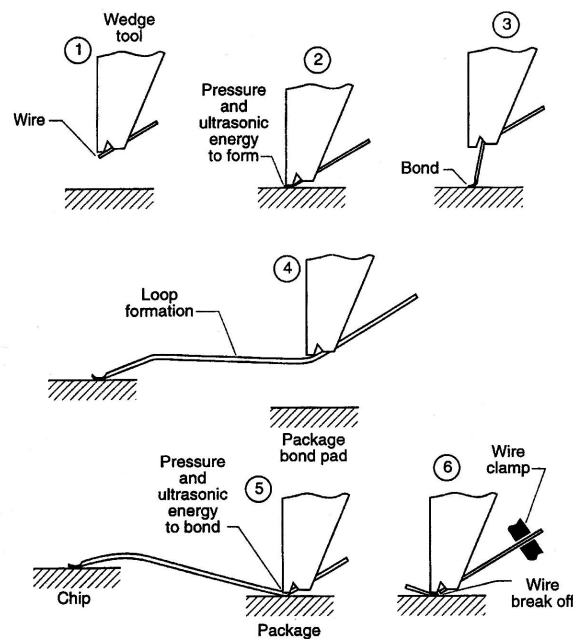


Figure 4-11 Physical stages of a single wire bond

A simplified procedure for making an ultrasonic wire bond between a chip-bond pad and the package with a typical wedge-type tool, is shown in Figure 4-2.

(1) Wire is located between the bonding surface of the tool and the bond. When used on an auto wire-bonding this height is specified as safety height.

(2) The tool is lowered and presses the wire against the bonding surface with a predetermined force. Ultrasonic energy is applied for a preset time to make the first bond (Source bond, see Figure 4-3).

(3) The tool is raised while the wire is paid out from the spool of wire (not shown).

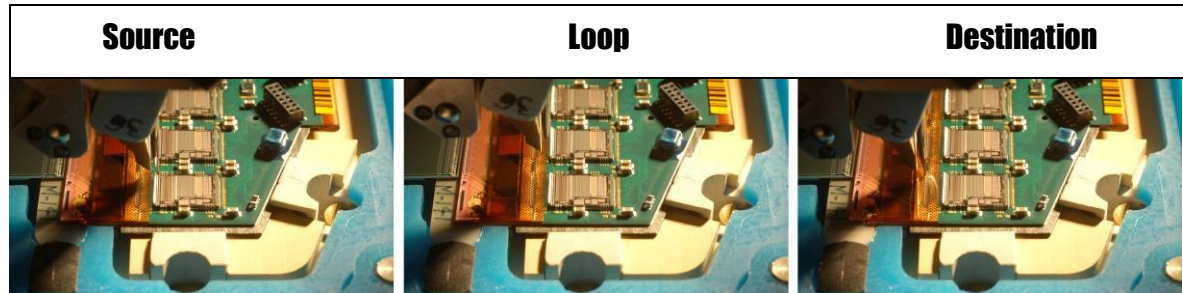


Figure 4-12 The three stages of bonding: source, loop and destination

(4) The bond head then moves the transducer and tool over the surface to the second bond (Destination, see Figure 4-3). The loop is formed and the tool lowers to the second safety height position.

(5) The tool is lowered to the bonding pad and the second bond is made.

(6) After the second bond has been made, a wire clamp (behind the tool) closes and pulls back on the wire to break it at the heel of the bond. The tool is raised, and the end of the wire is fed out underneath the tool until the end is located somewhat beyond the front of the tool (the tail length). The bonder is then ready to repeat the cycle. The most important stages of the bond are the source and destination stages. This refers to the first and second bond point respectively and will be referred to throughout chapter 6.

4.4 Parameters

As mentioned in section 4.2, all aspects of a wire bond are variable and in most instances programmable or at least adjustable. Parameters form one third of the requirements for successful wire bonding as will be described in section 4.5. With the

H&K 710 system parameters can be broken down into two sections, mechanically adjustable and programmable [25].

The mechanically adjustable parameters can be found mostly on or around the H&K bond-head (see Figure 4-4). The bond-head is mounted on the theta motion motor and it comprises the transducer, the wedge, the camera, the wire-clamp and all other components related to the bonding process (with the exception of the wire spool holder and feed which is mounted above the bond-head). The piezo bond-head can be rotated 400°.

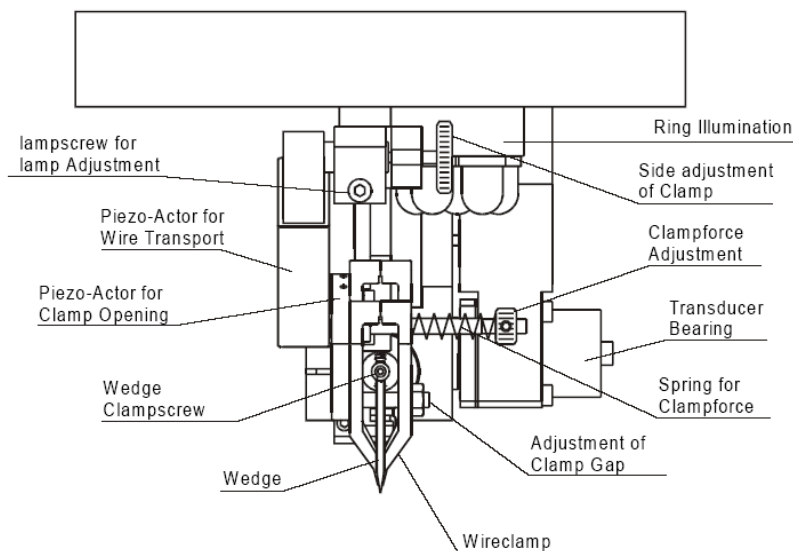


Figure 4-13 H&K 710 Bond-head

4.4.1 Mechanical Parameters

Opening of the wire clamps. This parameter can be adjusted to suit different wire widths by adjusting the screw that defines clamp gap (see Figure 4-4).

Wire clamp position. This position can be changed by adjustment of the side clamp adjuster. This is an important parameter and helps keep wire bond loops straight and parallel.

Clamp-force can be changed by increasing the pressure on the clamp exerted by the clamp spring to the right of the wedge. This is usually set with a gram gauge and should not exceed a certain factory set value. Incorrect setting of this parameter was to prove the cause of some poor bond reliability during the qualification and early production periods.

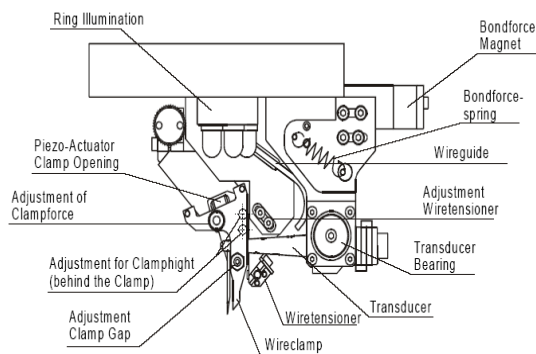
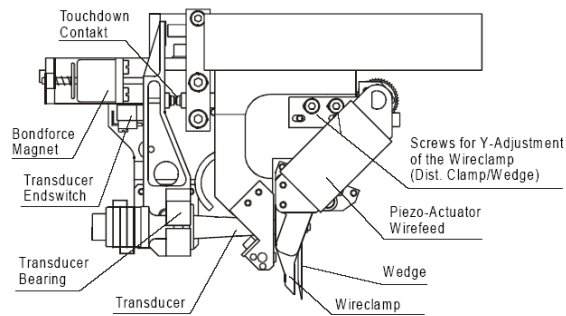


Figure 4-14 Left and right views of bond-head showing detailed layout of the bond-head components

Adjustment of Wire-clamp position (Horizontal). By default the distance between wedge and clamp is very small to prevent the wire “kinking”. This gap can be adjusted using the screws for “Y-Adjustment” (left side of bond-head, see figure 4-5)

Adjustment of Wire-clamp position (Vertical). As production continued it was found that the clamps started to wear. This problem could be counter-acted by adjusting the height of the clamps (right side of bond-head). This ensured an unworn section of the clamps were in contact with the wire.

Bond-force could be increased by replacing the bond-force spring for one of a higher value. 20 g spring was regularly used, decreased to 10 g for inner modules. This spring sets the minimum bonding power.

Wedge. The “wedge” or tool as it is otherwise referred to, is a crucial part of the bonding system. These tungsten carbide parts are clamped into the bond-head transducer. The base or point of the wedge has a 50 micron hole through which the wire is fed. The wedge is carefully positioned and clamped to a torque of 12 cNm, and the impedance is then matched. All these factors have to be closely monitored. Regular wedge cleaning and replacement was required to ensure good continuously bond quality.

4.4.2 Programmable parameters

All non-mechanically adjustable parameters can be viewed and refined in the parameters sub-section of the H&K PC based operating system (see Figure 4-6).

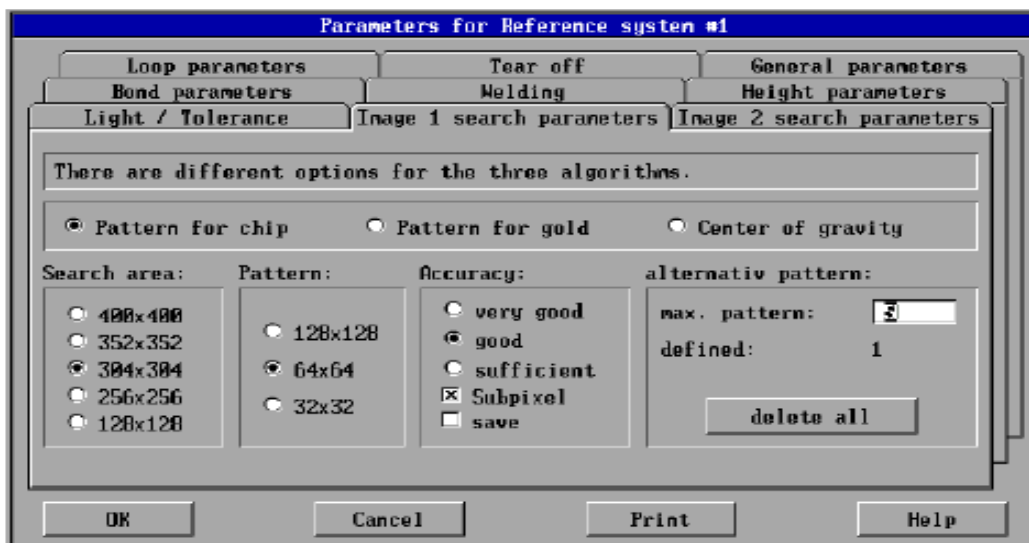


Figure 4-15 The parameter window, showing the range of adjustable parameters for one of the process windows

Within the parameters window there are three parameter sections which affect bond quality. These sections are welding, loop and bond. Welding parameters are deformation, bond-time, US power, bond-force and phase. Loop parameters are loop

height, loop length and loop shape. Bond parameters are accuracy, offshoot, safety height, safety radius, lower tolerance and touchdown velocity.

Deformation. For the best possible control of the bond process a proximity sensor measures the deformation of the bond wire in real-time. With this information it is possible to define the bond result (bond quality) and not just a defined bond time as a process parameter. Figure 4-7 shows the wire deformation over bond-time and a closely bundled collection of deformation curves. This diagram shows good bonding quality with little variance. These bonds deformed uniformly at the same speed over the same length of time.

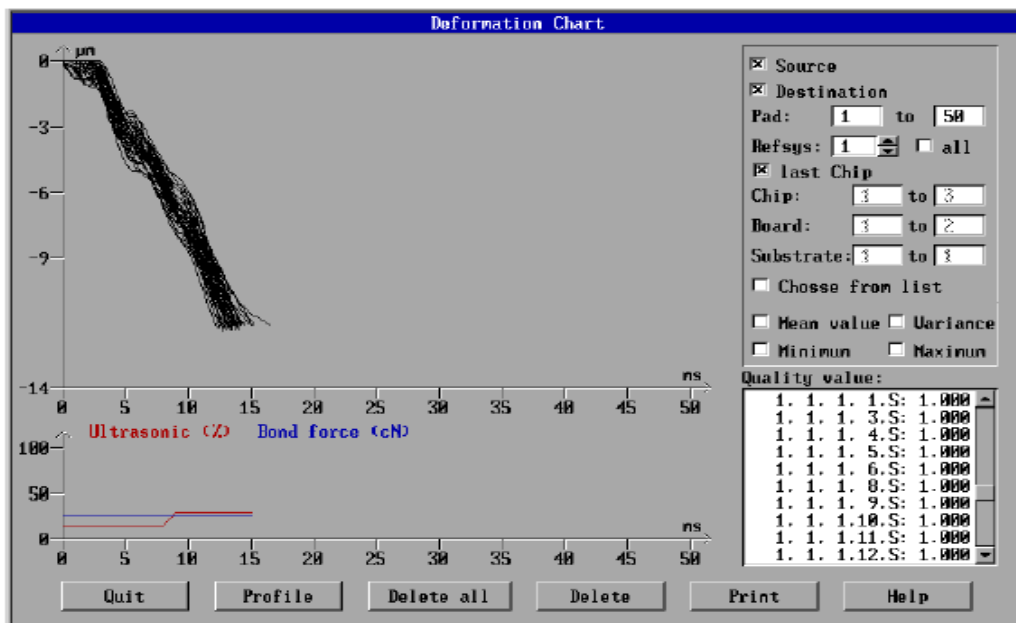


Figure 4-16 Deformation chart

Deformation is set by the user to a value of 1- 100%. This represents the percentage deformation of the wire with 1 being virtually none and 100 being almost completely flat. This parameter proved to be the most important and frequently adjusted of the programmable parameters. The deformation chart was constantly monitored during qualification and production stages.

Bond-time. As the wedge touches the surface of the module it waits for the deformation percentage to be reached. If that percentage is not reached then the wedge

will stay on the surface until the bond-time is reached. The bond-time is another parameter that allows the user to define how and when the bond is terminated. During the course of production however, deformation was used to define bonding termination.

Bond-force/US power. The process by which a bond is welded to the surface of the module is controlled by adjusting the bond-force and ultra-sonic power. The bond force is literally the force applied by the bond head and can be thought of as the weight of the wedge. The ultras-sonic power is produced by the US generator and the transducer which provide a sonic pulse which vibrates the wedge. These parameters are closely inter-related and an increase in one often required a decrease in the other. These are important parameters, which help control bond width and quality.

Phase. Each bonding step could be broken down into three phases, with each phase deploying certain percentages of power. As the bond wedge makes contact with a bonding surface the ultrasonic power is applied. If the US power is applied in phases it creates a short ramp up/down to full power. This parameter helps the bonder to accommodate poorly supported sections of the module, for example, by deploying 30% of US power at Phase 1 it is possible to take into account any module movement before deploying full power at Phase 2. Three phase bonding is possible but generally the bonder was set to two phase bonding.

4.4.3 Loop Parameters

Figure 4-8 illustrates the different stages to each bond. Each stage can be identified by a number, which corresponds to Table 1, where a detailed breakdown of the different parameters is presented.

Bonding Sequence

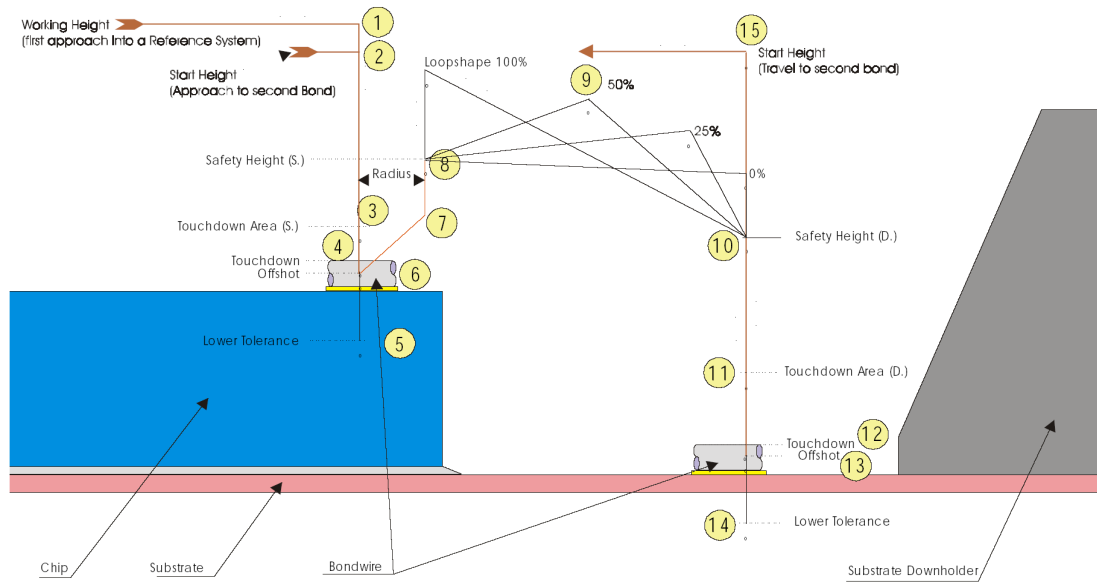


Figure 4-17 Detailed breakdown of loop height parameters

No.	Name	Menu Location	Explanation	Requirement	Default
1	Working Height	Reference-system/ parameter/ general parameters	Travel height of the bondhead when approaching the first product or before changing to the following reference system. This parameter has to be set in the general parameters and has no relation to the touchdown height of the product.	The value of this parameter has to be chosen that big, that the moving bondhead can not collide with the product downholder or other obstructions.	1.0 mm
2	Start Height	Reference-system / parameters / loop parameters	After the first completed loop in a reference system, the start height is the travel height to the next loop in the same reference system.	The value of this parameter has to be chosen that big, that wire loops or obstructions in the actual reference can not be touched by the bond tool.	1000 µm
3	Touch-down Area	reference system / parameters / height parameters	Starting at touchdown area, the bondhead. Travels in the slower touchdown speed. From this height on the bonder is expecting the touch down. The touchdown can happen between touchdown area and lower tolerance. The calculation of the process points „touchdown area“, „Offshoot“ and „lower tolerance“ is based on the height of the touchdown. (Best parameter for speed increase)	Theoretically the value of this parameter can be 0, if all touchdown points are very even in height. (typical setting for a CICOREL board is 30mm)	100 µm

4	Touch-down	reference system / parameters/height parameters	Measured height during height calibration. (no direct input possible) By adaptive height adjustment this data will be recalculated after any touchdown for the following wire.		N/A
5	Lower Tolerance	reference system / parameters / height parameters	Because of different product tolerances the touchdown point can be lower than expected. The lower tolerance sets a maximum deviation.	No influence in speed.	500 µm
6	Offshoot	reference system / parameters / bond parameters	The offshoot (overtravel) shall be about the way of the later wire deformation. After the touchdown the bondhead overtravels this programmed distance and opens the touchdown sensor without bonding into the wire. During the later bonding and deformation of the wire, the sensor stay's open.	At least as big as the defined wire deformation	About 0.5 x wire dia.
7	Radius	reference system / parameters / bond parameters / safety area	Radius and safety height create a cylinder around the first bond position. After the finished bond, the wedge moves straight up or under an angle to the edge of the cylinder and than straight up. If the radius is set "0", no slow down of the travel speed will happen at point 8. The cycle time can be increased by this movement. A radius will be chosen if heel damages occur.	If applicable, this setting should not be lower than 100mm	0.0 µm

8	Safety Height Source	reference system / parameters / bond parameters / safety area	The travel height of the bondhead for the second and all further wires. In order to prevent a contact with the neighbor wires. The radius determines the X-Y position of the bond-tool in safety height.	If a radius setting has been chosen, the safety height shall Not be lower than point 7.	200 μm
9	Peak of Loop Trajectory	automatically calculated	Highest point on the trajectory of the bond-tool. This point is determined by the distance between both bond positions, the programmed loop height and the programmed loop shape. The distance between point 6 and point 9 is equal to the free wire length of the loop.	N/A	

Table 1 Detailed breakdown of loop parameters

Table 1 describes the mechanics of the loop parameters. In the context of the bonding performed for ATLAS, the most relevant parameters were fine tuned throughout production. These parameters included:

Loop height is programmable within the parameter window but the parameter itself does not define the loop height. Instead it defines the height of the bond-head at the middle part of the bond. Increasing this parameter does increase the actual loop height but the parameter is more often used just to keep the height of the bonds in different programs the same.

Loop length is definable but not used in ATLAS Module production. It can be a very useful parameter when timing is critical.

Loop shape is a percentage that defines the shape of the bond. Like loop height it is not a true parameter with a high percentage providing loops with the loop high point near the source point of the bond. A high value was kept throughout production as this allowed bonds in high programs to clear low program bonds.

Accuracy parameter defines the accuracy with which the bond head places the bond. The maximum accuracy of the system is 3 μm (which matches the resolution of the camera). This parameter was set to 3 μm throughout production, but didn't really represent the true accuracy of the bonding, which also depends on other factors such as module clamping and calibration.

Offshoot is the last of the three methods of bond termination (the others being deformation and bond time). The offshoot is set to terminate the bond when the bond-head is lowered to a point (set by the user) beyond the initial touching point. This parameter is a fail safe to protect the module in the event of a failure and was usually set quite low (around 25 μm).

Safety height is the point to which the bond-head moves before descending to the module surface. It is a height above the touchdown point and has to be carefully monitored in order to prevent the bond-head colliding with components on the module hybrid.

Safety radius adds a stage to the physical movement of the bond head after the first bond (source). This movement is at an angle of 45° for a distance defined by the user. The object of this movement is to decrease the risk of bond heel break at the source point. This parameter was regularly set to a value of 80 μm throughout production.

Touchdown velocity is the speed with which the bond-head descends from the safety height to the module surface. This parameter is a balance between bonding speed and bond quality as too high a setting can affect bond welding.

Override controls the overall speed of the bond process and is again a trade-off between bonding speed and bond quality. This value was often changed but was regularly set to around 90% for outer modules and 60% for inner modules.

4.4.4 Other Bonder Parameters

Some other relevant parameters and their settings are presented in Table 2.

Parameter	Explanation	Spread	Default
Working Height	Travel height between two reference systems or to a different device.	Z-Axe movement Area	1.0 mm
Wire Buffer	Defines the sensitivity of the wire sensor.	(0-100)%	70%
Holder	shows the actual installed holder.		
Ultrasonic Gen-erat.	Shall not be touched by customers. The adjustment is done by H&K.		
Off Bonding	Defines the positions of the programmed off-bonding positions.		
Adjustment	Defines the order of activities. per substrate means: The entire substrate will be adjusted and then entirely bonded. per chip means: Chip adjust then chip bond and so on.		
Board Backwards	The adjustment starts at chip 1 and proceeds to chip n. Then the bonding starts at chip n and goes back to chip 1		

Table 2 Other useful bonding parameters

4.5 Criteria for good bonder performance

When all process variables are under control, ultrasonic wire-bonding can be a highly reliable manufacturing process. There are a number of basic requirements necessary to achieve successful and consistent wire-bonding: ultrasonic settings, module clamping and bonding surface/material conditions.

4.5.1 Ultrasonic settings

The success of the process relies upon the efficient transfer of the ultrasonic vibration from the transducer to the bonding tool. Therefore the tool must be set using the correct height gauge and securely held in the transducer arm using the correct grub screw tightened to the correct torque. In addition all bonding parameters (as explained in section 4.4) must be appropriate for the ATLAS SCT module specification. In order to achieve this an extensive period of bonder parameter optimisation was undertaken prior to production (see section 4.7).

4.5.2 Clamping

The substrate must be securely clamped to the work stage. Any movement will dampen the interfacial scrubbing action causing a degradation of bond quality.

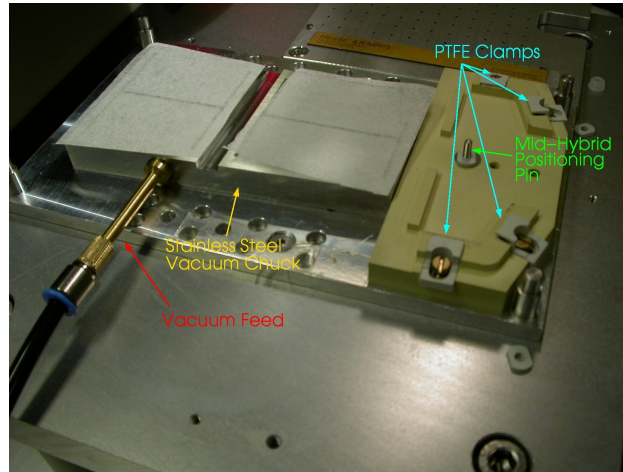


Figure 4-18 ATLAS module mounting jig

One of the major factors affecting a module bond-ability is the “bounce” factor. Modules are mounted on precision-machined jigs accurate to $1\mu\text{m}$ before wire bonding. This ensures that the flat module is as firmly supported as possible.

This final mounting jig is the result of many months of study and optimisation, which continued well into the production phase. Initial work concentrated on the flatness of the stainless steel vacuum chuck (see Figure 4-8). This chuck was machined and hand finished to an accuracy of $1\mu\text{m}$ providing as flat a support for the detectors as possible. Our next priority was to ensure the hybrid was equally well supported. The hybrid holder is made from a material called Noryl, which is suitable for its low static build up properties and for its ease of manipulation. The outer edge of the hybrid is clamped using small Noryl (PTFE) clamps. These clamps hold the hybrid down and help minimise “bounce”. During the qualification period it was observed that certain bonds were failing in the middle of the hybrid, both in the fan-in and chip bonding zones (Zones 2&3 in Figure 2-6). Initially the mid-hybrid positioning pin was used only to help locate the module onto the mounting jig, but it was thought that it could be used to help clamp the middle of the hybrid as well. Several different methods were tried including removing the positioning pin and screwing the hybrid down into the vacant hole, to re-working the hybrid holder to include a vacuum application. After considerable study, it was decided the ideal solution was to tap the existing positioning pin thus enabling a nylon bolt to be screwed down on the positioning pin

to clamp the middle of the hybrid. This improvement minimised mid-hybrid “bounce” and resulted in a decrease in the number of failed bonds and consequently the number of rework per module.

4.5.3 Material condition

Variations in material quality are the prime cause of failure. Inspection, storage and handling of components and bond wire must be carefully controlled to avoid contamination. All wire and wedge supplies were kept in a nitrogen cabinet throughout production. The clean room was temperature and humidity controlled to 22°C and 40%, this had proven to be the best balance between moisture in the air and potential electro-static build-up. Modules were regularly cleaned using a nitrogen gun to remove any dust, debris or loose wire bonds

4.6 External factors affecting bonding

During the initial stages of the production, several modules required large number of reworks. Initially this was considered to be either due to a clamping issue, or bond parameters. It was later decided that the bonder itself was the cause of the problem and after consultation with the service engineer, it was decided to keep to a constant temperature and humidity. The engineer also had concerns about the air circulation in the clean room, resulting in the limitation of the use of the A/C unit.

4.7 Bonding program optimisation

One of the main tasks during production planning was the writing of programs for the different sections of ATLAS outer modules. Later in the production period programs were also written for inner modules. The bonding map in Figure 4-10 illustrates the three different bonding zones (highlighted in red) on the ATLAS outer module. It also shows that all bonding is from top to bottom, general bonding rules dictate that if one surface is higher than another, always bond from the higher surface. The letters on the bonding map indicate the different reference points used to program the bonding system.

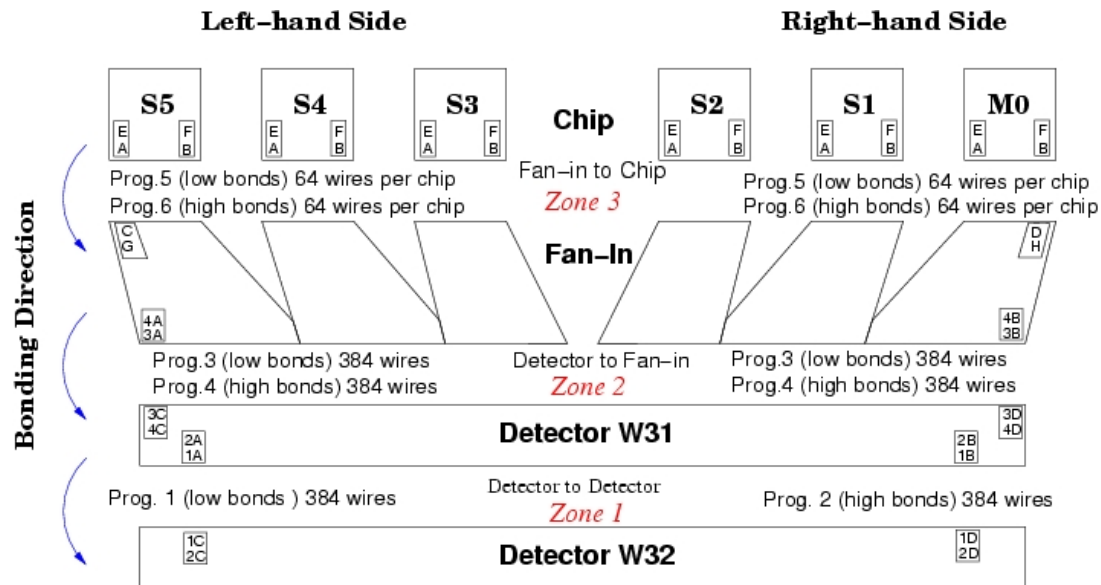


Figure 4-19 ATLAS outer module bonding map

The bonding map ^[26] also defines the different chip numbers. These are used to isolate defects. The bonding map also shows the reference system points. Each system has points that enable the bonder to place the source and destination of each bond within each system. The bond points within a reference system never change; the only thing that changes is the distance/angle between reference systems. The H&K bond jet can pick up these reference points using a Pattern Recognition System (PRS). The PRS searches for easily identifiable marks or features within a reference system. The PRS is pre-programmed to search in a certain place within specified tolerances. When the PRS finds the mark or feature, it uses it them as reference points with which to align the bond pads within that reference system to an accuracy of $\pm 3 \mu\text{m}$. Each reference system has 2 reference points and the bond pads of that reference system are always in exact relation to the reference points. The detector-to-detector programs have 2 reference systems as the bonds are between the two detectors. The fan-in to detector programs, have 3 reference systems: the left fan-in, the right fan-in and the detector. The chip programs have 8 reference systems: 6 different chip systems, the left fan-in and the right fan-in. The need for an area of bonding to be classified as a separate reference system is defined by deciding if that area of bonding can be expected to move within a program from module to module.

4.7.1 Bonding zones

For ease of programming the module was split into 3 bonding zones:

Zone 1. Detector to detector - these bonds connect the strips in Wafer 32 to the strips in Wafer 31.

Zone 2. Fan-in to detector – these bonds connect the strips on the detector to the fan-in/pitch adapter.

Zone 3. Chip to fan-in – these bonds connect the strip on the fan-in to the readout electronics.

All bonding zones were split in 2, high bonds and low bonds. This was a result of the necessity for channel pitch to be as low as possible, about 80 μm (see Figure 4-11).

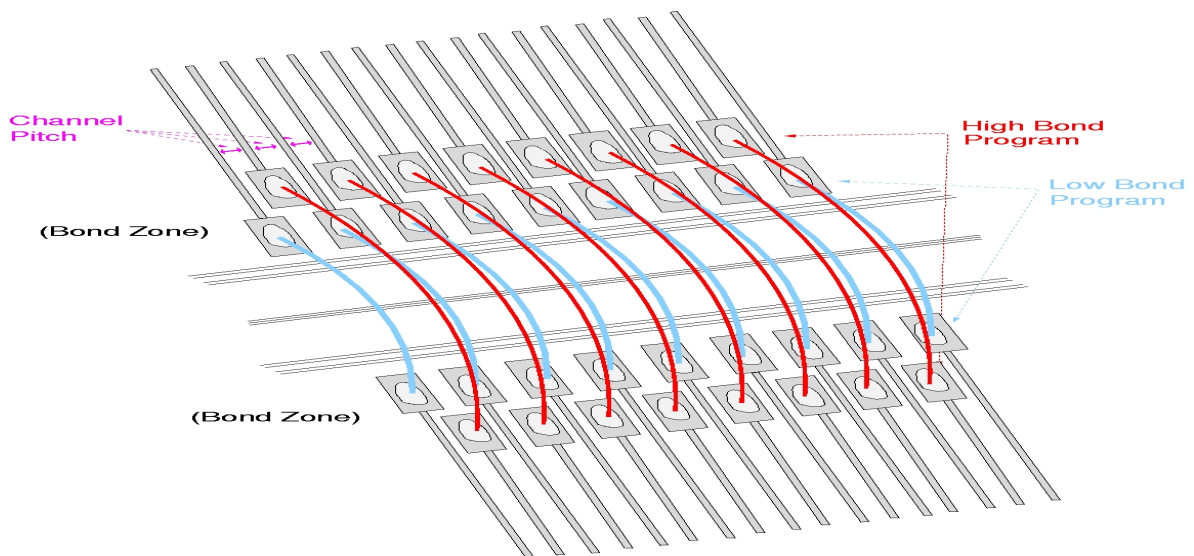


Figure 4-20 Close-in view of high and low bonds on module detector area

Program No.	Bonding Zone	Programme Code
1	Zone 1 Detector-to-Detector Low	OutK5mLo
2	Detector-to-Detector High	OutK5mHi
3	Zone 2 Fan-in to Detector Low	OutK5Fdl
4	Fan-in to Detector High	OutK5Fdh
	Zone 3	

5	ABCD3D (Chip) to Fan-in Low	OutK5LoCh1
6	ABCD3T (Chip) to Fan-in High	OutK5HiChP

Table 3 Final program list including H&K program codes used to generate program information

All program codes were derived from programs used in the Liverpool University bonding centre. All parameters for the programs have been modified to suit the different characteristics of the Glasgow ultrasonic generator and the different environment in which the modules are being bonded. These programs are used for both sides of the modules. The first programs run on the topside are programs No.1 and 2 “detector to detector”. Next the “fan-in to detector” programs are run and finally on the topside, the “chip to fan-in” programs. At this stage all the programs for the topside have been completed, there are now 4 extra bonds (not included in the programs) that are put down for the high voltage line to the detector. The module can then be turned over and the process run in reverse order – high voltage line bonds, “chip to fan-in” programs then “fan-in to detector” programs and finally “detector-to detector” programs. At this point a total of 4632 bonds have been made on the module. The module is then carefully removed and stored awaiting testing.

4.8 Bonder parameter optimization

There are two ways to determine bond quality. The first is by visual inspection. After completing a bonding program it is standard procedure to visually inspect the bonding. Points that are discussed in more detail in Chapter 6 are:

- Good adhesion to the surface.
- Length and width of the bond-print.
- Degree of deformation.
- Surface of the bond-print.
- Heel of the source bond.
- Length of the bond-tail.
- Loop form.
- Bond deformation diagram.

The other and main bond quality indicator is bond strength. Bond strength is measurable with a gram gauge bond pull tester and good bond strength is in the region of 6-12 grams. Extensive pull tests took place during the qualification period. Table 4 shows the results of bond tests done on two pre-qualification modules. The tests were done using a rudimentary destructive bond pull tester and fifty bonds were tested to produce each set of results. As the test is destructive, these tests were only performed on pre-qualification modules. The bonds destroyed during these tests were reworked to test reworking techniques. Having achieved satisfactory results on the pre-qualification modules, it was considered safe to proceed to qualification with the parameters used during the tests. These parameters have since been modified but remain similar to the original values.

Bond Strength (grams).	Mean	Max	Min	S.D.
Chip 1:	10.45	11.68	8.96	0.61
Chip 2:	10.38	12.29	8.80	0.58
Chip 3:	9.50	11.50	8.00	0.72
Det 1:	10.21	12.50	7.50	0.75
Fanin1:	7.38	9.50	6.00	0.88

Table 4 Results of pull tests on modules 52 and 53 (pre-qualification)

4.8.1 Over-bonding

An investigation into the IV-breakdown of ATLAS modules in conjunction with Rutherford Appleton Laboratories ^[28], has established two failure mechanisms on the silicon detectors during wire bonding that can be attributed to over bonding and high impact damage.

- **Micro-discharge**

Leakage current falls in time with high voltage maintained. It appears to be caused by over-bonding of detector bonds that could be attributed to small repetitive damage to the detector surface. Figure 4-11a shows an example of IV breakdown observed on

ATLAS outer module 253 after high voltage increase to 400v. Figure 4-11b represents the results of the long term test on this module (Chapter 5 will look at these tests in more depth).

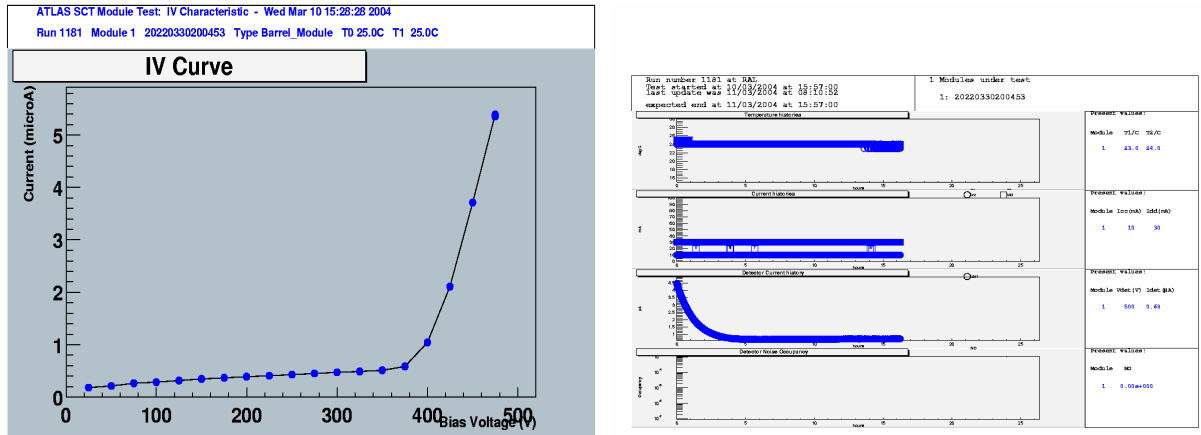


Figure 4-21a/b IV curve of module 253/falls of leakage current in time

- **Module IV Characteristic comparison**

Modules with bond showing evidence of over-bonding (Swaging) ^[27]. The pictures in Figure 4-13a show bonds that are considered over-bonded. The bond-feet on these bonds have an average width of 43 microns. Equivalent to 1.7 times the wire diameter. Figure 4-12a shows bond footprints that show evidence of swaging.

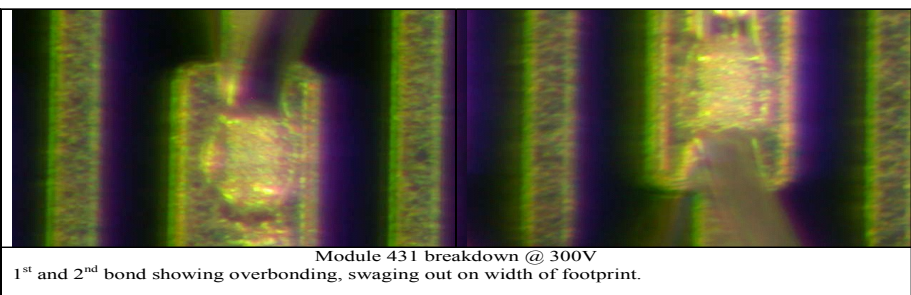


Figure 4-22a Examples of over-bonding

Having seen evidence of “swaging” a parameter adjustment was required. These bonds are over-deformed so a decrease in the deformation parameter and a slight decrease in bond-force was tried. Figure 4-13b show pictures of wire-bonds made after a reduction in the deformation parameter was made.

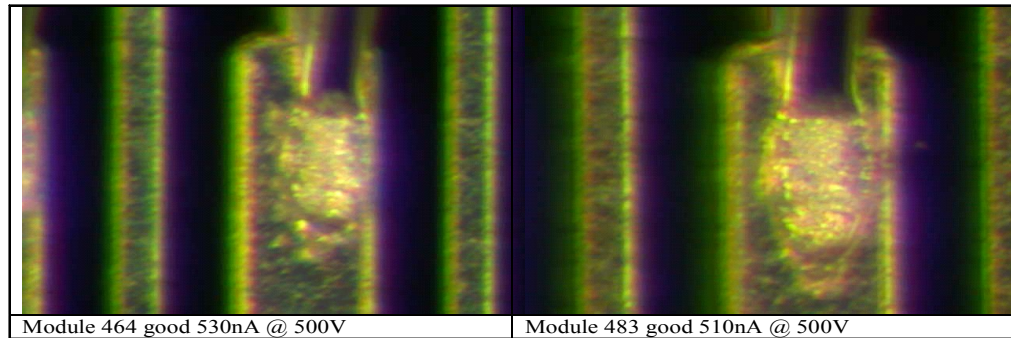


Figure 4-13b Bonds formed with the deformation parameter reduced

Measuring the bond width found that the average width was 36 microns, with standard deviation of 1.4, equivalent to 1.4 times the wire diameter. In addition the bonds have a better shape and form, which results in higher bond strength. While not all modules that are over-bonded fail, it has been found that since the date when the machine programmes were changed to reduce the width of the bonds on the detectors, to 1.3-1.5 times the wire diameter, subsequently produced modules showed much reduced incidence of this type of failure. The method used for reducing the bond width was to alter the machine parameters, complete a series of bonds, and then measure the width of the bonds.

4.8.2 High impact damage

Some modules showed high current where the only observable defect was slight damage to the HV bias line. Figure 4-14 show bias line bonds that have been reworked. The failed bond has left damage on the bias line and caused high leakage current (see Fig

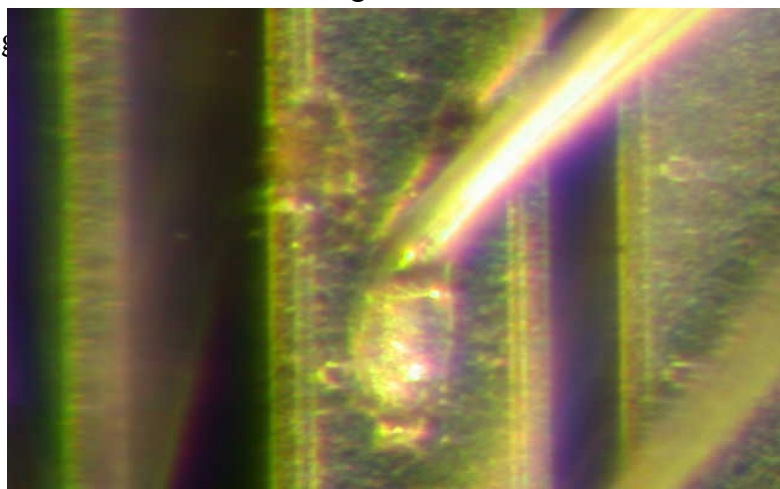




Figure 4-23 Module 236 showing evidence of high impact damage on the high voltage bias line

The high impact damage on the bias was occurring because the Hesse & Knipps machine was switched off at the end of the day, and because there was no air feed the wire retracted under the wedge. This led to insufficient wire available for the first bond (top left bias), causing high impact damage.

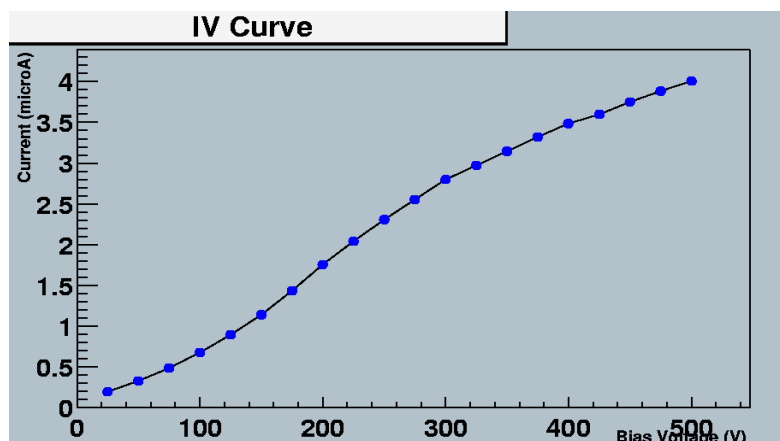


Figure 4-24 Module 236, high current 1 μ A@110 V and 6 μ A@400 V

All that was required to solve this problem was to leave the machine switched on, alternatively a bond off was done on the test substrate prior to resuming production [28].

4.8.3 Bond footprint profile analysis

During pre-qualification, bond footprints were analysed to identify bond failure modes and to compare footprint profiles of bonds from the different bonding zones of the modules. This form of profile analysis was preferable to bond pull tests at the

qualification stage as the test is non-destructive. A footprint can be considered the part of a wire bond that is in contact with the bonding surface

Figure 4-16 shows a 3D profile, taken using a Wyko NT1100 Optical Surface profiler, of a single bond-foot on the chip area of an outer module. Profiles such as these were used during qualification to analyse the form and structural rigidity of bonds. Profiles were also used to compare the quality of bonds made in each of the three bonding zones on a module (detector, fan-in and chip). The 3D images below present a height profile through different colours. In these images different height levels are represented by different colours. The programmable interface of the image software allows a datum level to be set. This level equals zero and is set at the height of the bonding zone surface. This level is seen as dark blue in the images. The colour gradually changes to green at the 5 micron level, to yellow at the 10 micron level, to orange at 15 microns and finally to red at 25 microns. With this colour code it is possible to form a reasonably accurate bond-foot profile.

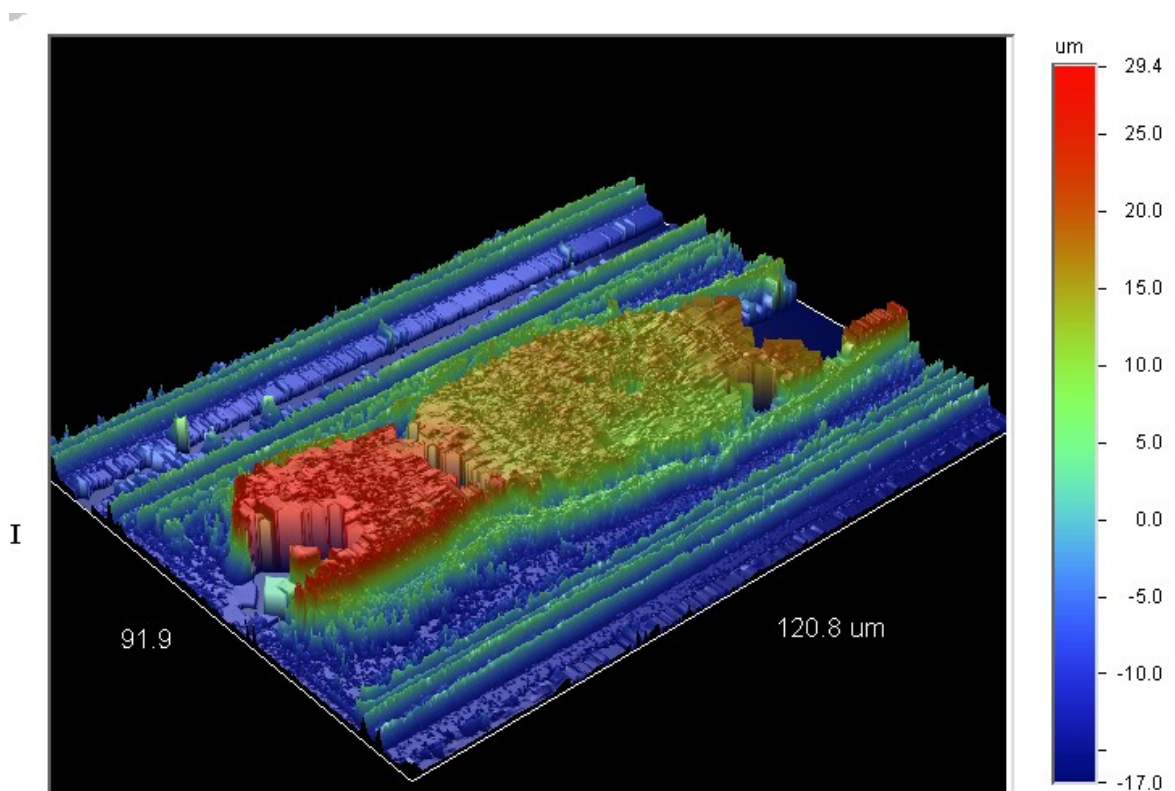


Figure 4-25 3D profile of wire-bond

The bond-foot in Figure 4-16 is a close to ideal footprint. The footprint itself shows an even spread of yellow and orange, indicating a solid foot-print base. The bond tail, indicated in red (the wire itself is 25 microns thick) is short and in line with the bond. The heel of the bond (to the right of the image) is substantial enough to suggest the risk of heel break is low. Additionally, the footprint is well centred within the bond pad and shows even deformation. A bond such as this would easily show a bond-pull strength in excess of 10 grams. Figure 4-17 shows the X plane and Y plane profiles used to calculate bond width. It is possible from these profiles to conclude that this bond has a width of around 40 microns and a length of around 70 microns. This facility was used during qualification to measure the bond width and assist prevention of the over-bonding described in Section 4.8.1.

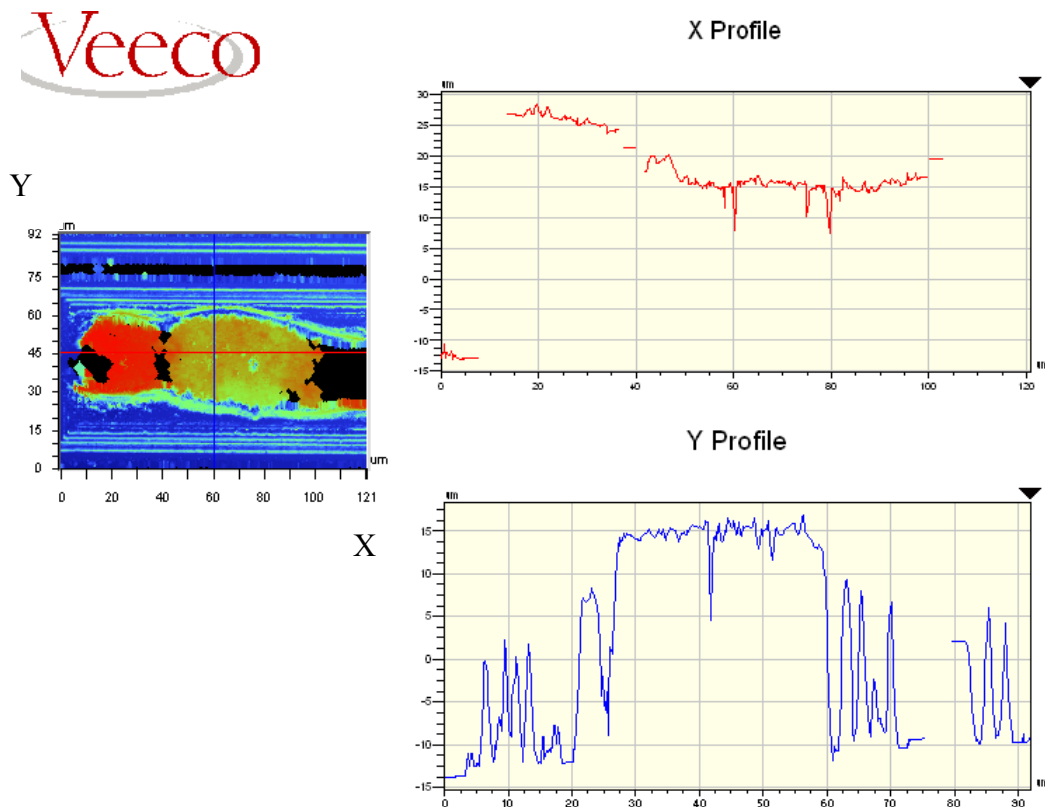


Figure 4-26 X and Y profiles of bond from previous figure

The graphs in Figure 4-17 provide height profiles in the X- and Y- planes. It is possible using this software to determine the average height of a bond-foot. This software was also useful for observing the consistency of tail lengths and heel

formations. While the footprint profiles enable analysis of form and shape, they can also be used to identify mechanical issues. As the wedge of the bond-head makes contact with a bonding surface, the surface can move if not properly clamped. As discovered during qualification, ATLAS modules can exhibit movement in different planes regardless of how well the module is clamped. In the following sections the concept of movement in a certain plane will be discussed. Movement within a plane will relate directly to the kinematic arrangement of the H&K bonding system (presented in Figure 4-18).

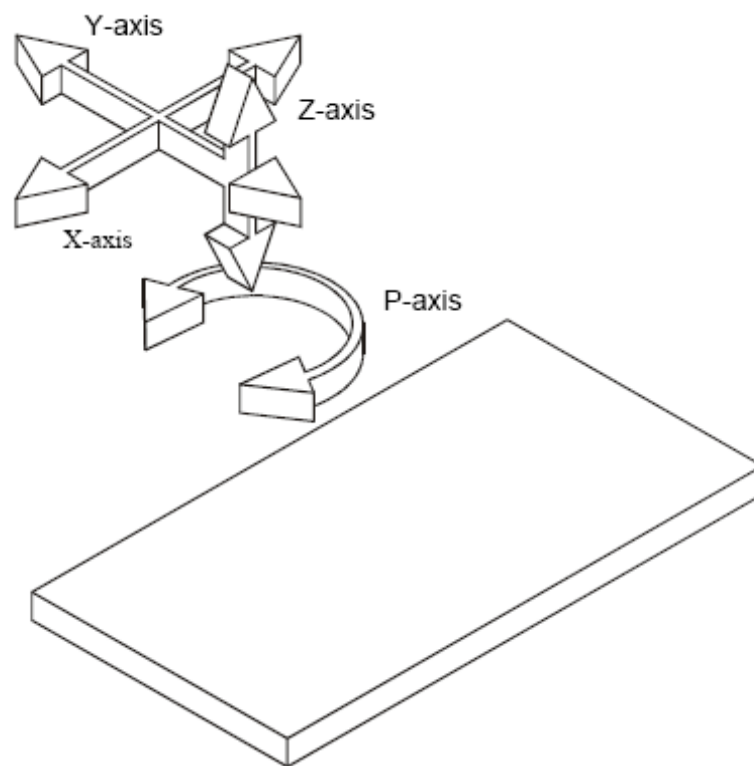


Figure 4-27 Kinematic arrangement of H&K bond-head

4.8.4 Bonding zone foot-print profile comparison

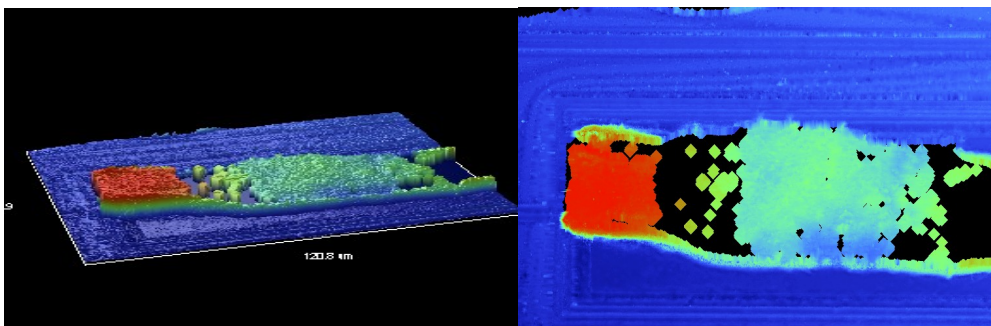


Figure 4-28 2D and 3D images of a single wire-bond footprint on the chip bonding zone

Tests carried out during qualification suggested that the chip zones displayed the best bonding quality. Figure 4-19 shows another chip bond profile and it is remarkably similar to the profile in Figure 4-16. All indications are that this is a good bond and tellingly the bond is in line and shows uniform characteristics. The horizontal view in Figure 4-20 provides further evidence of the strong bond-foot base.

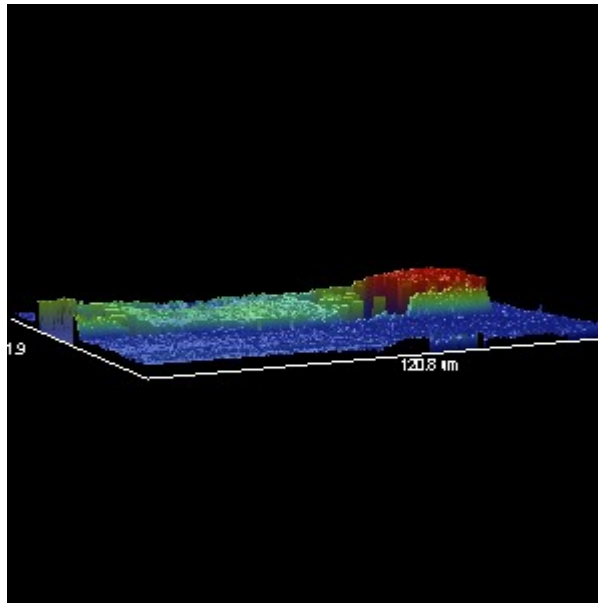


Figure 4-29 3D image from horizontal view point

Good bond quality on the chip zones was to become expected during production. The other bonding zones were to prove slightly less consistent and problems seen in footprint profiles taken during qualification would re-appear throughout production. Figure 4-21 for example, is a profile of a missed bond on the detector.

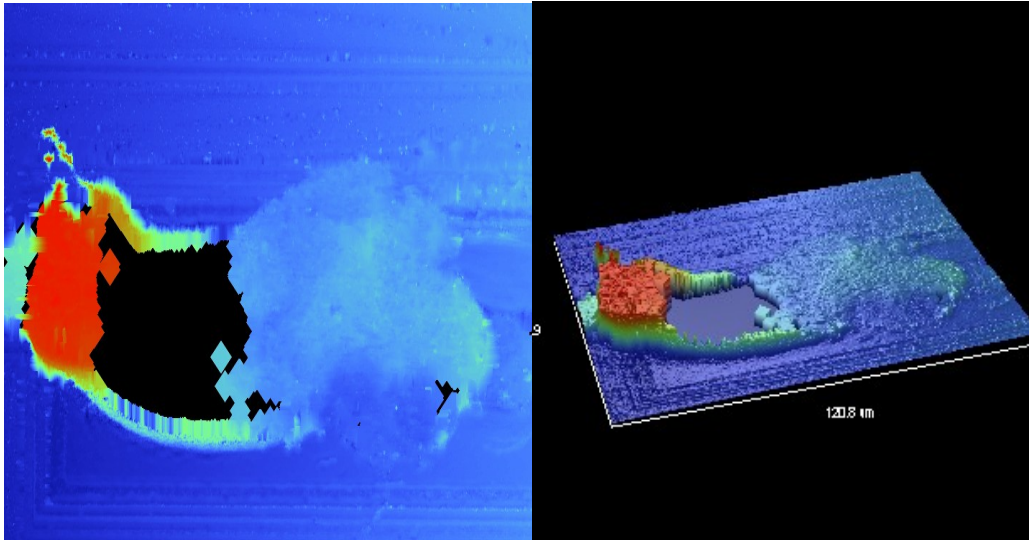


Figure 4-30 2D and 3D profiles of missed wire-bond on the detector

This profile obviously shows that the bond is incomplete; the bond has in fact broken at the heel. The footprint itself appears as a very low profile, most of the footprint remains blue in the image suggesting the footprint is below 5 microns high. This is a classic detector zone bonding fail. The low profile suggests the bonding system deformation parameter has been set very high. This is usually done to counteract movement in the Z-plane of the detector. Movement of this sort is usually a result of poor module clamping or Z-deviation in the module (Z-deviation will be discussed in Chapter 6). On closer inspection the bonding surface to the right of the footprint looks as if it has been scraped. This again lends weight to the theory of surface movement in the Z-plane. This scraped surface effect is known as “scrubbing”. Figure 4-22 further endorses the theory of surface movement in the Z plane. The 3D image clearly shows scrubbing to the left of the footprint. The footprint in this image is otherwise good, showing good form. The small bond tail is probably a consequence of the scrubbing during bond welding. The bond has a strong heel and consequently bond pull strength would be high.

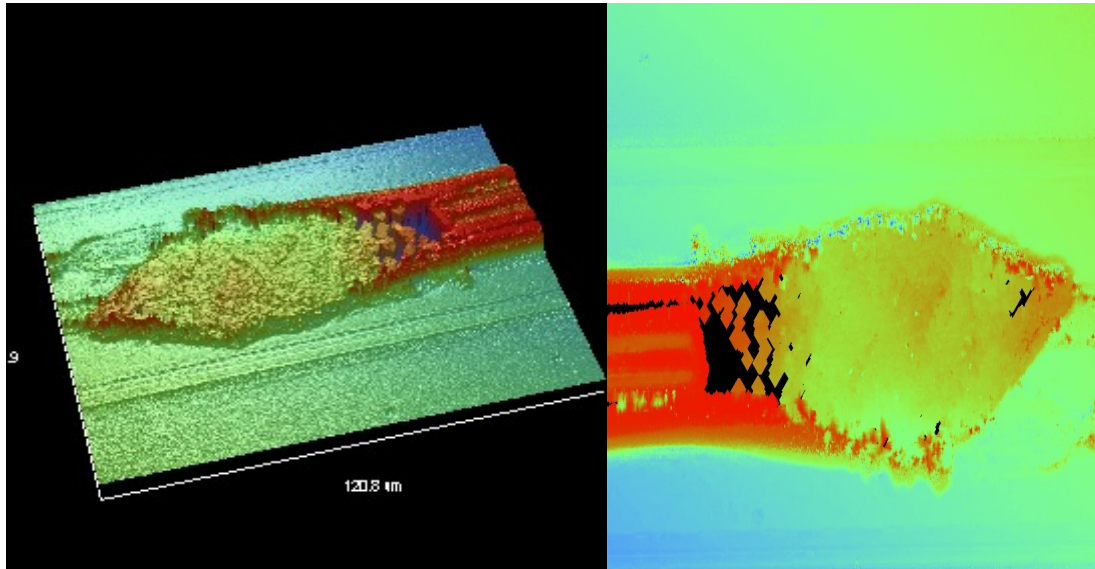


Figure 4-31 Footprint profile from bond on the detector

The different zones of the modules exhibited different bonding qualities throughout production and in the case of the fan-in failed bonds were often seen at a certain side. In general, bond quality was good in the detector zone throughout production.

The cause of this kind of fail trend was thought to be warping in the module that caused one end of the fan-in to “sit-up”. Both sides of the fan-in were unsupported therefore the fan-in relies on the clamping of the detector and hybrid areas for rigidity. If the module was in any way warped around the central axis it could result in one side of the fan-in sitting higher than the other.

One end of the fan-in sitting higher than the other can result in quite specific bond form. From the start of qualification, it was noticed that bond tails on the fan-in tended not to follow in the line of the bond itself (see Figure 4-23). These bent bond tails came to indicate a fan-in height inconsistency. If the fan-in was thought to be higher at one end than the other, the surface of the bond would move in the X -plane as the wedge of the bond head makes contact. This in turn would cause the tail of the bond to bend slightly depending on which side of the fan-in was higher. In this example the right hand side of the fan-in was higher than the left, the bond tails on some of the bonds would move to the left as in Figure 4-23.

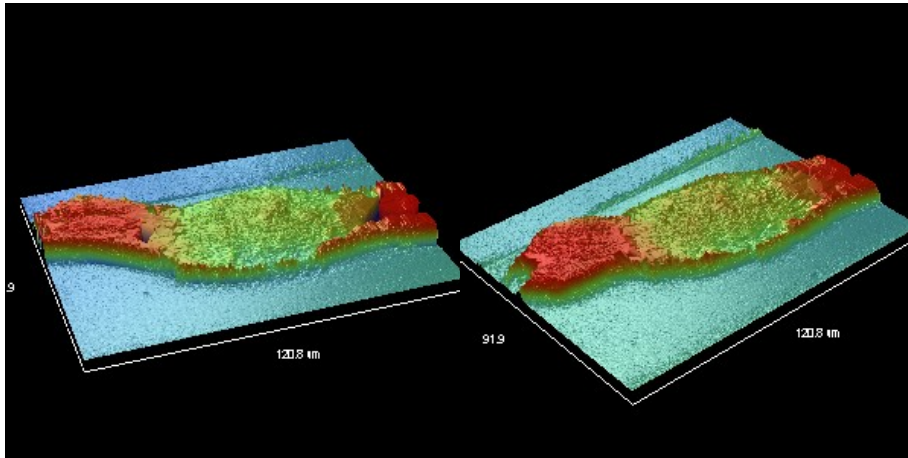


Figure 4-32 3D profiles of two bonds on the fan-in bonding zone

4.9 Summary

This chapter has covered a wide range of topics from the basics of wire-bonding to a description of the precise studies leading to successful bonding of ATLAS SCT modules. The need to find suitable parameters is a crucial element in the development of a reliable process and although there was a degree of parameter evolution during production (see Chapter 6) the fundamentals of the process remained largely unaltered. The generation of programme codes and the pull test work was carried out during the pre-qualification period. The work optimising parameters and identifying possible causes of bond failure and consequent rework was performed mostly during the qualification and early production stages. This work helped achieve a stable process where rework was minimized.

Chapter 5

5 Electrical testing

5.1 Introduction

This chapter describes the electrical measurements performed on the detector modules during production. Under the QA scheme, such tests are performed at many points in the production sequence. A basic set of tests has been defined, from which two standard test sequences have been drawn. The short sequence (Confirmation Test) is optimized for fast execution, focusing on detecting failures that might occur on detector modules. The long sequence (Characterisation Test) gives a more complete characterisation of the module, to detect more subtle deviations from the specification and provide a reference data set for macro assembly of detector modules onto the SCT barrel and end-cap disks. In addition to this, three long-term tests have been devised. These are performed to provoke infant mortality and to demonstrate the long-term stability of each detector module under nominal operating conditions. The test sequences are designed to monitor failures that might occur and to track the evolution of certain critical parameters.

5.2 The electrical characteristics of the SCT detector module

Each ATLAS SCT module is read out by 12 ABCD3TA ASIC's mounted on a copper/kapton hybrid circuit. Manufactured in the radiation hard DMILL process, each chip provides sparsified binary readout of 128 detector channels ^[29]. The amplified and shaped input signal is compared to a programmable threshold having two components: a single 8-bit DAC applied across the whole chip, and a channel specific 4-bit DAC designed to compensate for channel-to-channel variations. The resulting hit pattern is transferred into a binary pipeline, 132 cells deep. Upon receipt of a Level 1 Accept (L1A) trigger, the pipeline output is transferred into a de-randomising buffer that can store up to 8 events ^[30]. The first chip on each side of the module, designated as the master chip, is responsible for the electrical transmission of data to the read-out system. Within the module a token passing scheme is used to control the transfer of data to the master chip for onward transmission. This scheme incorporates several redundancy options such that, should any single chip fail, the remaining chips can still be read out. In ATLAS, an optical stage transmission system will be used for data communication with SCT detector modules. In the end-cap module, some components of the optical link are mounted directly on the hybrid leaving the PIN diode receiver and VCSEL diode transmitters to be added by means of an “opto plug-in”.

5.3 Electrical Test Equipment and Procedure

The tests described in this section, aim to verify the hybrid and sensor functionality after the module assembly and characterize the electrical performance of the completed module. The standard data acquisition system used to perform the electrical tests of the modules is also described.

5.3.1 Data Acquisition System (DAQ)

In some early measurements, the ABCD3TS's were powered and read out using the redundancy links, which are all electrical. This meant bypassing the optical ASIC's, thereby removing the need for expensive optical interfaces and delicate optical fibres.

However, there is a requirement for the optical ASIC's to be tested in the module readout, as this is the primary data route in the experiment. A scheme has been devised which reads out up to six modules using the optical ASIC's electrically while also testing the functionality of the module redundancy links. This system contains the following VME modules:

- **CLOAC**

(Clock And Control) CLOAC generates the clock, fast trigger and reset commands for the SCT modules in the absence of the timing, trigger and control system.

- **SLOG**

(Slow command Generator) SLOG generates slow commands for the control and configuration of SCT front-end chips for up to 6 modules. It fans out clock and fast commands from an external source (CLOAC). Alternatively an internal clock may be selected, allowing SLOG to generate clock and commands in stand-alone mode. When the SLOG runs in stand-alone mode, the CLOAC is not used in the set-up.

- **AERO (ATLAS End-cap Read-Out)^[30]**

One AERO card provides an electrical interface for up to 6 End-Cap modules. Data communication to and from the modules is via their onboard optical ASIC's - DORIC and VDC (data receiver and transmitter respectively). AERO encodes the module Clock and Command signals onto a single BPM (Bi-Phase Mark) carrier signal for transmission to DORIC ^[31]. The two module data links are transmitted back to AERO via the VDC and then routed to MuSTARD. Configuration of the channel allows the module to be read out using either the primary (optical) or redundant data routes.

- **MuSTARD (Multi-channel SCT ABCD Readout Device)**

MuSTARD receives, stores and decodes the data from multiple SCT modules. Up to 12 data streams (six modules) can be read out from one MuSTARD card.

- **SCTHV** ^[32]

A prototype high voltage unit providing detector bias to four SCT modules.

- **SCTLV** ^[33]

A custom-designed low voltage power supply for two SCT modules.

A module ‘patch card’ (see Figure 5-1) is also required to interface a single AERO channel to a module. The connections to AERO are made via two standard ethernet category 5(E) screened cables, allowing separation of the primary and redundant data routes onto the individual balanced cables. Using screened twisted pair cables and differential signals should result in a system with low electromagnetic interference and good immunity to external noise.

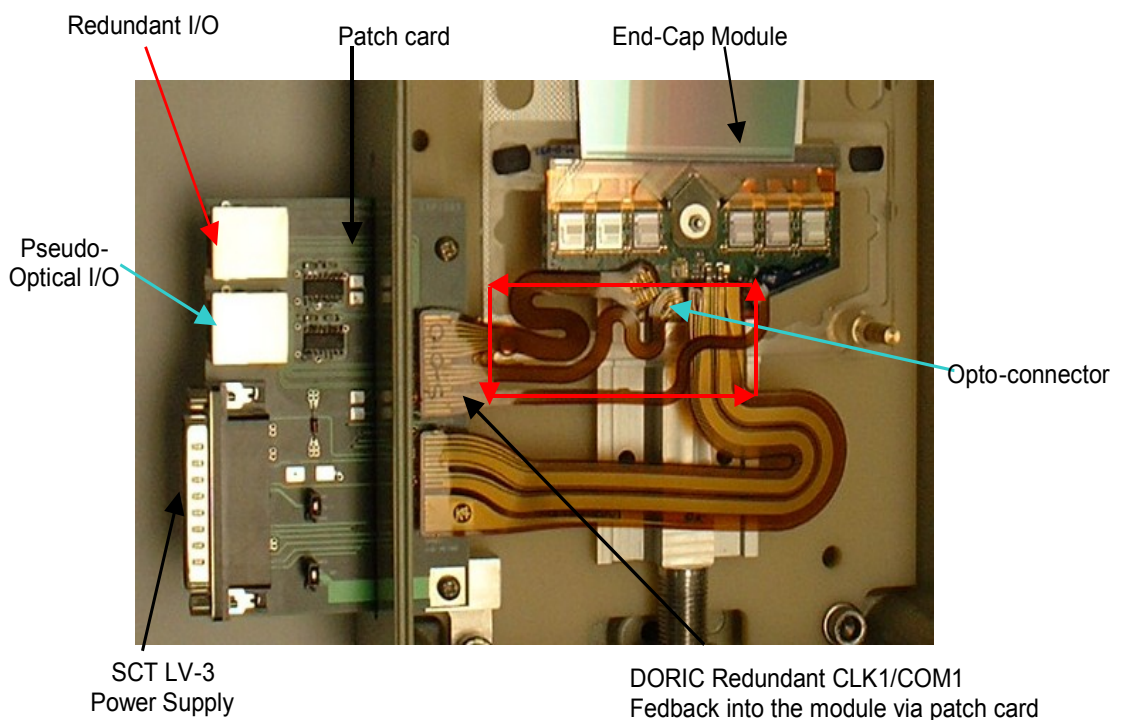


Figure 5-33 Photograph of a patch card linked to an end-cap module

AERO provides three readout modes (see Figure 5-2) for testing a module or hybrid, as follows:

Primary mode: the module is configured and read out via the Opto Chips DORIC and VDC.

VDC Bypass test mode: the module is configured via the DORIC outputs CLK/COM and the module data is read out via the Master ABCD3TAs. This scheme is used so that the VDC is bypassed for data transmission from the module whilst retaining the DORIC for module configuration.

Redundancy Mode: the module is configured via the redundant CLK1/COM1 provided from SLOG and the module data is read out via the Master ABCD3TA's.

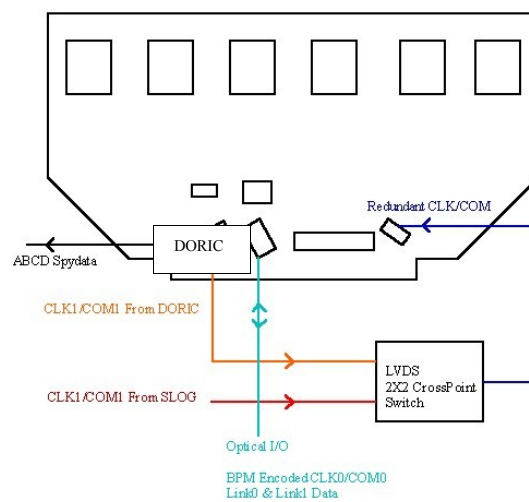


Figure 5-34 Module readout modes

The SCTDAQ software package ^[34] has been developed for testing both the bare hybrids and the modules using the VME units described above. SCTDAQ consists of a C++ dynamically linked library and a set of ROOT ^[35] macros which analyze the raw data obtained in each test and store the results in a database. A schematic diagram of SCTDAQ is shown in Figure 5-3.

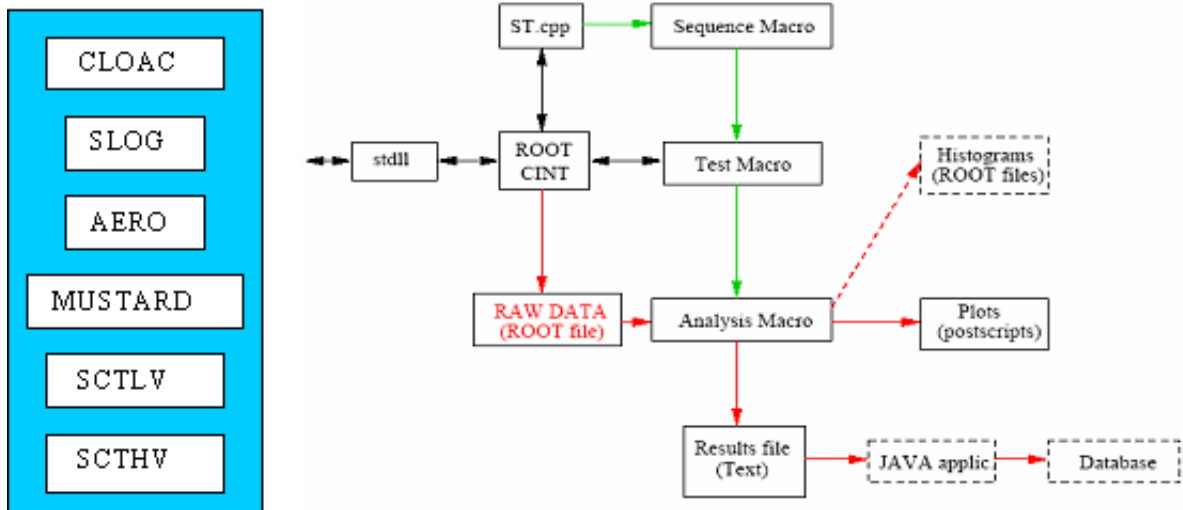


Figure 5-35 Schematic diagram of the SCTDAQ system

5.4 Thermal cycling

Each module was subjected to thermal cycling to prove that the module was capable of surviving the environment changes that can be expected in the ATLAS cavern.

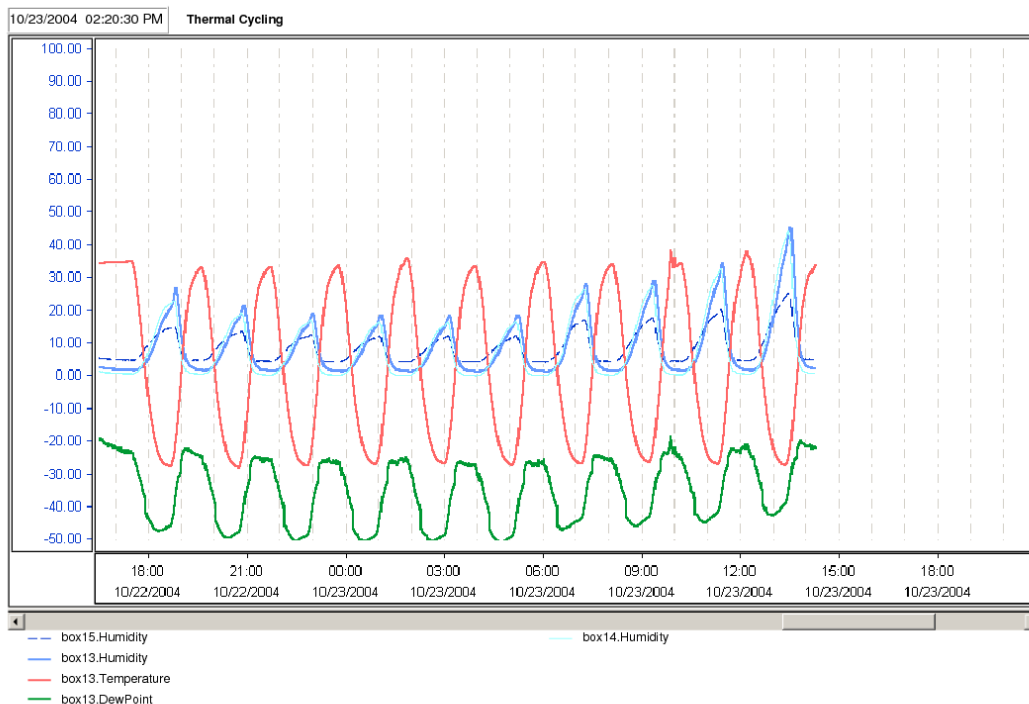


Figure 5-36 Thermal cycling humidity profiles

After an initial electrical test modules were mounted into aluminium cases (two cases each holding three modules) and placed into an environment chamber. Figure 5-4 shows the humidity plots of six modules tested during production. Each module is subject to the same conditions in the environment chamber and is cycled 10 times between -35 C to 35 C with ramp up/down times greater than 30 minutes (temperature in red in Figure 5-4). During the cycling, humidity in the cases is closely monitored (there are two temperature plots in Figure 5-4, both in blue, to represent the humidity in each case) this enables the dew point to be calculated and ensure that no water vapour is present in the cases.

5.5 Electrical Tests

After the thermal cycling, the module is placed inside a light-tight aluminium test box where it is supported at the two cooling blocks of the baseboard. The test box provides dry-air flow and cooling through a channel connected to an adjustable liquid coolant system (Figure 5-5). Up to six modules in their test boxes are placed inside an environmental chamber and tested simultaneously. Very careful optimisation of the grounding and shielding scheme was necessary.



Figure 5-37 Outer module supported by its transport frame inside an aluminium test box. The dry-air and coolant inlets are visible as is the support card on the lower right of the image

Every module is electrically characterized with the temperature on the hybrid, measured with an integrated thermistor, maintained at $(10 \pm 0.5) ^\circ\text{C}$. Using the internal

calibration circuit of the ABCD3TA chips to inject charge of adjustable amplitude in the preamplifier of each channel, the front-end parameters such as gain, noise and channel-to-channel threshold spread are measured. The characterisation sequence includes the following steps:

Digital tests are executed to identify chip or hybrid malfunction. These include tests of the redundancy links, the chip by-pass functionality and the 128-cell pipeline circuit.

Optimisation of the delay between calibration signal and clock (strobe delay) is performed on a chip-to-chip basis (see Figure 5-6).

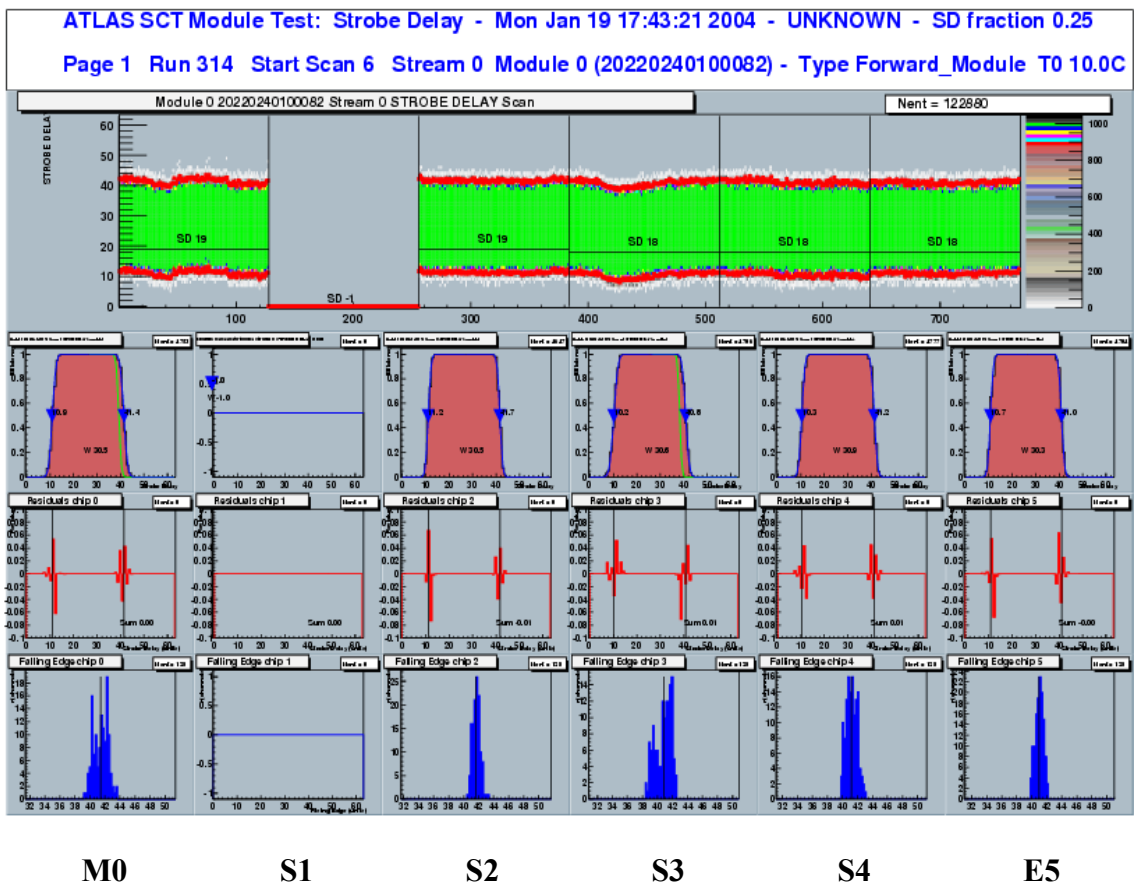


Figure 5-38 Strobe delay results from module 82. Each chip (top side of the module in this case M0 to E5) is readout simultaneously. This scan is performed to find the delay between the calibration pulse injection and comparator changing its state. The second row of results show the signal from the comparator must fall within a 25 ns window. (Note chip S1 is damaged and so is not reading out)

The channel by channel gain and electronic noise are measured by analysing S-curves obtained through repeated threshold scans performed for ten different values of injected charge, ranging from 0.5 to 8 fC. For each injected charge the threshold is scanned and the occupancy is fitted to a complementary error function. The value of the threshold in mV corresponding to 50% occupancy is the $vt50$ parameter. The gain, input noise and offset are deduced from the correlation of the voltage output in mV versus the injected charge in fC.

To minimize the impact of the threshold non-uniformity across the channels on the noise occupancy, the ABCD3TA allows one to adjust the local discriminator offset using a digital-to-analogue converter (TrimDAC) per channel with four selectable ranges (common for each chip). This trimming procedure is important due to the increase of the offset spread with radiation dose accumulated in ATLAS detector during its operation at the LHC. The effect of trimming on the threshold uniformity is evident by comparing the top plot of Figure 5-7 with Figure 5-8.

A threshold scan without any charge injection is performed to obtain a direct measurement of the noise occupancy (NO) at a threshold of 1 fC. NO is the probability for a channel to produce a hit for a certain event due to noise (Figure 5-9). Trimmed discriminator offsets are applied to ensure a uniform measurement across the channels. It is expected that the SCT modules will operate at a threshold set to 1 fC ENC, or slightly higher after heavy irradiation. This value is chosen to minimize noise occupancy and maximize signal sensitivity.

A dedicated scan is also executed to determine the time-walk. Setting the discriminator threshold to 1 fC for each value of injected charge ranging from 1.25 to 10 fC a complementary error function is fitted to the falling edge of a plot of efficiency versus strobe delay to determine the 50%-efficiency point. The time-walk is given by the difference between delays calculated for a 1.25 fC and for a 10 fC injected charge.

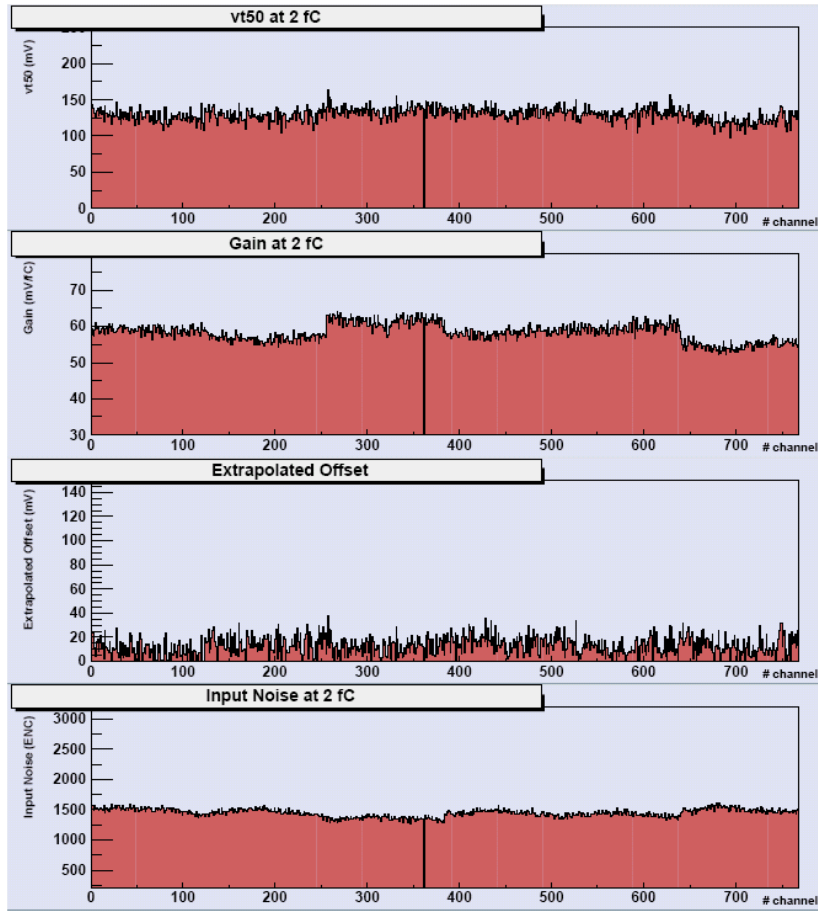


Figure 5-39 Typical set of plots obtained with the Response Curve procedure before trimming for one data stream, corresponding to six chips (768 channels). From top to bottom the vt50 value, the gain, the offset and the noise are shown for each channel

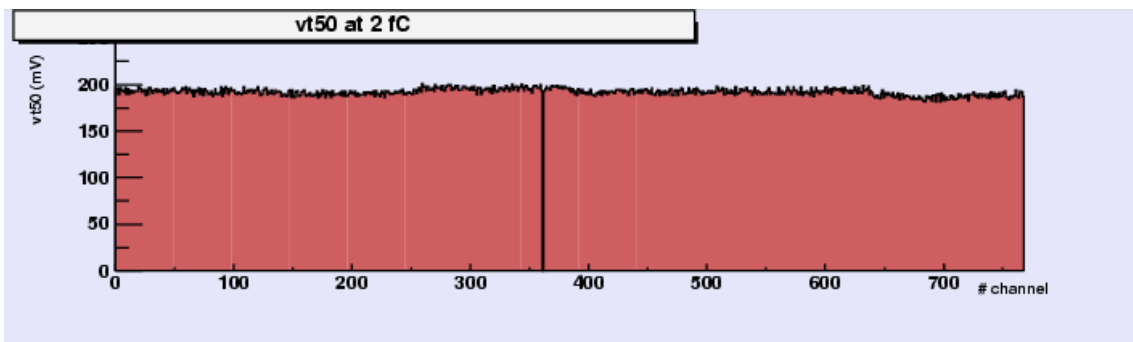


Figure 5-40 The vt50 value after trimming for the same module as in Figure 5-6

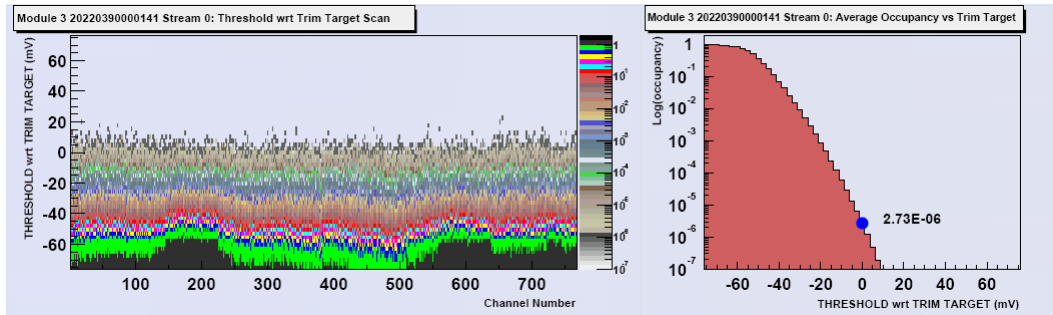


Figure 5-41 Noise occupancy plot for one data stream: 2D plot of occupancy vs. channel number and vs. threshold (left); average occupancy for the stream vs. threshold (right). The threshold is expressed with respect to the 1 fC point (0 mV) as determined during the trimming procedure

A long-term test with electrical readout is performed to confirm each module’s long term electrical and leakage current stability at low temperature. The ASIC’s are powered, clocked and triggered during at least 18 hours while the sensor bias voltage is 150 V and the temperature measured by the hybrid thermistor is (10±0.5) °C. The bias voltage, chip currents, hybrid temperature and the leakage current are recorded every 15 min. Every two hours a test is performed to verify module functionality and measure the noise occupancy (Figure 5-10).

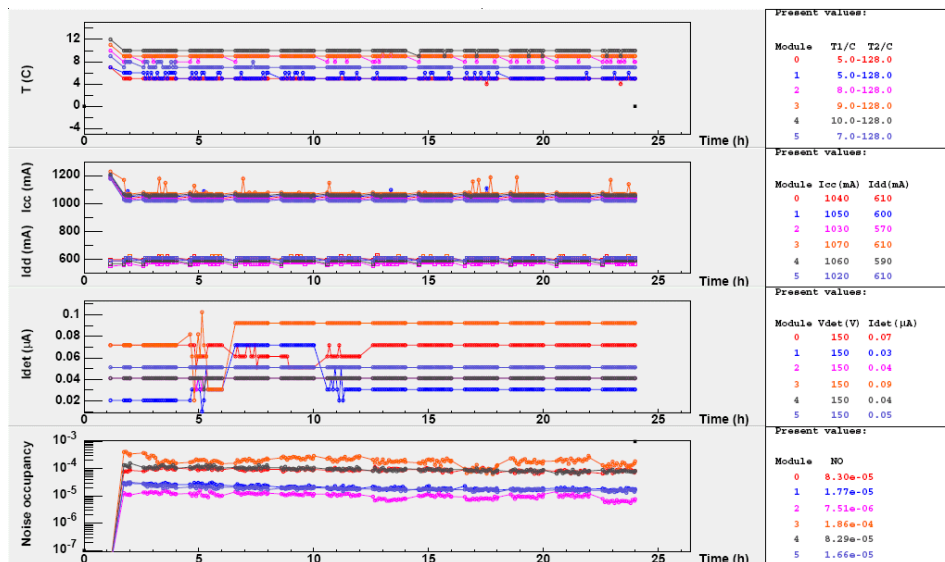


Figure 5-42 Long-term test results for six modules showing from top to bottom: hybrid temperature; analogue (I_{cc}) and digital (I_{dd}) current; detector leakage current (I_{det}); and noise occupancy as a function of time. Each modules results are represented using different colours as indicated on the right of the figure.

A final IV scan is performed at 20°C and the current values at 150, 350 and 500 V are recorded and compared with measurements before and after the module assembly. All the results are uploaded to the SCT production database.

5.6 Summary of Full Module Testing Sequence

On average, building a module took about 100 hours of which 70 hours were fully dedicated to testing the various aspects of the module. Three different sets of tests could be identified: reception of module components, tests made during assembly and, finally, the tests made on the module as a whole. Reception tests on components consisted mainly of visual inspection and confirmation that their critical properties were still within the specifications. In particular, for silicon sensors an IV characteristic curve (Figure 5-11) was measured. For spines the curvature along the TPG (Thermal Pyrolytic Graphite) and for hybrids the digital circuitry of the ASIC's as well as the gain, noise and dead channels were measured.

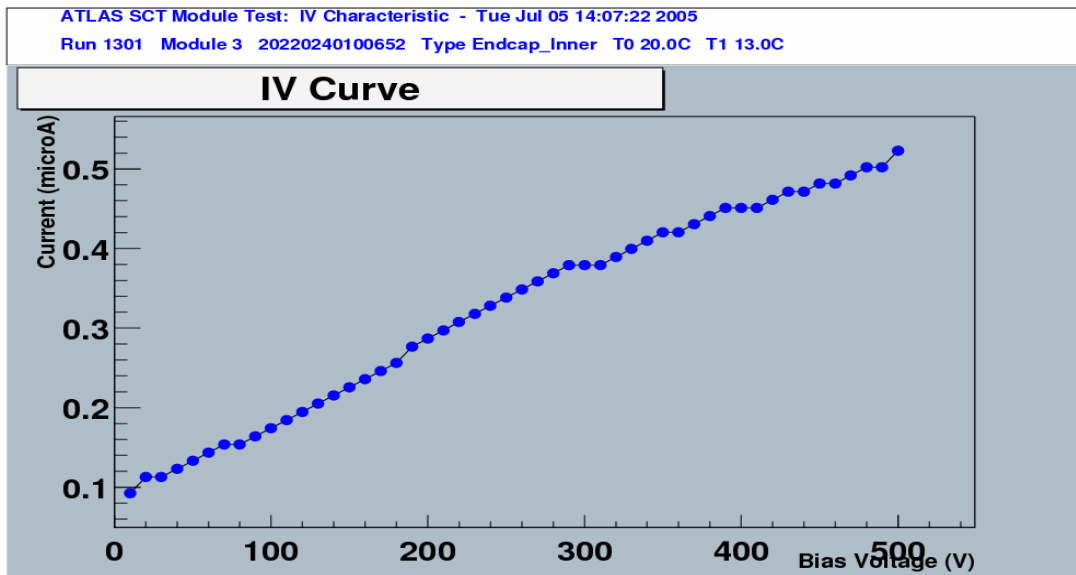


Figure 5-43 IV curve of module 652

During the assembly phase of the module, and before gluing the hybrid to the detector-spine assembly, an IV curve of each sensor was measured up to 350V. At the

end of this phase, and prior to the bonding process, all the metrology parameters were measured during the first period of the production in order to trace any mechanical deformation that could occur during the thermal cycle of the module.

A fully assembled module could therefore expect to undergo the following tests:

- Thermal cycling.
- Full metrology survey.
- IV curve measurement.
- Long-term test of electrical and leakage current stability: the modules were kept in a controlled environment and were clocked and configured during 24h with the detectors biased at 150 V. Every hour a minimal performance test was performed consisting on the gain, noise and dead channel determination as well as the configurability of the ASIC's.
- Full electrical characterization: in this test all the analogue and digital features of the module were tested.

5.7 Anomalous channel tolerances

During electrical testing a single channel can be flagged as anomalous by the DAQ system. These anomalous channels can be flagged as a result of any nine different channel defects. For a channel to flag as a defect it must show properties out with the accepted tolerances for a given attribute. For example, if the noise level of a single channel is 1.3 then this channel will be flagged as noisy as the levels exceeds the DAQ system upper tolerance limit of 1.15. Table 5 lists the defect types and the associated tolerances.

Defect	Condition	Default value of cut
DEAD	No output	-
STUCK	Continuous output	-
LO GAIN	Gain < (0.75 * mean chip gain)	-
HI GAIN	Gain > (1.25 * mean chip gain)	-
LO OFFSET	Offset < MIN OFFSET	-100 (mV)
HI OFFSET	Offset > MAX OFFSET	120 (mV)
UNBONDED	Noise < BONDED NOISE	800 (ENC)
PARTBONDED	Noise < MIN INNSE	1100 (ENC)
NOISY	Noise > (1.15 * mean chip noise)	-

Table 5 Anomalous channel defect tolerances

Channels with the following defects ^[20] are now masked at the end of a ThreePointGain test to reduce the probability of problems related to these defects being carried over to subsequent tests:

- low gain (< 0.75 * chip_mean_gain)
- high noise (> 1.15 * chip_mean_noise)
- DEAD
- STUCK
- high offset (>120mV)
- very low gain (< 0.3 * chip_mean_gain)
- The “PASS” field is set to “NO” if one or more of the following criteria are fulfilled:
 - A single chip is DEAD, STUCK or INEFFICIENT
 - A single chip has gain < 0 or gain > 100
 - More than 8 consecutive bad strips
 - More than 15 bad strips in total

In each case the reason why the test has failed is stated in the results file in the form of a DB comment. The database reporting structure must provide the possibility to set additional acceptance cuts on the mean and rms of vt50, gain, offset and noise,

together with cuts on the maximum number of allowable channel defects falling into each of the following two categories: Lost or Faulty. Lost channels include dead, stuck, un-bonded and noisy channels. Faulty channels include channels that are flagged as lo-gain, hi-gain, lo-offset, hi-offset, part-bonded or inefficient.

5.8 Criteria and Selection for Assembly to Disks

Modules were selected for assembly to discs according to an agreed set of criteria based on test results stored in the production database. Each grouping of production sites was responsible for evaluating the quality of its modules and placing them into four categories:

- **Good:** Pass all acceptance tests.
- **Pass:** Fails one test, but within ‘pass’ tolerance.
- **Hold/Rework:** Outside ‘pass’ tolerance. May be usable if reworked.
- **Fail:** Too bad to use, but stored safely.

The mechanical tolerances were originally set more tightly than required by spatial resolution requirements alone. In the light of experience we created a set of ‘pass’ tolerances for some parameters, which were 50 % wider. Modules with one parameter (or two *Z* parameters) in this ‘pass’ band are assigned to the “Pass” category. The RMS of the detector alignment distributions are still well within the spatial resolution requirements even when “Pass” modules are included, so there will be no effect on physics performance. For “Good” + “Pass” modules, the distribution of *midyf*, the most sensitive alignment parameter, has an RMS of 2.0 μm , well within the target of 4 μm .

‘Good’ and ‘Pass’ modules could be used anywhere in the end-cap; there was no selection for more or less demanding locations. Disc assembly went on in parallel with

module production, and some fine-tuning was done to allow for projected module yield while always preserving quality.

5.9 Summary

This chapter has looked at the testing of modules, the system test rig: the DAQ, and the criteria for allowing a module to be used in the experiment. A key element of the production process is the communication between different phases in the process. A system was established where information found at the testing stage was quickly fed back to the bonding and visual inspection stages. This resulted in some module problems being avoided from information logged during the process. One test not carried out in Glasgow is metrology which will be shown in Chapter 6, this was to highlight failures but required special equipment located in Liverpool.

Chapter 6

6 Production Results

6.1 Introduction

This chapter will present the results of ATLAS module production at Glasgow, both in their own right and with respect to results achieved by the other groups involved in the SCT production. The chapter will start with a closer look at the results of the qualification phase of production, highlighting the progress made at this stage toward a stable process. The causes of rework and the efforts made to combat re-work will be analysed. This chapter will also explain how the bonding system parameters evolved during production and the change from outer to inner module production. Attention will be paid to the total number of failed modules and their failure modes. Finally there will be a discussion of the main results and a look ahead to the start of the experiment.

6.2 Collaboration overview

The production of ATLAS SCT modules has been a long, complex and successful process that required around 24 months to complete. The production was planned with a contingency of 15%. In total there were 2350 end-cap modules built and tested within the collaboration with a yield of over 90% (see Table 6). Of this figure

Glasgow contributed 273 modules (40% of the UK deliverables) with a final yield of 94.5%.

Category	Inner	Middle (S+L)	Outer
Good	394	665	984
Pass	39	58	56
Hold/Rework	46	48	23
Fail	16	5	34
Good+Pass (G+P)	433	723	1040
G+P Required to equip End-Caps	400	640	936

Table 6 Module category statistics (as defined in Chapter 5)

Figure 6-1 shows the cumulative number of modules built as a function of time together with the yield both in terms of strictly GOOD modules and GOOD+PASS modules.

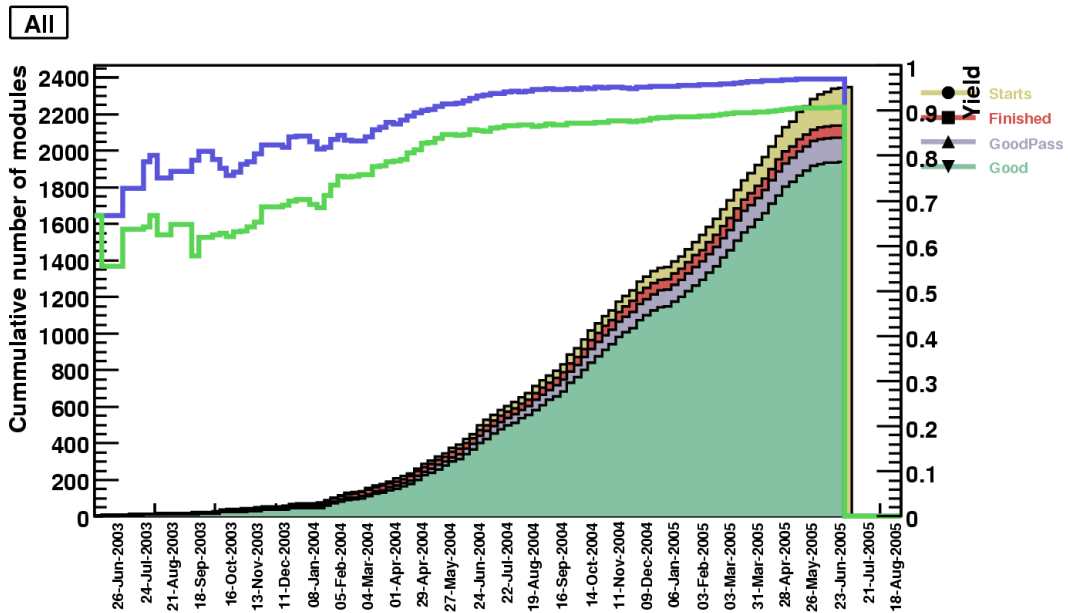


Figure 6-44 Module production performances, the filled histograms show the cumulative number of modules built as a function of time (Starts) and the number of finished, assembled and tested modules of each flavour. Also shown is the production yield (right scale) both considering just GOOD modules and also GOOD+PASS modules

Figure 6-1 describes the overall performance of all the SCT production sites. It displays the gradual production rate ramp up after the slow pre qualification and qualification periods. After these periods a production rate between 40 and 50 modules per week was achieved almost immediately with a constant yield above 90%.

6.3 Qualification

The production had two different phases. In a first phase, the different sites had to undergo a pre-qualification process in order to ensure that production tooling and procedures were in place to produce modules reliably within specifications. In order to exercise and test the procedures the production sites were supplied with second grade components. The full qualification process, however, was made with production grade components and was also intended as a short ramp-up to production. The delivery of components for the qualification also followed as closely as possible the production procedures in order to exercise and find the weaknesses of the component distribution. As part of the group's qualification attempt we were required to fully bond and test 5 modules. The module results would then be examined by the ATLAS SCT steering committee that would assess our suitability for production. The five modules were subsequently bonded using programs and parameters optimized in Glasgow and testing on the newly setup DAQ test system. Figure 6-2 charts the results. As explained in Chapter 3 the maximum number of permitted defects per module is 1% of the total number of channels. The total is 1536, which allows for 15 defect channels. The number of defects on module 41 and 43 both exceed this permitted tolerance – registering 19 and 25 defects respectively. Initially it was thought that this would delay the group's qualification, but it was decided that, given the defects caused by bonding were lower than 15 (6 and 12 respectively) Glasgow should be allowed to proceed to production. These modules had an unusually high number of defects channels already upon arrival from Manchester, these defects are stuck channels and dead channels and are often a result of mishandling during the module construction.

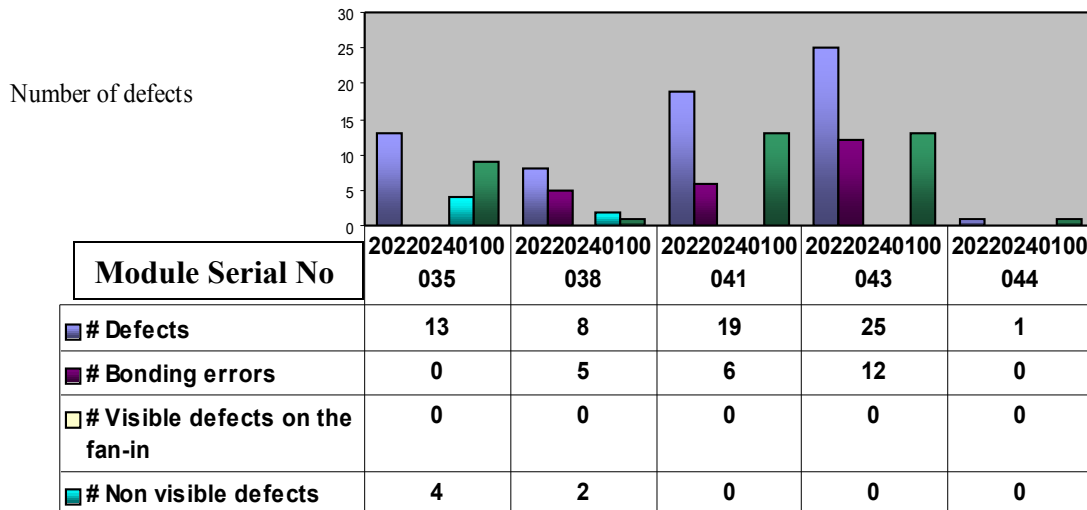


Figure 6-45 Results of qualification, this chart lists the number of defects per qualification module and the defect types. Bonding errors are defects that are deemed a result of poor bonding. Visible defects are defects that are seen at visual inspection (such as scratches). Non-visible defects are defects that are neither seen at visual inspection nor caused by poor bonding (such as dead/stuck channels

6.4 Production and early bonding problems

Figure 6-3 illustrates the problems encountered in the early stages of production. Rework numbers are generally too high with one module (module 118) recording as many as 117 reworked channels. During these early stages work concentrated on the module clamping as explained in Chapter 4 and then on fine tuning the process parameters.

Some of the modules in these early stages show low or no rework but this level of performance could not be sustained. After lengthy consultation with H&K service engineers and fellow bonders in the SCT community, steps were taken to control the temperature and humidity in the clean room bonding area, but the single greatest process improvement was achieved by increasing the tension of the wire clamps (see Figure 6-5). After this adjustment bond rework numbers became much more manageable. Bond quality also improved with much cleaner, stronger and reliable connections.

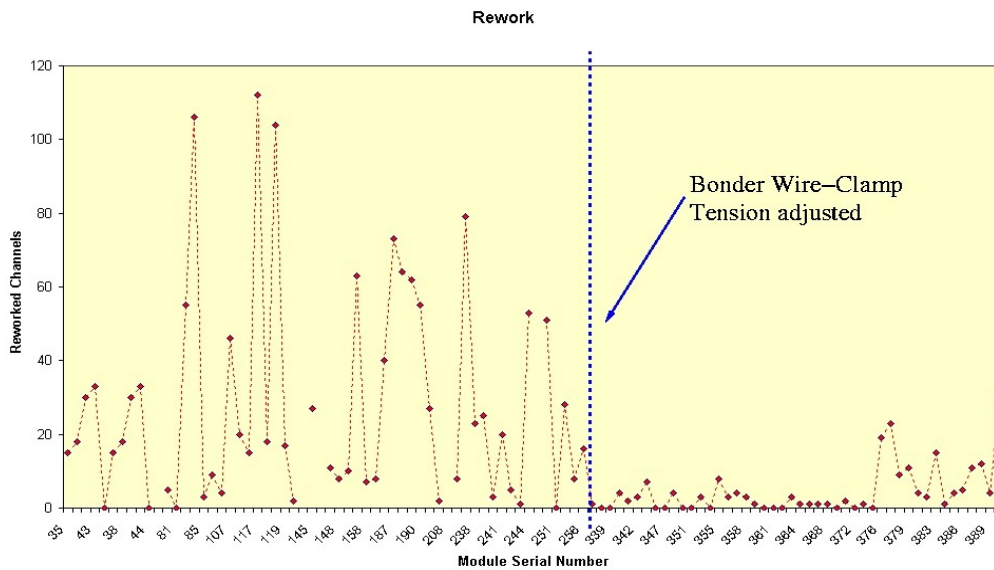


Figure 6-46 Number of reworked channels during early stages of production

The wire clamps are a very important component of the H&K 710 bond jet. During the bonding process they feed the wire through the wedge at different stages and crucially they tear off the wire at the end of a bond. As the wedge makes contact with a substrate at the second point of a wire bond (the destination point) the wire clamps close while the wedge is still making contact. This causes the wire to tear leaving a tail length in the wedge for the next bond. If the clamps fail to tear the wire at the destination point, the bond will not hold (see Figure 6-4).

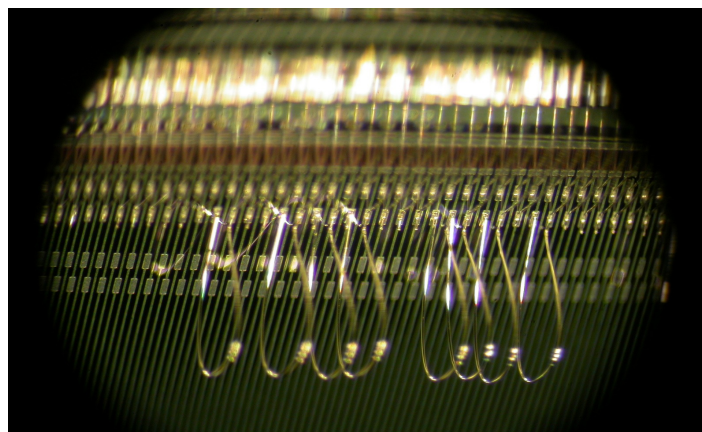


Figure 6-47 Failed wire-bonds caused by bonding system fault, wire is seen to form a loop between consecutive source points

It was discovered that this tearing process was not working efficiently; this was caused by the clamps failing to adequately grip the wire after the destination point contact. This in turn caused a variable tail length for the first contact point (source point) of the subsequent bond and in some cases the wire itself was failing to tear. After considerable experimentation it was discovered that there was a problem with the force exerted by the feed clamps onto the wire resulting in insufficient wire being fed through the tool for the next bond.

Figure 6-5 shows an image of the bonding wedge from the rear and the importance of the wire clamp to the bonding process. It was found that an increase in the force applied to the wire clamps via a spring was required. The adjustment of a small setscrew increased the tension of the wire clamps and eliminated the possibility of poor wire tear and variable tail length. This small setscrew had been at a default value as recommended by the service engineer of 6 cNm. This value was adjusted to 12cNm using a torque watch. During the initial stages of production, several modules required large number of reworks. Initially this was considered to be either a clamping issue, or due to bonding system parameters. It was later decided that the bonder itself was the cause of the problem and after consultation with the service engineer; it was decided to keep to a constant temperature and humidity. The engineer also had concerns about the air circulation in the clean room, resulting in the limitation of the use of the A/C unit. After these factors were brought under control and following the adjustment to the force applied to the wire-clamps, bond quality improved and re-work number started to stabilize at an acceptable level.

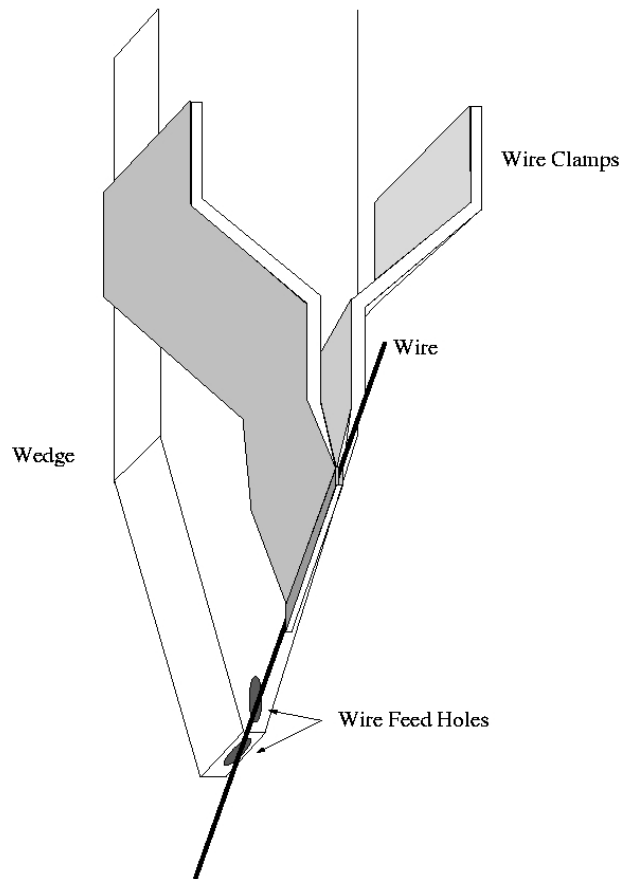


Figure 6-48 Graphical image of bonding system bond head

6.5 Wire-bond reworks

During production the first indication of poor bond quality is the number of reworks that were accumulated during the course of module bonding and this single factor became the greatest challenge to the overall success of the production. It could be assumed that a module which has a high number of reworks has some inherent differences to a module where few reworks are required. But in reality there are other factors that can cause high rework; these include user error, equipment fault, poor module clamping and atmospheric conditions. If a module requires a large number of rework it can be assumed that the overall quality and strength of the bonding on that module is not good. It can also be assumed that for every bond requiring rework, there are a few successful bonds that barely avoided rework. When all the elements were in

place the system provided nicely formed wire bonds with consistent footprint shape and loop form (see Figure 6-6).

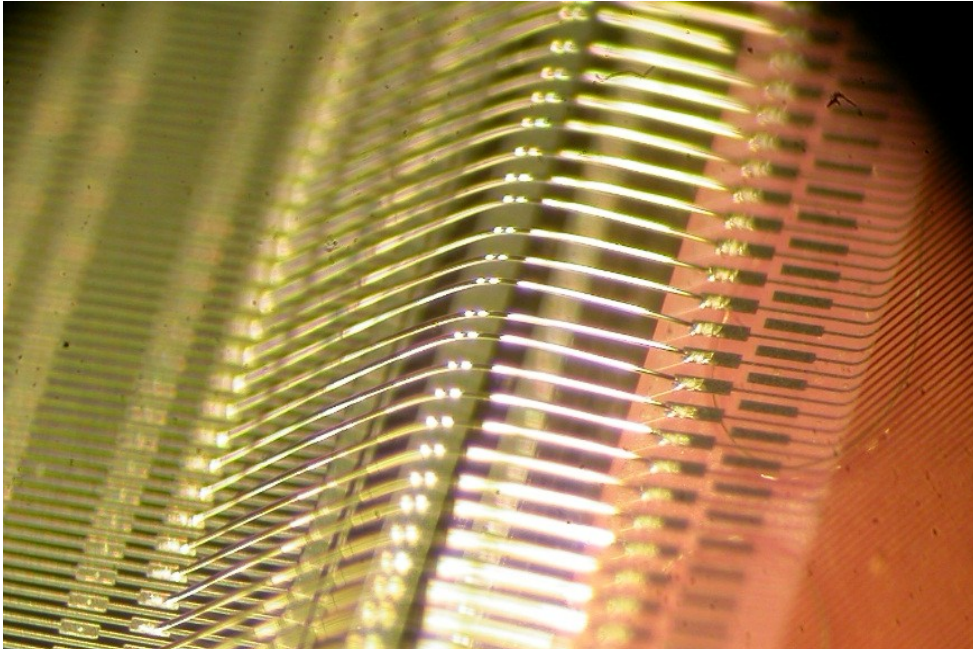


Figure 6-49 Example of good wire-bonding on the fan-in to detector zone of module 258

Through the course of production rework figures varied. As described earlier, during qualification and early production, high rework numbers were a result of bonding system faults and user error. However as production continued other factors became more prominent. Figure 6-7 shows the rework numbers performed on every module bonded in Glasgow. It shows that 14 modules required more than 50 reworked channels (see Figure 6-8). 50 reworks is the figure that became recognized as the maximum accepted rework number caused by inherent module tolerances, anything above this figure was considered to indicate a fault of a more substantial nature.

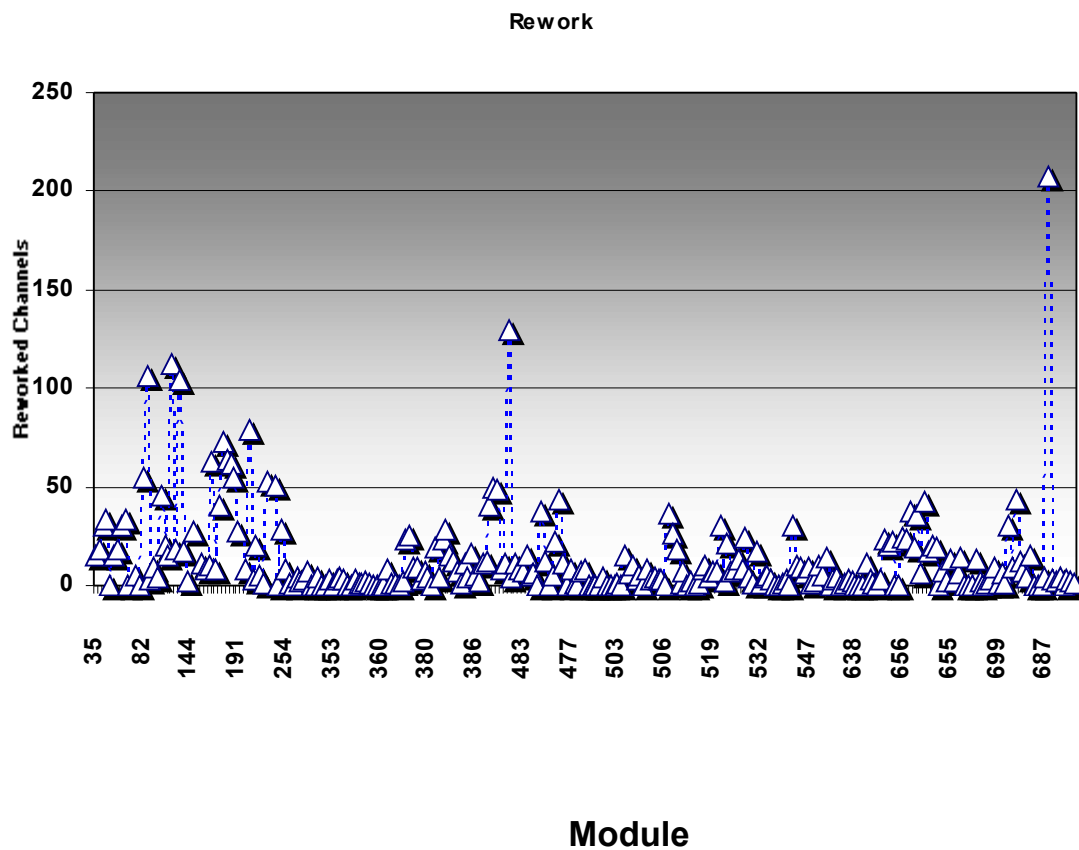


Figure 6-50 Final totals for reworked channels per module

Of these 14 modules requiring more than 50 rework, 12 occurred during the first 43 modules bonded and are attributed of bonding system faults and user inexperience. The other two modules requiring fifty plus reworks can be attributed to one-off user errors. As shown in Figure 6-7 after the initial problems, rework numbers stabilized with a high number of modules requiring less than 10 reworks. Despite decreasing rework over the production, there remained the possibility of a module requiring high rework and numbers were not brought fully under control.

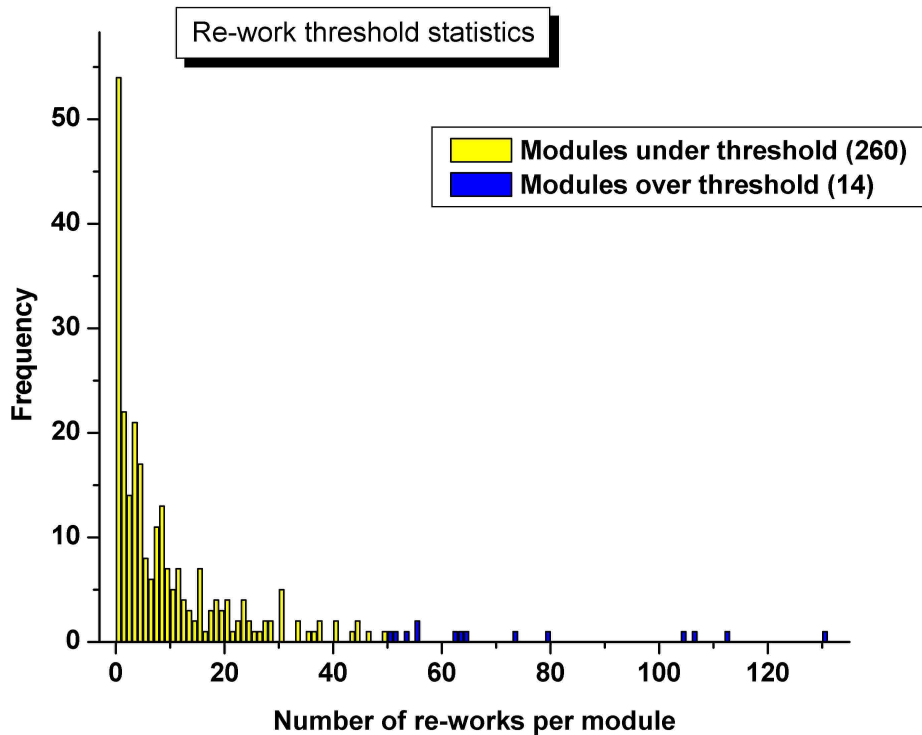


Figure 6-51 Frequency of reworked channels per module

6.6 Bonding parameter evolution

As described in Chapter 4, time was spent optimizing the bonding system parameters prior to Glasgow site qualification. This process was repeated before the switch to inner module production. However, once production is underway it is difficult to maintain the optimal parameter settings as the wire-bonding can not be tested, due to the destructive nature of the bond testing. Therefore parameter adjustments carried out during production were optimised to minimise rework numbers and to maintain consistent bond footprints and loop forms. Deformation charts provide an insight into the quality of bonding. Figure 6-9 is an illustration of the deformation charts provided by the H&K bonding system software. This shows the wire bond deformation as a function of time. If a deformation graph shows that a certain bond is taking longer to reach the deformation point as set in the parameters window, then it can be assumed that either the module is insufficiently clamped or has some tolerance variances. In

most cases altering the deformation value helped keep the deformation graphs within accepted levels. The deformation parameter increased gradually throughout production. Other parameters such as ultrasonic power and bond-force were increased for single bond fail and bond footprint quality control. Loop height and form parameters remained at the values set during pre-qualification.

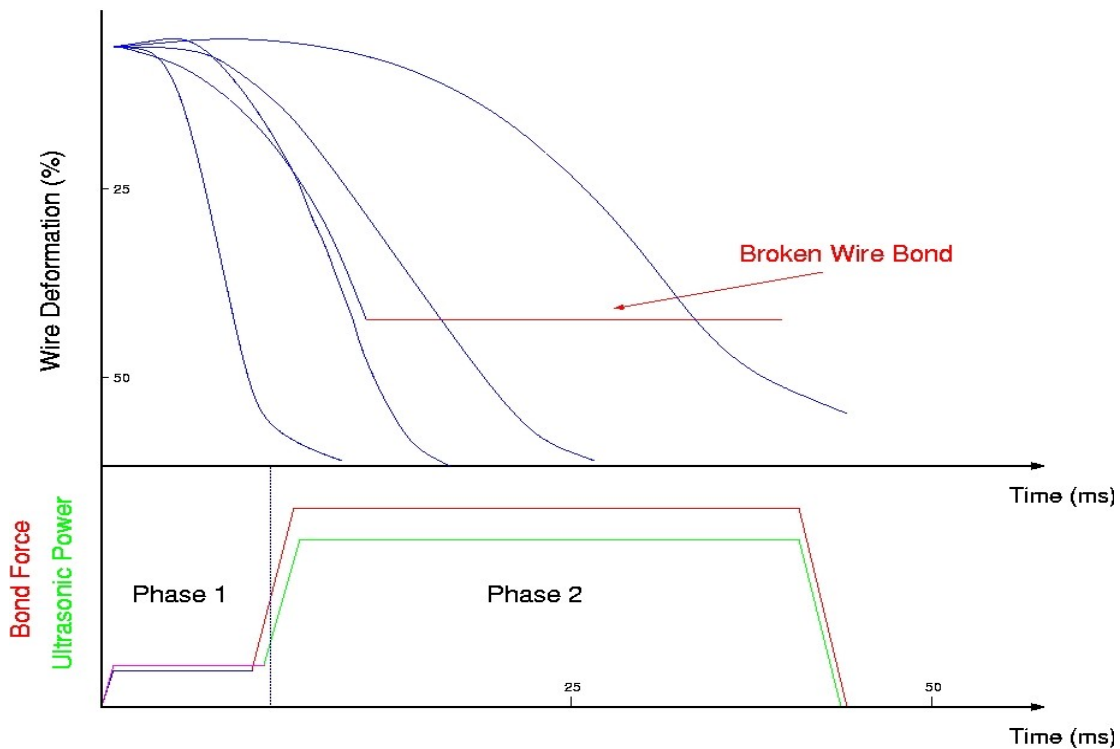


Figure 6-52 Deformation charts provided by the H&K bonding system software. Wire deformation is measured in the Z axis

It was found that bonding the fan-in zone on the inner modules was problematic and that attempts to solve this problem by altering deformation, ultrasonic and bond power parameters did not improve this. After changing some other parameters it was found that decreasing the over-ride speed of the bonder eliminated the problems. The over-ride speed is a parameter that sets the overall speed of the bonding and directly affects each time taken during the bonding process. Decreasing the value of this parameter and consequently increasing the time taken for each stage of bonding enabled successful bonding of the inner module fan-in zone. The over-ride speed was set to 90% (roughly 2 bonds/sec) during outer module bonding and was set to 50% for inner module production. There was no accepted explanation as to why this was necessary

but it was hypothesized that the overall structural rigidity of the clamped inner module was lower due to it having a much smaller detector area. The construction of an inner module is such that only one detector surface is required. This in turn reduces the size of the vacuum support chuck used during bonding. With less of the module being supported it was postulated that the overall strength of the inner module clamping was lower than that of the outer modules.

The far right hand side deformation track on Figure 6-9 is representative of a bond formed on an inner module fan-in. The longer a bond takes to reach the set deformation point, the greater the movement in the surface being bonded.

6.7 Rework Analysis

During production an exact count of rework numbers and rework locations was kept using an internal e-log. Module rework numbers were kept including details of which bonding zone the rework was performed on, and which channel number the reworked wire bond represented. The purpose of this exercise, besides maintaining records for the database, was to determine the bonding characteristics of each bonding zone, Figure 6-10 shows that rework numbers were fairly evenly spread over the three bonding zones on the modules. The detector bonding zones show the least number of re-works per module due to the relative ease of bonding these zones. Bonding is easier on these zones because the pad pitch is the highest (100 μm) and the pad size is the largest (70 μm by 150 μm) of the three bonding zones.

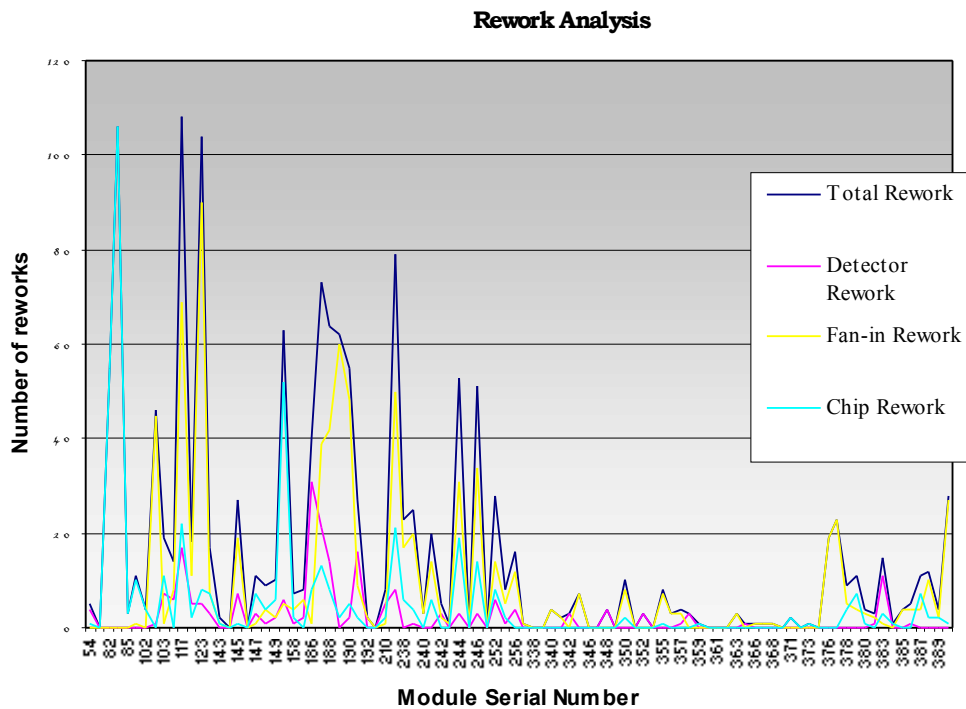


Figure 6-53 Breakdown of reworked channels per bonding zone on selected modules. This figure shows the total number of defects per module and breaks down that number into which bonding zone each rework was performed in.

It is clear that on certain modules (module numbers 83, 92,150) high rework is evident almost exclusively on the chip bonding zones. These reworks were attributed to serious user error and were not thought to be related to any other issues. As a whole the chip programs ran well with chip rework caused by user error as a result of the very fine pitch (50µm) of the bond pads on the chips. This narrowed down the issue of unexpected reworks to the fan-in and detector zones.

6.8 Mechanical tolerances

Every module is manufactured by hand at the Manchester site and is rigorously tested to ensure the hybrid, fan-in and detector are positioned within preset tolerances. During the course of research into the cause of high rework numbers on the detector and fan-in bonding zones, attention turned to modules that were closer to the tolerance limits (as detailed in figure 3-2 and 3-2). Due to the nature of the module construction,

no information was available on the position of the fan-in sections on the module, research was therefore restricted to the detector area. The information we received from Manchester related to the position of the detector with respect to Z (perpendicular to the detector surface). As the module detectors are glued onto the spine there can be variations in height (Z) due to inconsistencies in the amount of glue used, or slight warping of the detector or the spine. It was thought that a module that was slightly further out in Z could increase rework numbers. Figure 6-11 plots Z deviation on both sides of the detectors against rework numbers.

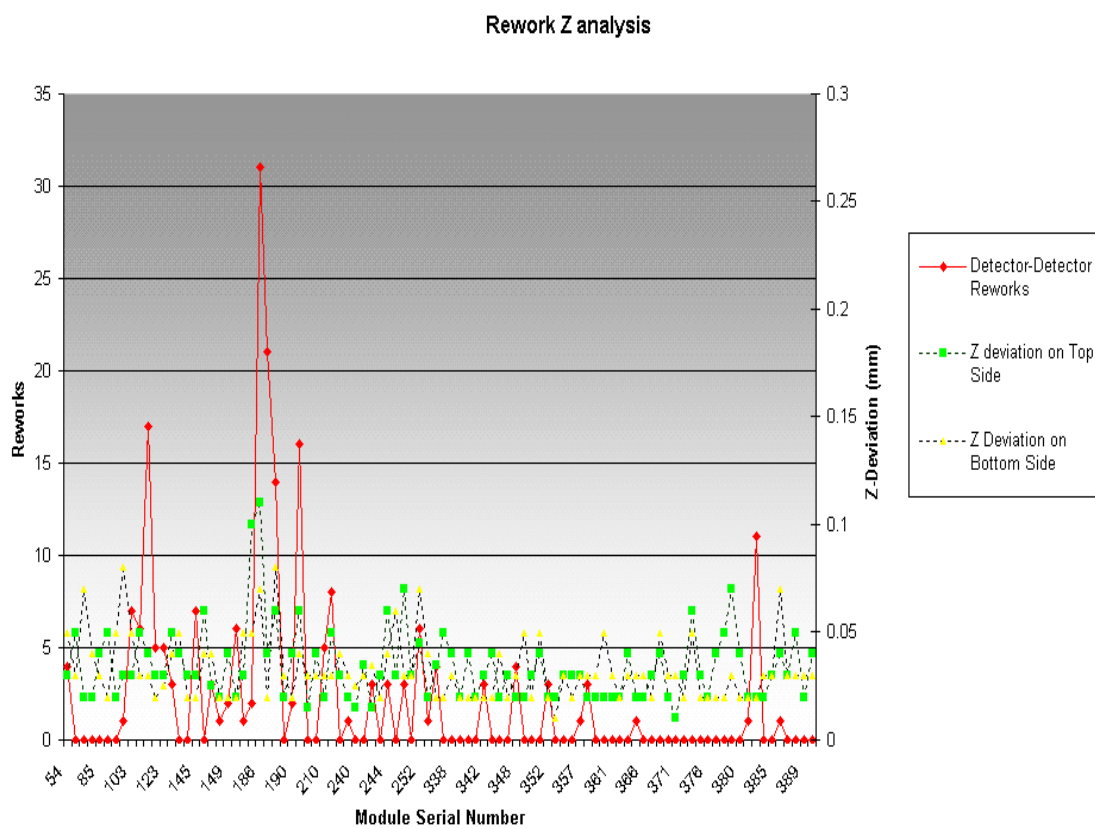


Figure 6-54 Analysis of the effects of Z-deviation in the detector on module rework numbers

Analysis of these results was inconclusive; it could be argued that module number 188 showed high Z-deviation on the top side which could be related to high rework, but module 123 and 384 show high rework and low Z-deviation. It was concluded that Z-deviation had little or no impact on rework numbers.

6.9 Module Failure Modes

By the end of production 292 inner and outer modules had passed through the Glasgow site. Of this figure 273 were deemed Good or Pass as defined in the ATLAS QA Acceptance guidelines. Of the 19 that did not meet the guidelines (see Appendix A), none were deemed to have failed as a direct result of the wire bonding process. Although it should be noted high leakage current could have been caused by high impact damage of bonding on the detector with excessive deformation. In addition module 81 failed due to a cracked ceramic spine, which although a result of mishandling at the bonding stage was logged as a visual inspection fail.

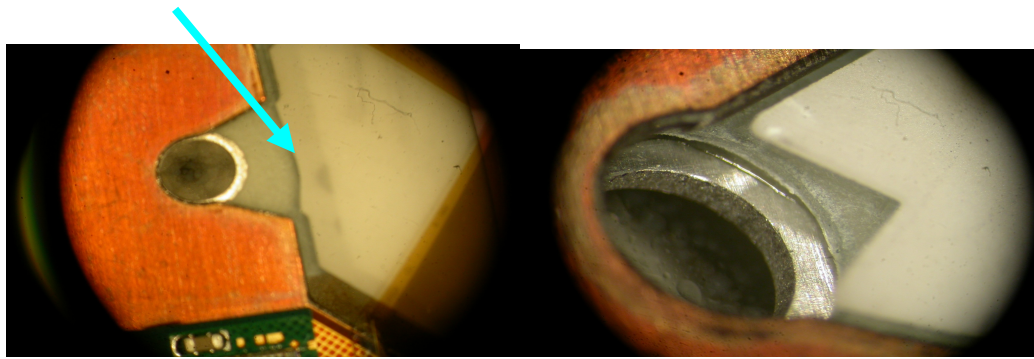


Figure 6-55 Module 81 cracked spine (left, identified by arrow) undamaged spine (right)

Module 81 suffered a damaged ceramic spine during clamping (see Figure 6-12), prior to wire bonding. After the module was damaged it was decided to tighten the clamping screws on the module using a torque watch to prevent further damaged modules.

Test	Modules Rejected
Visual Inspection	1.3%
IV	0.2%
Electrical	0.2%
XY Survey	3.3%
Z Survey	0.6%
Long Term Test	0.0%
Thermal Cycling	0.0%

Table 7 Failure modes of rejected modules

Table 7 shows the failure modes and their percentages. At the end of production, 5 failure modes had been encountered. The most common of which were XY-Survey, a test carried out in Liverpool. Next most common failure mode was visual inspection, accounting for 16% of the fails (see Appendix C). Module 81 is classified as a Visual Inspection fail due to the broken ceramic spine as is module 362 which was damaged in transit from Glasgow to Liverpool despite passing all tests while on site. Other failure modes include high IV characteristics. A module's IV characteristic rarely change during the bonding process but in the early stages of production it was thought that a high IV characteristic could be caused by high impact damage of bonding on the detector with excessive deformation. Two modules (144 and 544) failed for high IV. Other electrical failures are for high noise and scratches on the fan-in causing excessive faulty channels.

6.10 Final yield

As previously mentioned, the Glasgow production site achieved a final yield figure of 94.5%. The 273 modules bonded and tested in Glasgow were part of the 634 modules manufactured in Manchester and representing the deliverables of the ATLAS UK North cluster. The overall yield figure for the UK north cluster was 92.7% of modules achieving a "G" or "P" rating. Table 8 lists the final yield figure of all sites contributing SCT deliverables. The UK North combined figure of 92.7% good or pass

modules compares well with other production sites around the world.

Summary	Built	Good	Pass	Hold	Failed	Not tested	Yield (G)	Yield (G+P)	Done	Needed	Remaining
All	2349	1902	128	106	37	176	87.50%	93.40%	99.10%	-148	-8
Types	Built	Good	Pass	Hold	Failed	Not tested	Yield (G)	Yield (G+P)	Done	Needed	Remaining
Outer	1084	949	48	35	20	34	90.40%	94.80%	103.90%	-70	10
inner	490	369	35	32	10	44	82.70%	90.60%	96.20%	-24	-10
MidL	681	528	20	28	7	98	90.60%	94.00%	93.20%	-52	-9
MidS	94	56	27	11	0	0	59.60%	88.30%	98.80%	1	2
Sites	Built	Good	Pass	Hold	Failed	Not tested	Yield (G)	Yield (G+P)	Done	Needed	Remaining
Freiburg	223	142	22	15	1	43	78.90%	91.10%	88.20%	-17	-11
Geneva	653	600	15	8	9	21	94.90%	97.30%	107.50%	-63	1
MPi	423	272	30	22	2	97	83.40%	92.60%	82.20%	-24	-3
MPi-MidL	329	216	3	11	2	97	93.10%	94.40%	77.20%	-27	-5
MPi-MidS	94	56	27	11	0	0	59.60%	88.30%	98.80%	1	2
Man.	634	544	39	38	8	5	86.50%	92.70%	105.20%	-33	0
Man.-inn	162	141	9	11	0	1	87.60%	93.20%	105.80%	-9	0
Man.-Mid	195	175	9	8	2	1	90.20%	94.80%	109.50%	-17	-3
Man.-Out	277	228	21	19	6	3	83.20%	90.90%	101.80%	-7	3
Melbourne	29	12	1	2	4	10	63.20%	68.40%	41.30%	12	7
NiKHeF	105	86	4	6	9	0	81.90%	85.70%	97.40%	2	1
Valencia	282	246	17	15	4	0	87.20%	93.30%	107.00%	-17	-1
Valencia-Mid	157	137	8	9	3	0	87.30%	92.40%	106.20%	-9	-1
Valencia-Out	125	109	9	6	1	0	87.20%	94.40%	108.10%	-9	0

Table 8 Final yield figures of all SCT module production sites

The UK north clusters yield of 92.7% is one of the most impressive in the collaboration. Glasgow final yield of 94.5% is a figure only the production team in Geneva, who achieved an overall yield of 97% could improve upon. Other major contributors included Freiburg (91.1%), Munich (92.6%) and NiKHeF (85.7%).

6.11 Post production

All modules passed as “G” or “P” at the Glasgow production site were sent to Liverpool to be mounted. Figure 13 shows ring number 4 in Liverpool. On close inspection the inner modules (40 in total) lining the ring (52 in total) providing coverage. In this picture, this ring of the disk providing overlap



Figure 6-56 Disk 4 of SCT end-cap C

Once these rings have been populated with modules they are inserted in the end-cap cylinder and are connected to the various power and readout cables and cooling pipes.

Figure 6-14 shows end-cap C cylinder in the Liverpool laboratories just prior to shipment to the ATLAS cavern at CERN. The barrel section of the SCT is already at CERN and on the delivery of end-cap C from the NKHEF laboratories in Amsterdam the entire SCT will be on site.

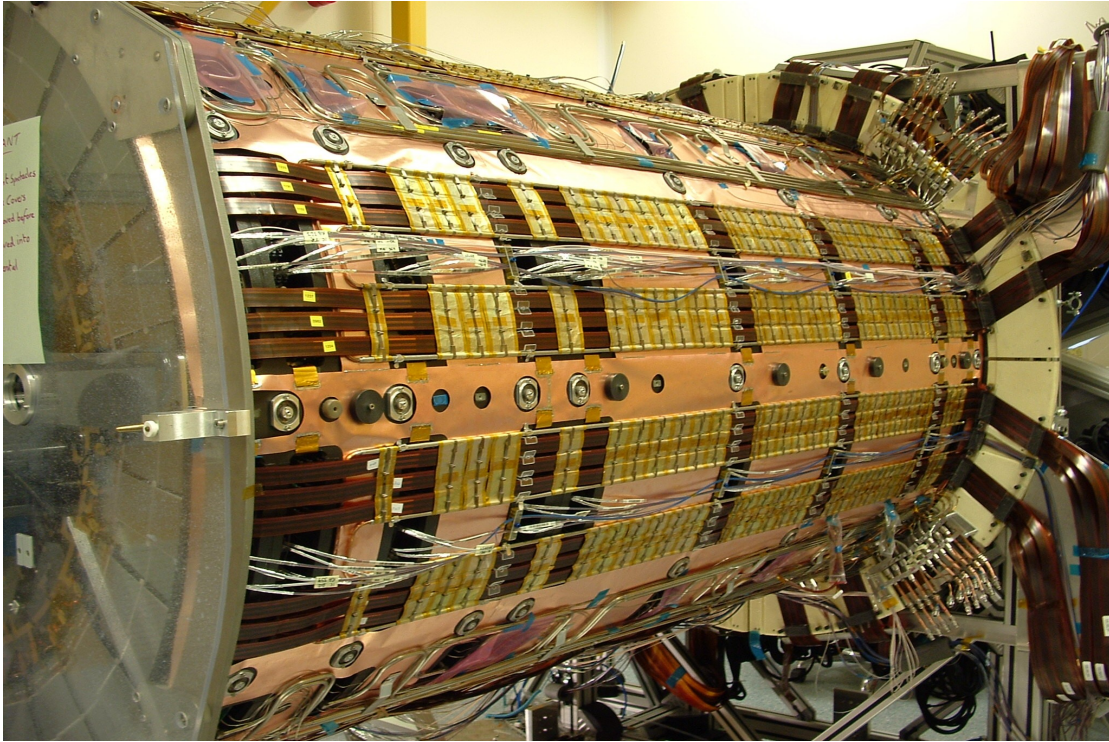


Figure 6-57 ATLAS SCT end-cap C

6.12 Conclusions and Summary

The work in this dissertation focused upon the creation and management of a process to bond and test modules for the ATLAS SCT end-cap C. As shown in Chapter 6, the operation was a success with very high yield figure achieved both by the Glasgow group and throughout the collaboration. Work on ATLAS production started in 2002 where the groundwork was started and the sourcing of equipment for bonding and testing took place. In late 2003 the first dummy modules were delivered for early bonding tests and to refine the SCT DAQ system. After a period of bonder program and parameter optimisation, the first pre-qualification modules were bonded and tested in December 2003. The start of 2004 saw Glasgow apply for and gain qualification on the strength of 5 modules successfully bonded and tested. In June 2005 the final inner module passed through the Glasgow production site, marking the end of ATLAS module production. In total 273 modules passed through during those two years, with a total of 1.2 million bonds being placed. At the end of production

Glasgow had achieved a figure of 94.5% of modules matching the “Good” or “Pass” criteria.

Module quality was high and consistently met expectations throughout. No new performance problems occurred after initial bonding problems in early production. The time spent during qualification optimising bonding programs and system parameters was invaluable in establishing a solid basis for the production process. The high quality of wire bonding during production was a key element in the overall quality of the work done. The high quality of wire bonding was a result of a sustained period of research and study into the science of wire-bonding and how that knowledge gained could be applied in a project like ATLAS. During the course of production the Glasgow site proved itself to be a world class facility for the production of detectors for use in large scale experiments. Communication was vital throughout, both internally and externally with weekly phone meetings, regular e-mails and reports submitted to the collaboration allowing contributors to pass on new information and address problems at the source. Much of the work was done by hand, such as mounting and clamping modules for bonding and preparing modules for testing. Module and bonding failures were often isolated incidents and due to different errors. Rarely was the same mistake made twice.

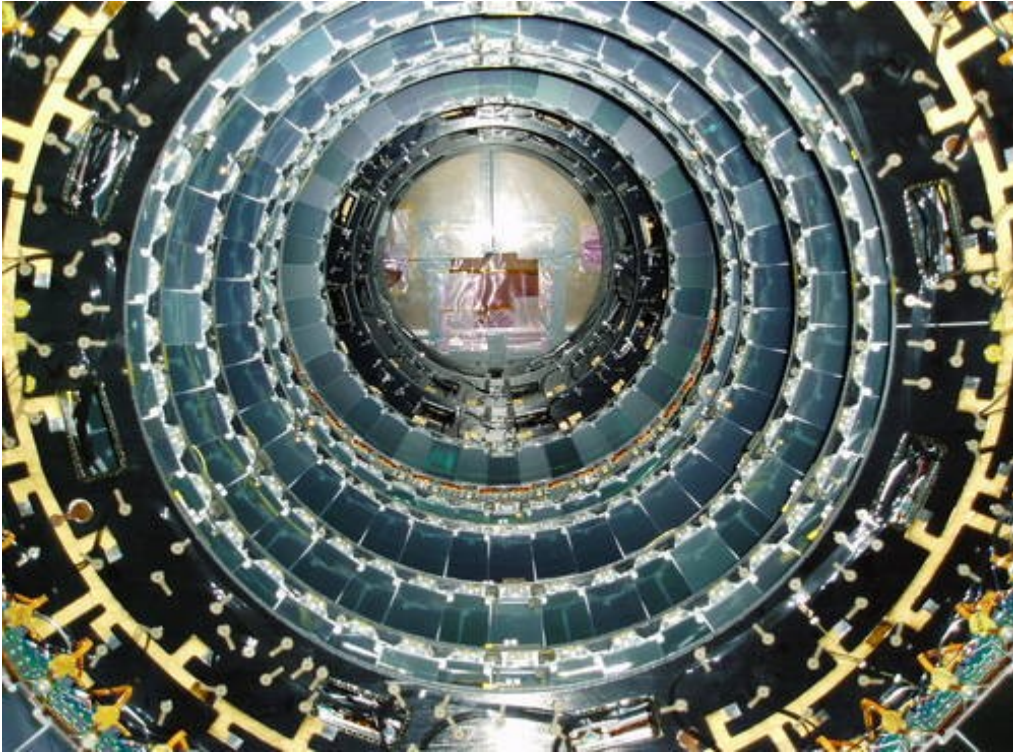


Figure 6-15 Beams eye view of end-cap C^[36]

In terms of the overall picture, around 2000 modules were prepared for the SCT end-cap and barrel sections. There was a component loss figure of only 7%, which is a factor of 2 lower than initially planned for. The total time spent on each module (component QA, assembly, wire-bonding, electrical testing, packing, shipping and database entry) was around 60 hours. The efficient timing and organisation of this effort was critical to the success of the ATLAS experiment. The Glasgow group has made a significant contribution to this success.

The SCT section of the ID (see Figure 6-15) has now been fully tested and is on site at the ATLAS cavern on the LHC ring at CERN where it will undergo further testing. The SCT should be in place on the beam line in the ATLAS pit by late July 2006. The ATLAS experiment should go ahead as planned in the summer of 2007.

Appendix A

List of information provided by SCT system DAQ

This is an extract of SCT DAQ confirmation sequence readout for module 630. Each electrical test and the result of that test is in bold text. The final defect list is at the end of the data. This module passed all tests.

SERIAL NUMBER : 20220240100630
TEST MADE BY : che
LOCATION NAME : Glasgow
Run number : 1147
TEST_DATE : 16/03/2005
PASSED : YES
PROBLEM : NO

%DAQ_INFOHOST
"PPELAB04"VERSION
"3.42"DUT
"Endcap_Inner"TIME
"13:16:59"
%DCS_INFO
#T0 T1
7.0 -128.0
#VDET IDET
150 0.020
#VCC ICC
3.50 1010
#VDD IDD
3.98 630
#TIME_POWERED

%HardReset

```
#NOCONFIG ICC  IDD
      720  580
#NOCLOCK ICC  IDD
      1010 360
#No defects found!
%NewTest
```

%FullBypassTest

```
#NConfigs 62
#Vdd = 4.0 - 3.5
#Vmin
#token r_tkn token r_tkn
#M0      S1
3.50    3.50 3.50  3.50
#S2      S3
3.50    3.50 3.50  3.50
#S4      E5
3.50    3.50 3.50  3.50
#M8      S9
3.50    3.50 3.50  3.50
#S10     S11
3.50    3.50 3.50  3.50
#S12     E13
3.50    3.50 3.50  3.50
#Comment
#M0      S1
"Minimal tested" "Minimal tested" "Minimal tested" "Minimal tested"
#S2      S3
"Minimal tested" "Minimal tested" "Minimal tested" "Minimal tested"
#S4      E5
"Minimal tested" "Minimal tested" "Minimal tested" "Minimal tested"
#M8      S9
"Minimal tested" "Minimal tested" "Minimal tested" "Minimal tested"
#S10     S11
"Minimal tested" "Minimal tested" "Minimal tested" "Minimal tested"
#S12     E13
"Minimal tested" "Minimal tested" "Minimal tested" "Minimal tested"
#No defects found!
%NewTest
```

%RedundancyTest

```
#RedundancyTest Summary - not for the database
#chip pass good stuck dead adr0 adr1 com0 com1 com
# 0 1 128 0 0 0 0 0 0 0
# 1 1 128 0 0 0 0 0 0 0
# 2 1 128 0 0 0 0 0 0 0
# 3 1 128 0 0 0 0 0 0 0
```

```

# 4 1 128 0 0 0 0 0 0 0
# 5 1 128 0 0 0 0 0 0 0
# 6 1 128 0 0 0 0 0 0 0
# 7 1 128 0 0 0 0 0 0 0
# 8 1 128 0 0 0 0 0 0 0
# 9 1 128 0 0 0 0 0 0 0
#10 1 128 0 0 0 0 0 0 0
#11 1 128 0 0 0 0 0 0 0
#No defects found!
%NewTest

```

%PipelineTest

```

#NGOOD
#M0 S1 S2 S3 S4 E5
128 128 128 128 128 128
#M8 S9 S10 S11 S12 E13
128 128 128 128 128 128
#No defects found!

```

```

%NewTest

```

%StrobeDelay

```

#DELAY
#M0 S1 S2 S3 S4 E5
21 23 22 22 22 22
#M8 S9 S10 S11 S12 E13
23 23 21 22 22 21
#No defects found!

```

```

%Comment

```

```

COMMENT      : Strobe Delay Fraction 0.40

```

```

%NewTest

```

%ThreePointGain

```

#Loop A - Fit
#      func  p0    p1    p2
#M0
4      14.39  58.91  0.00
#S1
4      12.13  59.71  0.00
#S2
4      9.68   61.37  0.00
#S3
4      12.44  59.92  0.00
#S4
4      5.55   59.91  0.00
#E5
4      11.24  58.63  0.00
#M8
4      3.35   63.65  0.00
#S9

```

```

4      7.34  59.77  0.00
#S10  4      13.52  57.35  0.00
#S11  4      8.02   59.82  0.00
#S12  4      14.28  57.05  0.00
#E13  4      12.12  59.87  0.00
#
#Loop B - Gain, Offset, Noise at 2.00fC
#      vt50  rms   gain  rms   offset rms   outnse innse  rms
#M0   133.0  8.86  58.9  1.38  14.4  9.01  9.78  1038  46
#S1   132.1  9.70  59.2  4.10  12.2  9.65  9.85  1031  29
#S2   133.4  8.64  61.3  1.17  9.8   8.77  9.54  972   27
#S3   132.3  10.18 59.9  0.99  12.4  10.11 9.70  1012  29
#S4   126.3  9.17  59.9  1.34  5.7   8.02  9.57  999   25
#E5   128.7  8.10  58.6  1.12  11.2  8.59  10.16 1084  27
#M8   132.1  7.49  63.5  1.28  3.6   6.53  9.89  973   24
#S9   127.1  8.90  59.8  1.23  7.4   7.92  9.62  1007  23
#S10  127.5  9.02  57.3  1.17  13.5  9.03  9.52  1038  25
#S11  127.7  9.69  59.3  4.24  8.5   7.94  9.45  988   26
#S12  127.9  9.77  57.1  1.07  14.3  9.32  9.70  1063  26
#E13  131.7  10.27 59.9  1.44  12.1  9.14  9.88  1032  25
#
#Loop C - Comment
#M0 S1 S2 S3 S4 E5
"OK" "OK" "OK" "OK" "OK" "OK"
#M8 S9 S10 S11 S12 E13
"OK" "OK" "OK" "OK" "OK" "OK"
#BadChannelSummary - not for the database
# at 2.00fC
#      lost  dodgy  dead  stuck  ineff  unbon  lo_gn  hi_gn  lo_off
#      hi_off partbon          hi_nse
#Chip 0:  0    0    0    0    0    0    0    0    0
#      0    0

```

#Chip 1:	0	2	0	0	2	0	2	0	0	0
0	2									
#Chip 2:	0	0	0	0	0	0	0	0	0	0
0	0									
#Chip 3:	0	0	0	0	0	0	0	0	0	0
0	0									
#Chip 4:	0	0	0	0	0	0	0	0	0	0
0	0									
#Chip 5:	0	0	0	0	0	0	0	0	0	0
0	0									
#Chip 6:	0	0	0	0	0	0	0	0	0	0
0	0									
#Chip 7:	0	0	0	0	0	0	0	0	0	0
0	0									
#Chip 8:	0	0	0	0	0	0	0	0	0	0
0	0									
#Chip 9:	0	2	0	0	2	0	2	0	0	0
0	2									
#Chip 10:	0	0	0	0	0	0	0	0	0	0
0	0									
#Chip 11:	0	0	0	0	0	0	0	0	0	0
0	0									
#Link 0:	0	2	0	0	2	0	2	0	0	0
0	2									
#Link 1:	0	2	0	0	2	0	2	0	0	0
0	2									
#Link 2:	0	4	0	0	4	0	4	0	0	0
0	4									

%Defect

DEFECT NAME : PARTBONDED

FIRST CHANNEL : 113

LAST CHANNEL : 113

%Defect

DEFECT NAME : LO_GAIN

FIRST CHANNEL : 243

LAST CHANNEL : 243

%Defect

DEFECT NAME : LO_GAIN

FIRST CHANNEL : 245

LAST CHANNEL : 245

%Defect

DEFECT NAME : LO_GAIN

FIRST CHANNEL : 1214

LAST CHANNEL : 1215

#4 defects found affecting 5 strips

#2 maximum consecutive defects

%Comment

COMMENT : Channel 243 masked: low gain (26.4mV/fC, cut 44.4mV/fC)

#

%Comment

COMMENT : Channel 245 masked: low gain (29.2mV/fC, cut 44.4mV/fC)

#

%Comment

COMMENT : Channel 1214 masked: low gain (28.4mV/fC, cut 44.5mV/fC)

#

%Comment

COMMENT : Channel 1215 masked: low gain (26.8mV/fC, cut 44.5mV/fC)

#

#

%TEST Rawdata

FILENAME : E:\sctvar\results\20220240100630_RC_1147_12.txt

Appendix B

List of Failed Modules

The final number of modules that failed or were held at Glasgow was 19

20220240100054 (fmModuleOutK5) - **HOLD**

Failed module XY survey, measured at Manchester before shipping to Glasgow.

20220240100158 (fmModuleOutK5) - **HOLD**

Failed survey before and after thermal cycling.

20220240100208 (fmModuleOutK5) - **HOLD**

Failed Z survey after thermal cycling.

20220240100211 (fmModuleOutK5) - **HOLD**

Failed Z survey after thermal cycling.

20220240100245 (fmModuleOutK5) - **HOLD**

Failed the initial IV test after bonding. The module has a scratch on one of the detectors which was noted at Manchester.

20220240100362 (fmModuleOutK5) - **FAILED**

Failed module evaluation. Top W32 wafer was broken during transit from Glasgow to Liverpool.

20220240100372 (fmModuleOutK5) - **HOLD**

Mhy out by 10.8 microns, a change of 11.6 from the Manchester measurement, and 0.8 outside the pass band.

20220240100381 (fmModuleOutK5) - **HOLD**

Has 16 defects. 15 of these match scratches on the fanin.

20220240100386 (fmModuleOutK5) - **HOLD**

It is in the hold category because it has two survey parameters (zminf, zminb) which are out of spec.

20220240100396 (fmModuleOutK5) - **HOLD**

The module appears tilted about the X axis.

20220240100472 (fmModuleInnK5) - **HOLD**

Misy out of tolerance by 2 microns, midyf out by 8.2 micron.

20220240100478 (fmModuleInnK5) - **HOLD**

Midyf out of tolerance by 13 microns

20220240100488 (fmModuleInnK5) - **FAILED**

Unstable noise. Suspect HV bias connection.

20220240100501 (fmModuleInnK5) - **HOLD**

Midyf out of tolerance by 3.4 micron. Electrically ok.

20220240100517 (fmModuleInnK5) - **HOLD**

Midyf out of tolerance by 3.6 micron. Electrically ok.

20220240100518 (fmModuleInnK5) - **HOLD**

Midyf out of tolerance by 4.3microns. Electrically ok.

20220240100542 (fmModuleInnK5) - **HOLD**

Midyf out of tolerance by 3.8 microns.

20220240100544 (fmModuleInnK5) - **HOLD**

Passes IV only after long training.

20220240100658 (fmModuleInnK5) - **HOLD**

Midyf out of tolerance by 0.6 $\hat{\text{A}}\mu\text{m}$.

Appendix C

Visual Inspection Failures

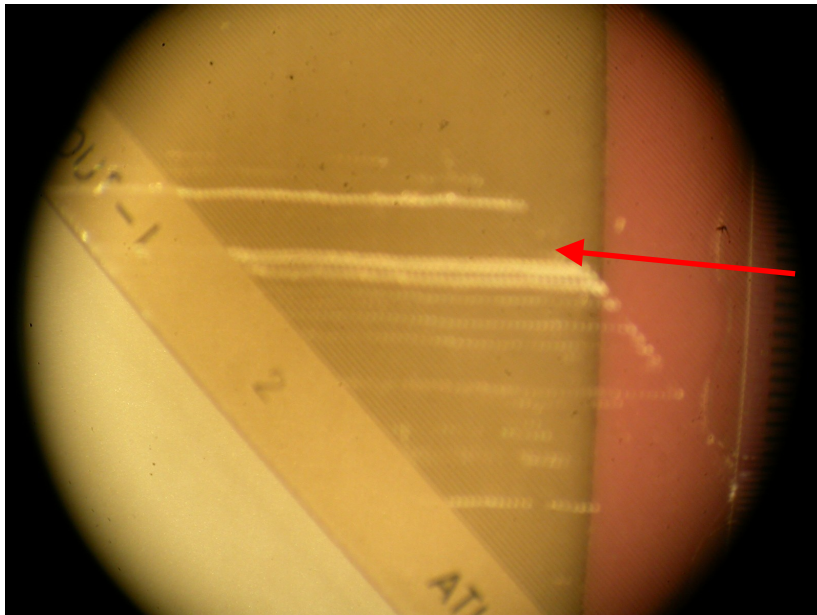


Figure C-0-58 Module 144 Scratches on fan-in

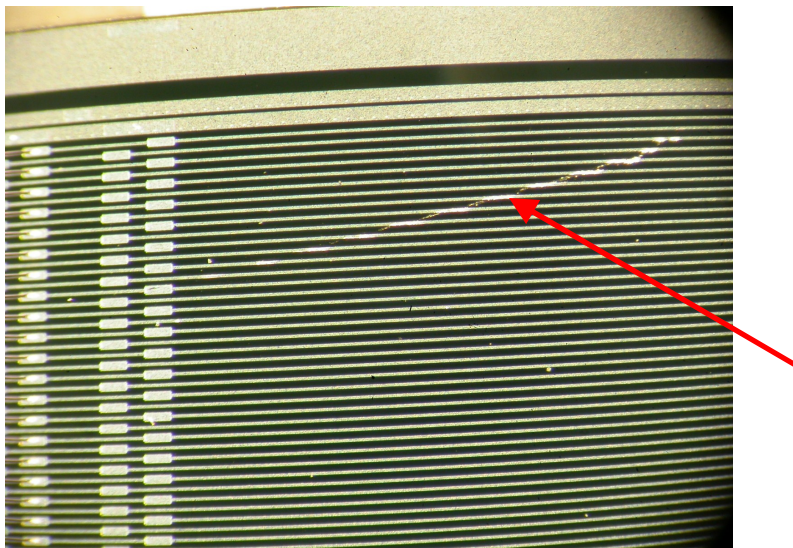


Figure C-0-59 Module 245 failed IV. Scratch on detector



Figure C-0-60 Scratches on fan-in of Module 488

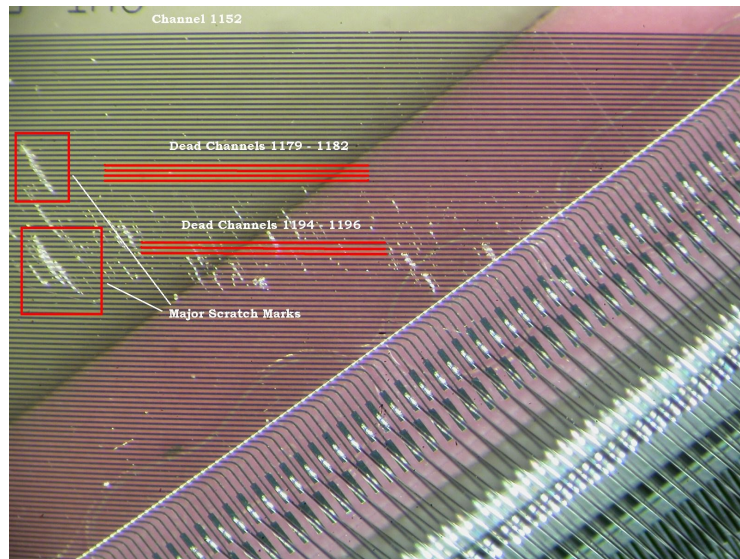


Figure C-0-61 Module 38 Dead channels on fan-in, caused by scratches

Bibliography

1 Neutrino Mass and New Physics, Annu. Rev. Nucl. Part. Sci. 2006. 56:569-628

2 Weinberg, S., "A Model of Leptons", Physical Review letters 19:1264-1266, (1967)

3 Salam, A., Elementary Particle Theory, N Svartholm, ed. (Stockholm: Almquist and Wiksell, 1968).

4 C. Alvisi et al., Nucl. Instr. and Meth. A305 (1991) 30

5 Erik H.M Heijne, Semiconductor micro-pattern pixel detectors: A review of the beginnings, Nucl.
Instrum. Meth 465(2001) 1-26

6 L.A.Ch. Koerts et al., Nucl. Instr. and Meth. 92 (1971) 157 and following articles.

7 The ATLAS Technical Proposal for a General Purpose pp Experiment at the Large Hadron Collider at
CERN, CERN/LHCC/94-43 (1994)

8 Y.Unno., ATLAS silicon micro-strip Semiconductor Tracker (SCT), Nucl. Instrum. Meth A 453 (2000)
Issues 1-2 109-120

9 ATLAS Detector and physic performance, Technical Design Report, CERN/LHCC/97-15 (1999)

10 F.Parodi., Vertexing strategy and algorithms at ATLAS , Nucl. Instrum. Meth A 560 (2006) 79-83

11 ATLAS Inner Detector, Technical Design Report, CERN/LHCC/97-16 (1997)

12 Gelmini, G., Beyond the Standard Model, Proceedings of the Eighth Lake Louise Winter Institute,
Lake Louise, Alberta, Canada, February, 1993.

13 J.Wess and J.Bagger, Supersymmetry and Supergravity, ISBN 0691085560 (1992)

14 G.F.Tartarelli., ATLAS B-physics performance, Nucl. Instrum. Meth A 408 (1998) 110-118

15 ATLAS Detector and physics performance Technical Design Report, CERN/LHCC/99-14 (1999)

16 F. Campabadal et al, Design and performance of the ABCD3TA ASIC for readout of silicon strip
detectors in the ATLAS semiconductor tracker ABCD3T, Nucl. Instrum. Meth. 552(2005) 292-328

17 I.M. Gregor et al, Optical links for the ATLAS SCT and Pixel detector, Nucl. Instrum. Meth
465(2001)131-134

18 The Quality Assurance of the ATLAS SCT end-cap detector modules, ATL-IS-QA-0004,
https://edms.cern.ch/file/316208/1/ModuleQAv9_00.pdf

19 S.Snow, Thermal and mechanical specifications and expected performance of the forward SCT
module.ATL-IS-EN-0007 (2001)

20 S.Snow, Thermal and mechanical performance results from forward SCT modules.ATL-IS-EN-0002
(2002)

21 Ph.Clark. et al, The ATLAS SCT production DB, ATL- INDET- 2002- 015 (2002)

22 P. Demierre, D. Ferrère, A Database for Silicon Microstrip Detectors in the SCT Central Cluster Working
Group, ATL-INDET-98-219 (1998)

- 23 J. Foster, S. Snow, Proposal for a Database for the ATLAS SCT Construction, ATL-INDET-96-144
(1996)
- 24 G.Harman, Wire-bonding in Micro-electronics, Materials, Processes, Reliability and Yield. 2nd Edition
25 Hesse and Knipps BondJet BJ710 User Manual (2001)
- 26 J. Bizzell, Wire-bonding of assembled ATLAS SCT middle forward modules, private communication
(2002)
- 27 J. Bizzell V.Davis, Investigation in to causes of poor IV Characteristics, private communication (2003)
- 28 J.Bizzell, V.Davis, High Impact damage caused by wire-bonding, private communication (2001)
- 29 C.Lacasta, SCT end-cap module production document, SCT Collaboration , <http://www.uv.es/lacasta/ECpaper>
- 30 A. Greenhal, ATLAS SCT AERO, http://hep.ph.liv.ac.uk/~ashley/ATLAS_AERO.html
- 31 O.Runolfsson, Quality assurance and testing before, during and after construction of semiconductor
tracking detectors, Nucl. Instrum. Meth A 383 (1996) 223-228
- 32 E. Gornicki, P. Malecki and S. Koperny, Multi-channel system of fully isolated HV power supplies for
silicon strip detectors Proc. 6th Workshop on Electronic for LHC Experiments, Cracow, Poland, 11-15 September
2000 [CERN-2000-010] 376-379
- 33 J. Bohm, et al, Power Supply and Power Distribution System for the ATLAS Silicon Strip Detectors
Proc.7th Workshop on Electronics for LHC Experiments, Stockholm, September 2001,CERN-2001-005, 363-367
- 34 L. Eklund, J. Hill, G. Moorhead and P. W. Phillips, Atlas SCT Test DAQ Online Documentation,
<http://sct-testdaq.home.cern.ch/sct-testdaq/sctdaq/sctdaq.html>, P.W.Phillips System Performance of ATLAS SCT
Detector Modules, Proc. 8th Workshop on Electronics for LHC Experiments, Colmar, France, 9-13 September 2002
[CERN-2002-003], p. 100-104 (2002)
- 35 R. Brun and F. Rademakers, Nucl. Instrum. Meth. A 389 (1997) 81; <http://root.cern.ch>
- 36 ATLAS collaboration, Information available [from http:// hep.ph.liv.ac.uk/atlas/](http://hep.ph.liv.ac.uk/atlas/)